

**NOVEL THERAPEUTIC APPROACHES FOR THE TREATMENT OF CHILDHOOD
OCULAR GENETIC DISEASES**

by

Vahitha Shameem Nizamudheen

M.Phil. in Biochemistry, Thiruvalluvar University, 2010

M.Sc. in Biotechnology, University of Madras, 2008

A THESIS SUBMITTED IN PARTIAL FULFILLMENT OF
THE REQUIREMENTS FOR THE DEGREE OF

DOCTOR OF PHILOSOPHY

in

THE FACULTY OF GRADUATE AND POSTDOCTORAL STUDIES
(Experimental Medicine)

THE UNIVERSITY OF BRITISH COLUMBIA
(Vancouver)

July 2021

© Vahitha Shameem Nizamudheen, 2021

The following individuals certify that they have read, and recommend to the Faculty of Graduate and Postdoctoral Studies for acceptance, the dissertation entitled:

Novel therapeutic approaches for the treatment of childhood ocular genetic diseases

submitted by Vahitha S Nizamudheen in partial fulfillment of the requirements for

the degree of Doctor of Philosophy

In Experimental Medicine

Examining Committee:

Dr. Cheryl Y. Gregory-Evans, Professor, Dept of Ophthalmology & Visual Sciences, UBC
Supervisor

Dr. Fabio M. Rossi, Professor & Director, Dept of Medical Genetics and BRC, UBC
Supervisory Committee Member

Dr. Orson L. Moritz, Professor, Dept of Ophthalmology & Visual Sciences, UBC
Supervisory Committee Member

Dr. Hakima Moukhles, Associate Professor, Department of Cell & Physiological Sciences, UBC
University Examiner

Dr. Robert Molday, Professor, Dept of Ophthalmology & Visual Sciences, UBC
University Examiner

Additional Supervisory Committee Members:

Dr. Elizabeth M. Simpson, Professor, Dept of Medical Genetics, UBC
Supervisory Committee Member

Abstract

Aniridia and Usher syndrome 1D are rare congenital defects that lead to vision loss in childhood. Here we tested several different approaches to treat animal models of these diseases. Aniridia is a pan-ocular condition caused by deletion or mutation of the *PAX6* gene itself or by downstream intragenic abnormalities. We tested two approaches to target the aniridic-glaucoma phenotype in *Pax6*^{Sev/+} mouse model of aniridia. First, since *Tgfb2* is a direct downstream target of Pax6, we tested whether injection of Tgfb2-secreting mesenchymal stem cells into the *Pax6*^{Sev/+} mouse eye could improve development of anterior segment tissue abnormalities. We observed complete formation of Schlemm's canal (SC) and a partially repopulated trabecular meshwork (TM). Secondly, we tested whether nonsense suppression strategy could rescue the TM defect in the mouse model harboring a nonsense mutation. Either an aqueous suspension of Ataluren® was injected subcutaneously, or topical eyes drops were instilled twice daily from P5 - P45. We found improved structural anatomy, and increased levels of Tgfb2, Pitx2 and Foxc1 proteins. Furthermore, nonsense suppression via the topical route rescued the developmental defects of TM and SC better than by systemic treatment.

Usher syndrome 1D (USH1D) is an autosomal-recessive condition characterized by deafness, vestibular dysfunction and vision loss caused by absence of CDH23 protein. We obtained a mouse model Y2209X line (*Cdh23*^{mtblr+/-}) which carries a *Cdh23* nonsense mutation. Homozygous *Cdh23* mice show profound head shaking, circling behavior, deafness, and reduced ERG response. Here, we used prenatal and postnatal nonsense suppression with Ataluren®. We observed a reduction in severity of phenotypic features in Ataluren-treated mice compared to mock-treated mice as well as corrected localization of photoreceptor proteins. We also studied *ex vivo* nonsense suppression therapy in Usher patient-specific cells. Induced pluripotent stem cells

(iPSCs) were derived from a patient's blood cells and three-dimensional (3D) retinal eyecups were generated in culture. The retinal eye cups were treated with Ataluren® which restored CDH23 protein levels, as well as other photoreceptors proteins including arrestin, recoverin and S-opsin. These results suggest patient-derived retinal eyecups are a useful tool for preclinical testing of small molecule drugs.

Lay Summary

In my study, I tested different therapeutic strategies in mouse models of two childhood genetic eye conditions (Aniridic glaucoma and Usher syndrome) caused by lack of PAX6 and CDH23 proteins, respectively. I used a drug molecule (Ataluren®) to increase the amount of Pax6 or Cdh23 protein in the mutant mouse eye. In another approach, to bypass the lack of Pax6 protein, I also used a stem cell therapy approach to increase the level of Tgfβ2, which is one of the targets of Pax6. Both drug and stem cell approaches were able to rescue the structural abnormalities in the eye and improve visual function. Furthermore, to test Ataluren® in a human model I converted patient blood cells into retina-like structures in a dish. These artificial retinas were also treated with Ataluren®. These novel treatments help us to understand and potentially improve vision in patients with inherited eye diseases.

Preface

All the data collection and analysis were performed in the Gregory-Evans developmental neurobiology lab in UBC, VGH Campus. All procedures involving animals were approved by the UBC Animal Care Committee under certificates (A18-0166, A17-0252, A13-0255) issued to Dr. Cheryl Gregory-Evans and in accordance with University of British Columbia policies, animal ethics certification (Certificate #: 6523-14), Animal care training (RBH-36-14 RA-26-14, RSx-37-14) and biosafety training(2019-yRCLJ).

In Chapters 2 and 3, all experiments were designed by me along with suggestions from my Supervisor Dr. Cheryl Gregory-Evans. Ocular injection experiments in mice were performed with the assistance from Xianghong Shan. Tissue processing and data collection were performed by myself. The manuscript is in preparation for both chapters for a peer reviewed journal. ERGs were done alongside Dr. Ishaq A. Viringipurampeer (Research Associate). A part of chapter 2 was presented in Association for Research in Vision & Ophthalmology (ARVO) International eye conference held at Hawaii, USA in 2018. Abstract was published in *Investigative Ophthalmology & Visual Science*, ARVO annual meeting abstract, July 2018.

Nizamudheen, V. S., Shan, X., Viringipurampeer, I. A., Bashar, E., Wang, X., & Evans, C. Y. G. (2018). Novel therapeutic strategies to rescue the developmental abnormalities in aniridic glaucoma. *Investigative Ophthalmology & Visual Science*, 59(9), 3967-3967. Retrieved from <https://iovs.arvojournals.org/article.aspx?articleid=2691694>

Chapter 3 was also presented in ARVO virtual meeting May 2021, Abstract was published in Investigative Ophthalmology & Visual Science, ARVO annual meeting abstract, June 2021.

Nizamudheen, V. S., Yanai, A., Gregory-Evans, K., & Gregory-Evans, C. Y. (2021). Nonsense suppression therapy in an animal model of usher 1D syndrome.

Investigative Ophthalmology & Visual Science, 62(8), 3074-3074. Retrieved from <https://iovs.arvojournals.org/article.aspx?articleid=2776345>

In Chapter 4, iPSCs were generated in Centre for Commercialization of Regenerative Medicine (CCRM), Toronto. Differentiation of cells and treatment protocols were carried out by myself and Dr. Anat Yanai, (Research Associate) in our collaborator's lab. All tissue processing, data collection was performed by myself, Anat Yanai, and Ishaq A. Viringipurampeer. A manuscript is in preparation for this chapter as well.

Table of Contents

Abstract.....	iii
Lay Summary	v
Preface.....	vi
Table of Contents	viii
List of Tables	xiv
List of Figures.....	xv
List of Abbreviations	xvii
Acknowledgements	xx
Dedication	xxi
Chapter 1: Introduction	1
1.1 Overview of the eye	1
1.2 The anterior segment of the eye.....	2
1.3 The retina	3
1.4 Genetics of ocular diseases	4
1.4.1 Development of anterior chamber angle of the eye	6
1.4.2 Congenital human eye disorders with anterior chamber abnormalities.....	8
1.4.2.1 Importance of the <i>PAX6</i> gene in early ocular morphogenesis	9
1.4.2.2 Role of <i>Tgfb2</i> in the anterior chamber angle of the eye.....	12
1.4.2.3 Experimental model: <i>Pax6</i> ^{Sey/+} mouse model of aniridia.....	12
1.4.2.4 Current treatments.....	13
1.4.3 Usher syndrome	14
1.4.3.1 Symptoms and pathophysiology	14

1.4.3.2	USH1D - mutation in <i>CDH23</i>	15
1.4.3.3	Role of <i>Cdh23</i> in the retina and cochlea.....	16
1.4.3.4	Experimental model: <i>Cdh23</i> ^{m1btlr/-} mouse model of USH1D syndrome	20
1.4.3.5	Current treatments.....	20
1.4.4	Nonsense-mediated mRNA decay (NMD).....	21
1.5	Promising therapies.....	22
1.5.1	Mesenchymal stem cells (MSCs) as a promising approach for cell-based therapy..	22
1.5.2	Translational readthrough for genetic eye disorders.....	24
1.5.3	Induced pluripotent stem cells (iPSCs) in clinical therapies	25
1.6	Modes of delivery of therapeutics.....	27
1.6.1	Ocular injections versus topical eye drops.....	27
1.6.2	Vectors	27
1.6.2.1	Viral vectors.....	28
1.6.2.2	Non-viral systems	28
1.6.2.3	Efficiency and limitations	28
Chapter 2: Therapeutic strategies for the treatment of anterior chamber abnormalities....		30
2.1	Chapter Introduction	30
2.1.1	Therapeutic strategies for the treatment of anterior chamber abnormalities	31
2.1.1.1	Specific hypotheses.....	31
2.1.1.2	Rationale	31
2.1.1.3	Experimental plan	33
2.2	Methods.....	34
2.2.1	Animal housing and husbandry	34

2.2.2	Genotyping of <i>Pax6</i> ^{Sey/+} mouse	35
2.2.3	Cell-based gene therapy	35
2.2.3.1	Cloning of <i>Tgfβ2</i> cDNA.....	35
2.2.3.2	Isolation and expansion of MSCs from adipose tissue	36
2.2.3.3	Transfection of MSCs with <i>Tgfβ2</i> -containing expression vector.....	37
2.2.3.4	Anterior chamber ocular injection	38
2.2.4	Pharmaceutical therapy	39
2.2.4.1	Ataluren® preparation for topical eye drops and systemic injection	39
2.2.5	Histology.....	39
2.2.6	Immunohistochemistry	39
2.2.7	Transmission electron microscopy (TEM)	40
2.2.8	Western blot	40
2.2.9	Enzyme-linked immunosorbent assay (ELISA)	41
2.2.10	Statistical analysis.....	42
2.3	Results.....	42
2.3.1	Anterior segment morphogenesis in the <i>Pax6</i> ^{Sey/+} mouse eye	42
2.3.2	Comparative localization of Pax6 and <i>Tgfβ2</i> in the anterior chamber region	45
2.3.3	Characterization of genetically modified MSCs expressing <i>Tgfβ2</i> protein	46
2.3.4	Outcomes of cell-based delivery of <i>Tgfβ2</i> and non-suppression therapy to the <i>Pax6</i> ^{Sey/+} eye.....	50
2.3.4.1	Structural benefits	50
2.3.4.2	Quantification of anterior segment proteins in the eye	52
2.3.4.3	Analysis of other proteins in the development of anterior chamber angle	54

2.4	Discussion	56
Chapter 3: Nonsense suppression therapy in an animal model of Usher 1D syndrome		62
3.1	Chapter introduction	62
3.1.1	Nonsense suppression therapy for USH1D syndrome.....	62
3.1.1.1	Specific hypothesis	63
3.1.1.2	Rationale	63
3.1.1.3	Experimental design.....	64
3.2	Methods.....	64
3.2.1.	Animal husbandry and breeding	64
3.2.2.	Genotyping of <i>Cdh23</i> ^{m1btlr-/-} mice	65
3.2.3	Systemic injection of Ataluren® in <i>Cdh23</i> ^{m1btlr-/-} mice	66
3.2.1.1	Immunohistochemistry	66
3.2.1.2	Electroretinography.....	67
3.2.1.3	Statistics	67
3.3	Results.....	68
3.3.1	Preclinical model of USH1D	68
3.3.2	Assessment of incidental mutations in the <i>Cdh23</i> ^{m1btlr+/-} mouse	68
3.3.3	Reduced body weight in homozygous <i>Cdh23</i> ^{m1btlr-/-} mice	80
3.3.4	Decreased survival rates in <i>Cdh23</i> ^{m1btlr-/-} homozygous mice.....	80
3.3.5	Sequencing of <i>Cdh23</i> ^{m1btlr-/-} with Y2207X mutation	81
3.3.6	PCR genotyping of the mice	81
3.3.7	Immunohistochemistry in retinal and cochlear <i>Cdh23</i> ^{m1btlr-/-} tissue sections	82
3.3.8	Ataluren® treatment corrects the abnormal photoreceptor protein translocation.....	84

3.3.9	Photoreceptor synaptic terminal protein expression in <i>Cdh23^{m1bitr/-}</i> retina	86
3.3.10	Ataluren® treatment reverses functional responses.....	87
3.3.11	Transmission electron microscopy analysis of retinal photoreceptors	90
3.3.12	Real-time circling behavioral after Ataluren® treatment	91
3.4	Discussion.....	93
Chapter 4: Nonsense suppression therapy in human iPSC-derived 3D retinal organoids ...		97
4.1	Chapter introduction	97
4.1.1	Specific hypothesis	97
4.1.2	Rationale	98
4.1.3	Experimental design.....	98
4.2	Methods.....	99
4.2.1	Culture, maintenance, and characterization of patient-derived iPSCs.....	99
4.2.2	Differentiation of 3D retinal organoid derived from patient iPSCs.....	100
4.2.3	Quantitative polymerase chain reaction (qPCR).....	101
4.2.4	Western blotting.....	102
4.2.5	Immunohistochemistry	102
4.2.6	Terminal deoxynucleotidyl transferase dUTP nick end labeling (TUNEL).....	103
4.2.7	Statistical analysis.....	104
4.3	Results.....	104
4.3.1	Generation and characterization of iPSCs from patients with <i>CDH23</i> mutations..	104
4.3.2	Generation of 3D retinal organoids for disease modeling	107
4.3.3	Effect of <i>CDH23</i> mutation on photoreceptor protein expression in patient-derived retinal organoids.....	109

4.3.4	Nonsense suppression therapy in retinal organoids	110
4.4	Discussion	115
Chapter 5: Conclusion.....		120
Chapter 6: Future directions		125
Bibliography		128
Appendix A Supplemental data for chapter 1.....		167
A.1	3% TBE Agarose gel preparation	167
A.2	Confirmation of <i>Tgfb2</i> gene in the plasmid pIRES Ds Red 2 vector by restriction digestion analysis.....	168
A.3	Optimization of Electroporation of MSCs at different voltage	169
A.4	START formulation for topical treatment.	169

List of Tables

Table 1.1: Genetic heterogeneity in ocular disease	5
Table 1.2: Genes causing abnormalities of the anterior segment.	9
Table 1.3: Known genes causing 3 types of Usher syndrome	15
Table 3.1: Primers for other null mutations in <i>Cdh23^{m1btlr-/-}</i> Y2207X mouse strain	65
Table 4.1: Test results for characterization of control iPSC line.....	105
Table 4.2: Test results for characterization of <i>CDH23</i> iPSC line.....	105

List of Figures

Figure 1.1: Overview of the eye.	1
Figure 1.2: Anterior segment of the eye.	2
Figure 1.3: Diagrammatic representation of the retina	3
Figure 1.4: Morphogenesis of anterior segment.	7
Figure 1.5: Graphical representation of development of anterior chamber.	8
Figure 1.6: Cartoon image representing normal and Usher syndrome phenotypes.	18
Figure 1.7: Tip link of the stereocilia in the ear	19
Figure 2.1: Overview of the cell-based gene therapy approach.	33
Figure 2.2 : Overview of Ataluren® treatment.	34
Figure 2.3: Ocular anterior segment morphogenesis <i>Pax6</i> ^{Sey/+} mouse eye.	44
Figure 2.4 : Localization of Pax6 and Tgfb2 in the anterior segment.	46
Figure 2.5: Characterization of MSCs from adipose tissue	47
Figure 2.6: Characterization of genetically modified <i>Tgfb2</i> -expressing MSCs	49
Figure 2.7: Efficacy of cell-based delivery compared to nonsense suppression therapy at P21. .	51
Figure 2.8: Protein expression analysis in treated <i>Pax6</i> ^{Sey/+} mutant mouse eye tissue lysates	53
Figure 2.9: Analysis of other proteins in the development of anterior chamber angle.	55
Figure 3.1: Effect of mutation of <i>Aggf1</i> in <i>Cdh23</i> ^{m1btlr/-} Y2207X mouse strain.	70
Figure 3.2: Sequence analysis of <i>Aggf1</i> in <i>Cdh23</i> ^{m1btlr/-} Y2207X mouse strain.	71
Figure 3.3: Effect of mutation of <i>Carmil3</i> in <i>Cdh23</i> ^{m1btlr/-} Y2207X mouse strain.	73
Figure 3.4: Sequence analysis of <i>Carmil3</i> in <i>Cdh23</i> ^{m1btlr/-} Y2207X mouse strain.	74
Figure 3.5: Effect of mutation of <i>Tiprl</i> in <i>Cdh23</i> ^{m1btlr/-} Y2207X mouse strain.	76
Figure 3.6: Sequence analysis of <i>Tiprl</i> in <i>Cdh23</i> ^{m1btlr/-} Y2207X mouse strain.	77

Figure 3.7: Effect of mutation of <i>Txndc16</i> in <i>Cdh23^{m1btlr-/-}</i> Y2207X mouse strain.	79
Figure 3.8: Lifespan of homozygous <i>Cdh23^{m1btlr-/-}</i> mice.	80
Figure 3.9: <i>Cdh23</i> BLAST result for <i>Cdh23^{m1btlr-/-}</i> mice.	81
Figure 3.10: Representative image of genotyping of <i>Cdh23^{m1btlr-/-}</i> mice by restriction digestion analysis:.....	82
Figure 3.11: Immunohistochemical staining of retinal and cochlear sections.	83
Figure 3.12: Light-induced translocation of retinal proteins in wildtype and <i>Cdh23^{m1btlr-/-}</i> mice.	85
Figure 3.13: Synaptic ribbons in the retinal photoreceptors.	87
Figure 3.14: Representative scotopic ERG recordings with Ataluren® Therapy.....	88
Figure 3.15: Representative 30Hz flicker ERG recordings with Ataluren®Therapy.....	89
Figure 3.16: Electronmicrographs of retinal photoreceptors at P120.	91
Figure 3.17: Circling behavior.....	92
Figure 3.18: Finger-like calyceal processes in primate photoreceptors.....	95
Figure 4.1: Pluripotent human iPSCs express pluripotency markers.	106
Figure 4.2: Expression of PAX6 in retinal organoids.....	108
Figure 4.3: Generation of 3D retinal organoids for disease modeling.....	109
Figure 4.4: CDH23 and photoreceptor protein expression in patient-derived retinal organoids.....	110
Figure 4.5: Formation of neuroepithelium in control and <i>CDH23</i> -mutant organoids.....	111
Figure 4.6: Cell death in retinal organoids.....	112
Figure 4.7: The effect of nonsense suppression on photoreceptor protein expression at day 150.	114
Figure 4.8: Transmission electron microscopy of <i>CDH23</i> mutant retinal organoids treated with 10 mg/ml Ataluren®.	115

List of Abbreviations

3D	3-dimensional
AD	Autosomal dominant
adMSCs	Adipose derived mesenchymal stem cells
ANOVA	Analysis of Variance
AR	Autosomal recessive
C-MYC	Cellular Myelocytomatosis
CB	Ciliary body
CC	Connecting cilium
CDH23	Cadherin-23
CMV	Cytomegalovirus
CRISPR	Clustered regularly interspaced short palindromic repeats
Cas9	CRISPR associated protein 9
CTGF	Connective tissue growth factor
DAPI	4', 6-diamidino-2-phenylindole
DMEM	Dulbecco's Modified Eagle Medium
DNA	Deoxy ribonucleic acid
DPBS	Distilled phosphate buffered saline
DsRed2	Discosoma red fluorescent protein
ECM	Extracellular matrix
EDTA	Ethylene diamine tetra acetic acid
EGTA	Ethylene glycol tetraacetic acid
ELISA	Enzyme linked immuno sorbent assay
ERG	Electroretinogram
ES	Embryonic stem cells
Foxc1	Forkhead Box C1
GCL	Ganglion cell layer
hESCs	Human embryonic stem cells
IHC	Inner hair cells
INL	Inner nuclear layer

IOP	intra ocular pressure
IPL	Inner plexiform layer
iPSCs	Induced pluripotent stem cells
IRD	Inherited retinal disease
IRES	Internal ribosome entry site
IS	Inner segment
KLF4	Kruppel-like factor 4
LCA	Leber congenital amaurosis
MET	Mesenchyme epithelial transition
mRNA	Messenger ribonucleic acid
MSCs	Mesenchymal stem cells
NR	Neuro retina
OCT4	Octamer-binding transcription factor 4
OHC	Outer hair cells
OLM	Outer limiting membrane
OMIM	Online Mendelian inheritance in man
ONL	Outer nuclear layer
OPL	Outer plexiform layer
OS	Outer segment
<i>PAX6</i>	Paired box-6 gene
PBMCs	Peripheral blood mononuclear cells
PBST	PBS + 0.1% Tween 20
PC	Pillar cells
PCR	Polymerase chain reaction
PEG	Polyethylene glycol
PFA	Paraformaldehyde
Pitx2	Paired-like homeodomain transcription factor 2
POAG	Primary open angle glaucoma
POM	Periocular Mesenchyme
pre-mRNA	Pre-messenger ribonucleic acid

qPCR	Quantitative polymerase chain reaction
RHO	Rhodopsin
RNA	Ribonucleic acid
RP	Retinitis Pigmentosa
RPE	Retinal pigment epithelium
RT	Room temperature
SOX2	SRY-Box Transcription Factor 2
START	Sodium chloride, Tween 80, powdered Ataluren, caRboxy meThyl cellulose
TUNEL	Terminal deoxynucleotidyl transferase dUTP nick end labeling
Tgf β 2	Transforming growth factor beta 2
TM	Trabecular meshwork
USH1D	Usher syndrome 1D
WAGR	Wilms tumor, aniridia, genitourinary malformations, and mental retardation syndrome

Acknowledgements

I would like to convey my sincere and heartfelt gratitude to my Supervisor Prof. Cheryl Gregory-Evans, who was with me throughout my graduate journey. She was such a great mentor who was always there for her graduate students. I sincerely thank her for her continuous support, guidance and encouragement throughout my graduate study.

I would also take this moment to appreciate and thank my committee members Dr. Elizabeth Simpson, Dr. Orson Mortiz, and Dr. Fabio Rossi and for their valuable suggestions and guidance throughout my PhD journey.

I would like to thank our lab collaborator Prof. Kevin Gregory-Evans and my lab members Ms. Xianghong Shan (Lab manager), Dr. Xia Wang (PDF), Dr. Anat Yanai (Research Associate), Dr. Ishaq A. Viringipurampeer (Research Associate), Mr. Naif Sannan (graduate student), Dr. Emran Basher (graduate student), Ms. Jess Morrice (graduate student) and Ms. Aisha Soliman (graduate student), for their time and suggestions during my graduate study.

I would like to thank members of UBC Bio-imaging facility Garnet, Derrick and Brad for providing guidance and help for my electron microscopy studies.

I sincerely acknowledge the family of Usher patients, who provided blood samples and their generous donation to carry out project. Without them I could not have performed the study in Usher Syndrome type 1D.

I would like to acknowledge Sharon Stewart trust, CIHR Transplantation Training program and Foundation Fighting blindness (FFB) for their financial support for this research.

Last, but not least, I would like to thank my family, friends and my well-wisher Dr. Jyothi Jayaraman, who gave unconditional love and support throughout my PhD journey.

Dedication

To my wonderful parents (*Nizamudheen & Shakeela*) and my husband (*Ishaq*) and my lovely girls
(*Inaaya & Aisha*)

Chapter 1: Introduction

1.1 Overview of the eye

The eye is a spherical fluid filled structure which helps to process and visualize the surrounding world. It consists of 3 different layers; the outer fibrous layer consisting of the cornea and sclera, an inner layer containing mainly retina, iris and part of ciliary body, and the vascular layer comprised of the uvea and choroid (Fig. 1.1). It can also be subdivided into two segments, anterior and posterior. The anterior segment of the eye consists of anterior chamber, the cornea, iris, ciliary body, and lens. The posterior segment of the eye includes choroid, retina, fovea, vitreous chamber, sclera and optic nerve. Vision is the process of light passing through cornea, pupil, and ocular lens. The light is refracted by the lens and passes through the vitreous and reaches the retina, before being converted into electrical signals, that pass through the optic nerve, which is then interpreted by the brain.

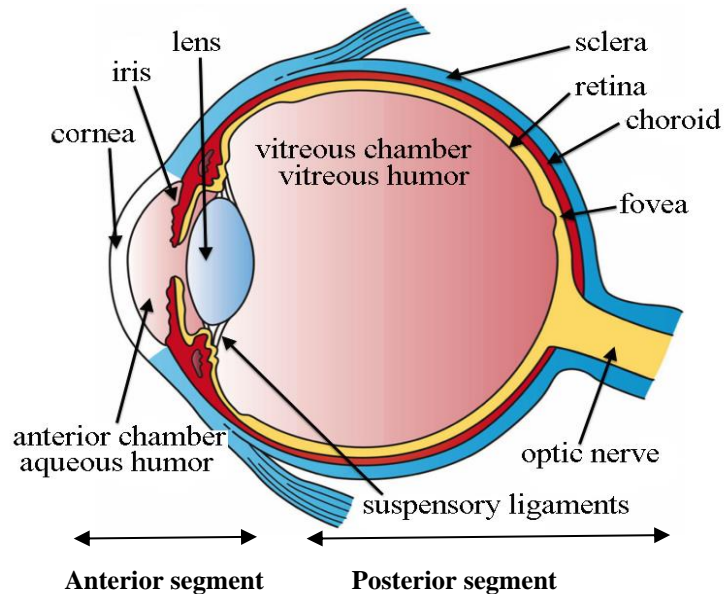


Figure 1.1: Overview of the eye.

Cross section image of eye showing the anterior segment and posterior segment structures. Adopted and modified from "File: Three Main Layers of the Eye.png" by Artwork by Holly Fischer that is licensed under CC BY 3.0.

1.2 The anterior segment of the eye

The anterior segment of the eye consists of an outer layer of conjunctiva which covers the sclera and extends over the transparent cornea of the eye, ciliary body, lens, iris, and drainage structures such as Schlemm's canal and trabecular meshwork. The light is refracted through the iris and passes through the pupil and reaches the retina where the image is processed. The ciliary body (CB) is the structure which produces the aqueous humor and additionally holds the lens in position by zonules contained within the suspensory ligaments. The aqueous humor produced by the ciliary body passes through the narrow space between the iris and lens circulates and filters through the trabecular meshwork, and finally drains into the Schlemm's canal (Fig. 1.2). The aqueous humor provides nutrients to the cornea, lens, and eliminates the metabolic waste and drains into Schlemm's canal. Any obstruction in the drainage of aqueous humor may increase the intraocular pressure of the eye leading to glaucoma and eventually to loss of vision if untreated.

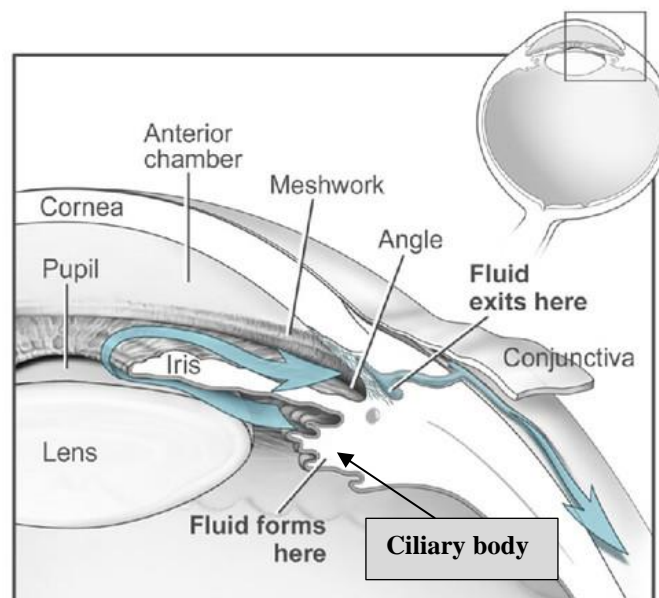


Figure 1.2: Anterior segment of the eye.

Sagittal section of the anterior segment of the eye adapted and modified "Drawing of the Eye" by National Eye Institute is licensed under CC BY 2.0.

1.3 The retina

The retina is a thin light sensitive tissue located in the posterior part of the eye. The retina is divided into two parts, the retinal pigment epithelium (RPE) and the neurosensory retina. The neurosensory retina consists of neuronal cells types including photoreceptors, secondary order neurons (bipolar cells, horizontal cells and amacrine cells) and retinal ganglion cells (Fig. 1.3).

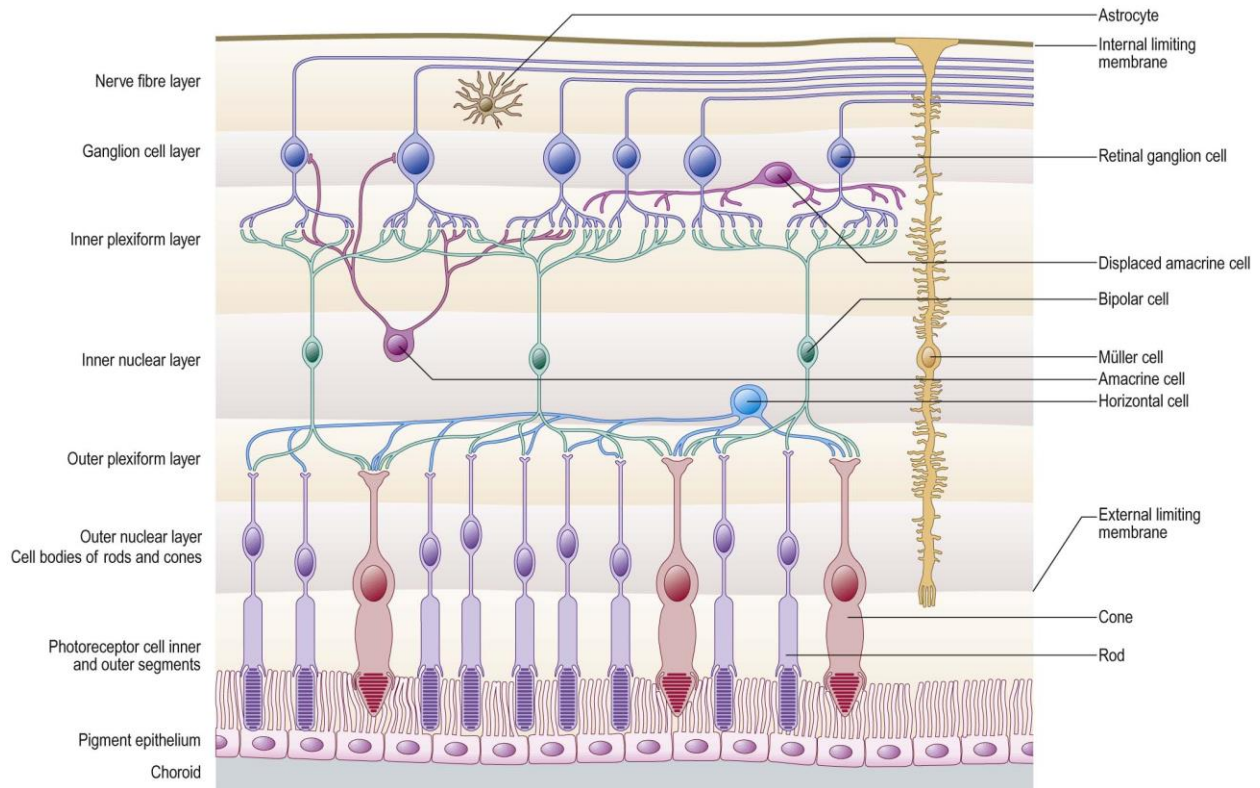


Figure 1.3: Diagrammatic representation of the retina

Image adapted from the book Grays Anatomy by Juan C Fernandez-Miranda 2016 with permission from the Elsevier books License # 485197017155.

These cells are arranged in specific layers consisting of a photoreceptor layer with rod and cone photoreceptors; the outer nuclear layer (ONL) containing the photoreceptors nuclei; the outer plexiform layer (OPL) where photoreceptors synapse with secondary order neurons; the inner nuclear layer (INL) where bipolar, horizontal and amacrine cells nuclei are located; the inner

plexiform layer (IPL) containing the axons of the secondary order neurons that synapse with retinal ganglion cells; the ganglion cell layer (GCL) consisting of nuclei of the ganglion cells; and the nerve fiber layer (NFL) which directs the ganglion cell axons to the optic nerve.

1.4 Genetics of ocular diseases

Genetic ocular disease is one of the leading causes of vision loss or impaired vision. There are several genetic eye disorders such as retinitis pigmentosa, Stargardt disease, Aniridia, retinitis pigmentosa, hereditary optic neuropathy, pediatric cataract, pediatric glaucoma, and Usher syndrome. Currently, about 100,000 people in the United States, and over a million people globally, are losing their vision from progressive retinal dystrophies, caused by genetic defects (Frick, Roebuck, Feldstein, McCarty, & Grover, 2012). Inherited ocular diseases are both genetically and clinically heterogeneous making this group of disorders a significant health concern. Although, substantial advances have been made in understanding the pathophysiology and molecular basis of these diseases, only a handful of treatments are available.

A genetic disease is a condition that is directly transmitted from a parent to their offspring's through the genetic information present in the genes (MacDonald & Mah, 2000; Mathebula, 2012; Young, 2003). Mutations in a gene can be inherited in an autosomal recessive, autosomal dominant, X-linked or sex linked and mitochondrial fashion. Some genes are expressed during ocular development which can cause malformation defects at birth (e.g., *PAX6* mutations causing aniridia), whereas other genes code for structural components of the retina and cause childhood or adult-onset diseases (e.g. *RHO* mutations causing retinitis pigmentosa). Some examples of inherited ocular disease genes are listed in Table 1.1, where some genes cause multiple different phenotypes that contribute to the complexity of understanding the mechanisms of disease.

Furthermore, in some genes like Rhodopsin there are over 100 different mutations in the gene that cause the same phenotype (RetNet: <https://sph.uth.edu/retnet>).

Inherited Ocular Disease	Inheritance pattern	Some of the genes involved
Aniridia	Autosomal dominant	<i>PAX6</i>
Cone-rod dystrophy	Autosomal dominant	<i>CRX, GUCY2D, GUCA1A,</i>
Cone-rod dystrophy	Autosomal recessive	<i>ABCA4, AIPL1, SEMA4A, RIMS1, RPGRIP1, ADAM9</i>
Juvenile retinoschisis	X-Linked	<i>RS1</i>
Leber congenital amaurosis	Autosomal recessive	<i>AIPL1, CRB1, CRX, RDH12, RPE65, CNGA3, RPGRIP1</i>
Leber optic neuropathy	Mitochondrial	<i>MT-CYB, MT-ND2, MT-ND4L, MT-TA, MT-CO3, MT-ATP6</i>
Peters anomaly	Autosomal dominant/recessive	<i>FOXC1, PAX6, PITX2, CYP1B1</i>
Retinitis pigmentosa	Autosomal dominant	<i>RHO, RPI, IMPDH1, PRPF3, PRPF31, PRPF4, CA4, NR2E3</i>
Retinitis pigmentosa	Autosomal recessive	<i>ABCA4, CNGB1, FAM161A, MERTK, PDE6A, PDE6B, PDE6G, RBP3, RPI</i>
Retinitis pigmentosa	X-linked	<i>RP2, RPGR</i>
Stargardt disease	Autosomal dominant	<i>ELOVL4</i>
Stargardt disease	Autosomal recessive	<i>ABCA4</i>
Retinoblastoma	Autosomal recessive	<i>RB1</i>
Usher syndrome	Autosomal recessive	<i>MYO7A, USH1C, CDH23, PCDH15, SANS, CIB2, ESPN, USH2A, GPR98, WHRN, CLRN1, HARS1, PDZD7</i>

Table 1.1: Genetic heterogeneity in ocular disease
Genes in bold cause multiple phenotypes

1.4.1 Development of anterior chamber angle of the eye

Neural crest cells are very important for the development of the anterior chamber of the eye. Anterior chamber originates from the neural fold of the neural ectoderm. As part of the normal neurulation process, the neural folds converge along the midline forming the neural tube. The neural crest cells at the convergence point undergo an epithelial to mesenchymal transition and then migrate ventrally from the neural tube to the periphery (Kalcheim, 2015), where they differentiate into various cell lineages contributing to proper eye morphogenesis. The neural crest-derived mesenchymal cells envelop the developing optic cup (Fig. 1.4.a). The outer surface ectoderm of the optic cup forms the lens, corneal epithelium and conjunctiva. The ciliary body epithelium, corneal endothelium, sclera, ciliary muscles, and endothelium lining of anterior chamber are formed from the neural crest-derived mesenchymal cells. The peripheral retina is derived from inner layer of neuroectoderm and RPE is developed from the outer layer of neuroectoderm (Ken & Sowden, 2016). After the separation of the lens vesicle, the surface ectoderm develops the corneal epithelium of the eye. (Fig. 1.4.b) (Sowden, 2007). Between the 5th and 6th month of gestation in humans the anterior chamber structures are well developed and aqueous humor production and outflow begins to function. The anterior segment structures which are derived from mesenchymal origin including the iris, trabecular meshwork and Schlemm's canal (Baulmann et al. 2002) (Fig. 1.4 c). Genes including *PITX1*, *FOXC1* and *PAX6* are involved in the development of anterior chamber structures (Gould, Smith, & John, 2004). Absence of these genes or even a small variation in the expression of this protein can affect the anterior chamber morphogenesis.

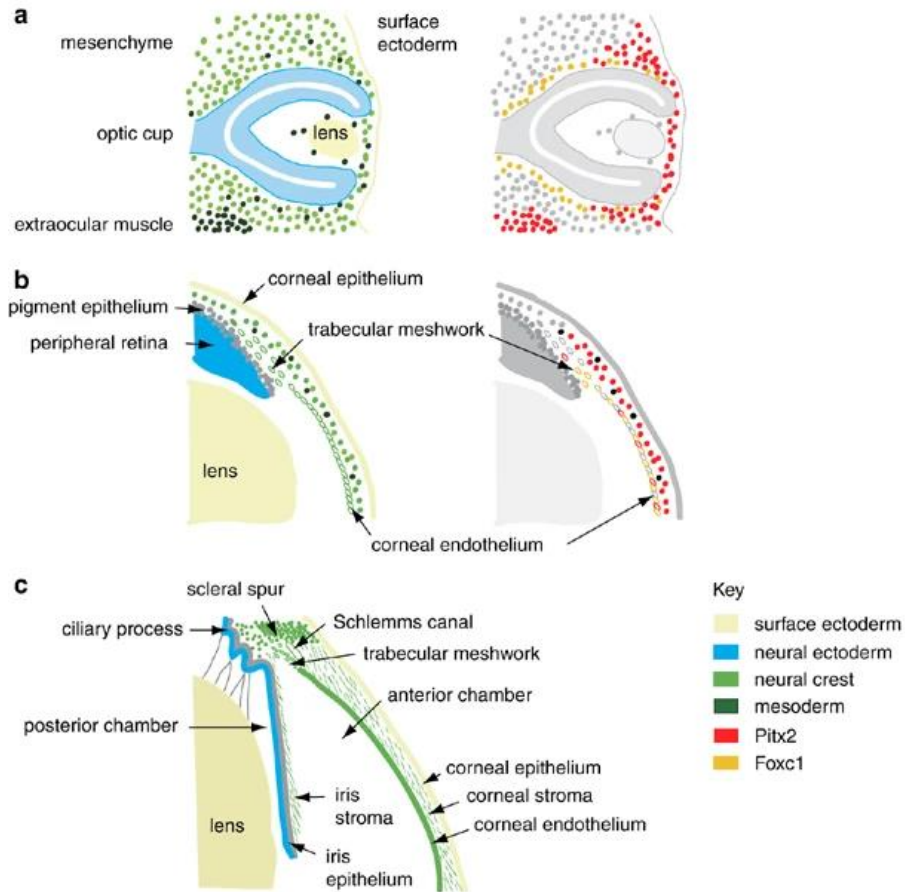


Figure 1.4: Morphogenesis of anterior segment.

Image adapted from (Sowden, 2007) with permission from Springer nature license # 4856040702240.

In mice the morphogenesis of anterior chamber structures occurs postnatally from postnatal day P4 to P21 and mature completely by P45. Around P1-P4, a mass of mesenchymal cells migrates towards the chamber angle (arrows in Fig 1.5 A). From P4-P10, the extracellular fibers fill the spaces between the chamber angle cells (solid arrows), while the scleral vesicles appear in the immediate adjacent sclera (open arrows) (Fig: 1.5 B). From P11-P14, the extracellular fibers integrate themselves with the trabecular meshwork cells to form trabecular beams (arrows in Fig. 1.5 C), further the scleral vessels which are present near to the chamber angle merge to form Schlemm's canal (open arrow in Fig 1.5 C). The outer surface margin of the anterior chamber

moves posteriorly, and the inner surface margin of the trabecular meshwork becomes exhibited to the anterior chamber (Cvekl & Tamm, 2004).

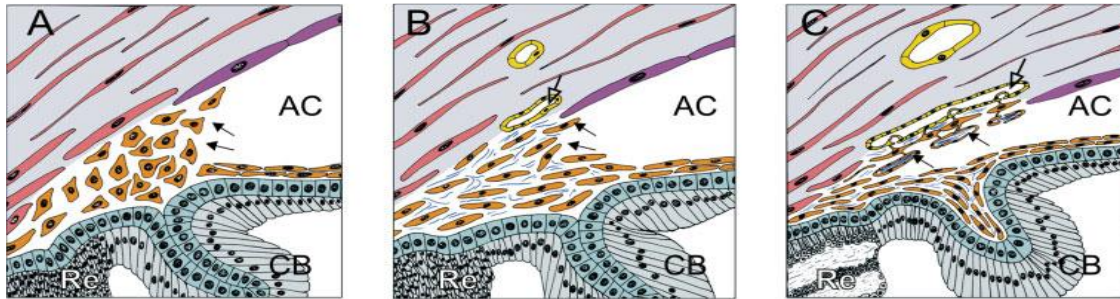


Figure 1.5: Graphical representation of development of anterior chamber.

Image adopted from the (Ernst R. Tamm, Aleš Cvekl 2004) with permission from John Wiley and Sons (license # 4856241239279). Re,retina; CB,ciliary body; AC,anterior chamber.

1.4.2 Congenital human eye disorders with anterior chamber abnormalities

The anterior chamber angle of the eye is a complex array of interacting tissues are very important for the normal eyesight. The cornea, iris tissue, and the outermost epithelium of the lens form the edges of the anterior chamber angle also known as irideocorneal angle (Ken & Sowden, 2016). The development of the anterior segment of the eye depends on several transcription factors during early embryonic development. These “master control” genes are either activate or suppress the expression of direct downstream target genes. Errors in the homeobox genes of transcription factor causes genetic ocular conditions like corneal opacity, congenital glaucoma and anterior segment dysgenesis (ASD) (Robert & Colby, 2017). Table 1.2 lists some of the genes which causes anterior segment abnormalities.

OMIM number	Gene name	Chromosome location	Inheritance	Type of protein	Disease
601771	<i>CYP1B1</i>	2p22	AD	TF	Congenital glaucoma
601090	<i>FOXC1</i>	6p25	AD	TF	Axenfeld-Rieger syndrome
602091	<i>LTBP2</i>	14q24	AR	Latent TGF- β binding protein	Congenital glaucoma
601542	<i>PITX2</i>	4q25	AD	TF	Peters anomaly, iris hypoplasia
106210	<i>PAX6</i>	11p13	AD	TF	Aniridia
112262	<i>BMP4</i>	14q22-q23	AD	Regulatory molecule	ASD with microphthalmia, or with/without anophthalmia
602575	<i>LMX1B</i>	9q34	AD	TF	Nail-patella syndrome
601094	<i>FOXE3</i>	1p23	AR	TF	Axenfeld syndrome, Peters anomaly

Table 1.2: Genes causing abnormalities of the anterior segment.

AD, autosomal dominant; AR autosomal recessive; TF, transcription factor; ASD, anterior segment dysgenesis.

Table adapted and modified from (Summers, Withers, Gole, Piras, & Taylor, 2008) with licensed under Creative Commons Attribution license.

1.4.2.1 Importance of the *PAX6* gene in early ocular morphogenesis

PAX6 is expressed from the early embryonic stage of ocular development and is often referred to as the “master control” gene in the eye (Gehring, W. J. & Ikeo, 1999; Gehring, Walter J., 2002). *PAX6*, a member of the paired box gene family, regulates transcription of several genes that are involved in the development of the eye and other tissues such as like pancreas, brain, spinal cord and that also have a maintenance function in adult tissues (Simpson & Price, 2002). The *PAX6* gene is highly conserved and expressed in both vertebrates and invertebrates (Altmann, Chow, Lang, & Hemmati-Brivanlou, 1997; Glaser et al., 1994; Mishra, Gorlov, Chao, Singh, & Saunders,

2002). The anterior surface ectoderm and neuroectoderm of the optic cup continuously express *PAX6* throughout the morphogenesis of eye (Ma, Grigg, & Jamieson, 2019). The master regulator *PAX6* is expressed in the evolving lens, pigmented layers of the iris and ciliary body, in the cornea, and during the development of retina (van Heyningen & Williamson, 2002). Furthermore, in the mouse *Pax6* is also expressed postnatally in the mesenchymal derived developing trabecular meshwork cells (Cvekl, Aleš & Tamm, 2004). Lens epithelium cells express *Pax6* which is involved in the anterior chamber morphogenesis and in maintaining retinal organization and corneal cells arrangement (Ashery-Padan, Marquardt, Zhou, & Gruss, 2000; Collinson, Quinn, Hill, & West, 2003). *Pax6* regulates the expression of several downstream targets, including cell signaling molecules, transcription factors and structural proteins (Collinson, Hill, & West, 2000; Cvekl, Ales & Callaerts, 2017; Hanson, Isabel & Van Heyningen, 1995; Liu, W., Lagutin, Mende, Streit, & Oliver, 2006; Machon et al., 2010; Wolf et al., 2009a).

Human *PAX6* covers about ~28 kb of genomic DNA comprising 14 exons and it contains three different promoters (P0, P1, P α), thus, its able to produce different splice variants including full length *PAX6* and the *PAX6-5a*. To date, over 500 pathogenic mutations have been identified and were deposited in the ClinVar database, the Exome Aggregation Consortium (ExAC) and the Human *PAX6* allelic variant database (http://lsdb.hgu.mrc.ac.uk/home.php?select_db=PAX6). Mutation in *PAX6* causes a panocular condition of eye known as Aniridia syndrome (OMIM 106210). It is an autosomal dominant condition affecting the developing cornea, iris and retina of the eye. Aniridia patients present with some, but not necessarily all the following ocular symptoms: nystagmus, corneal pannus, refractive error, dry eye, foveal hypoplasia, iris hypoplasia, and strabismus (Netland, Scott, Boyle, & Lauderdale, 2011). About 50-70% young or early adolescent aniridic patients develop increased intraocular pressure (IOP) that damages the optic nerve leading

to glaucoma (Brauner, Walton, & Chen, 2008; Kroeber et al., 2010a; Lee, Khan, & O’Keefe, 2008). In addition, some patients also exhibit systemic features including obesity, loss of olfaction, hearing problems and cognitive abnormalities (Grant, M. K., Bobilev, Pierce, DeWitte, & Lauderdale, 2017; Sisodiya et al., 2001).

In most cases, aniridia occurs due to the functional loss of one copy of the *PAX6* gene, a condition known as haploinsufficiency (Hanson, I. M. et al., 1994). About 50% of *PAX6* mutations are nonsense mutations causing premature termination codons, about 25% are missense mutations causing a less severe form of aniridia and about 15% of cases are due to chromosomal deletions or rearrangements (Hingorani, Hanson, & van Heyningen, 2012). In a subset of patients (less than 10%) abnormalities have been identified in the genomic region downstream of *PAX6* that controls its expression (Fantes et al., 1995; Hingorani et al., 2012; Lauderdale, Wilensky, Oliver, Walton, & Glaser, 2000). Ultra-rare homozygous *PAX6* mutations result in anophthalmia and brain malformations that are incompatible with life (Glaser et al., 1994; Hodgson & Saunders, 1980).

Similar, but often more severe, ocular phenotypes are also seen in mice with *Pax6* mutations. Mice with heterozygous mutations of the *Pax6* gene exhibit microphthalmia, absence of the anterior chamber, corneal keratopathy, abnormal folding of the retina and cataracts (Chang et al., 2001; Hill, 1991; Kaufman, Chang, & Shaw, 1995). Defects in the iridocorneal angle of the eye such as failed morphogenesis of the trabecular meshwork and Schlemm’s canal (Kroeber et al., 2010b), surrounded by fragments of iris tissue, blocks the outflow of aqueous humor and leads to an rise in the intraocular pressure (IOP) of the eye (Hanson et al., 1994). In the *Pax6* homozygous state there are eye and brain abnormalities, as well as the inability to suck milk due to failure of palate closure that results in perinatal lethality (Grindley, Hargett, Hill, Ross, & Hogan, 1997; Kaufman, Chang, & Shaw, 1995).

1.4.2.2 Role of *Tgfb2* in the anterior chamber angle of the eye

Tgfb isoforms are expressed by various tissues and involved in early embryonic development (Akhurst, FitzPatrick, Gatherer, Lehnert, & Millan, 1990; Saika, Shizuya, 2006). One of these isoforms, Transforming growth factor- β 2(Tgfb2), is a dimeric polypeptide growth factor which is under the direct control of Pax6 (Saika, S. et al., 2001; Wolf et al., 2009b). Pax6 expression from lens epithelium regulates the expression of Tgfb2 in the ciliary body, iridocorneal angle, corneal cells and it is even involved in regulating the formation of retinal architecture (Kroeber et al., 2010). Tgfb2 regulates the proliferation and production of extracellular matrix (ECM) in the developing trabecular meshwork and is involved in the proper differentiation of anterior chamber angle in the developing eye (Kroeber et al., 2010a). Studies in *Tgfb2*^{-/-} null mice exhibited a smaller number of keratocytes and had thin corneal stroma with less ECM components. Histological analysis demonstrated fusion of the lens to the cornea (Peters' anomaly), and a failure of corneal endothelium formation. Yet, these mice differentiated normal corneal epithelium (Saika et al., 2001). In contrast, other Tgfb isoform knockouts do not have any ocular phenotype, presumably because they are not regulated by Pax6, but exhibit lymphocytic inflammatory disease and cleft palate (Proetzel et al., 1995; Saika et al., 2001).

1.4.2.3 Experimental model: *Pax6*^{Sey/+} mouse model of aniridia

The *Pax6*^{Sey/+} mouse model of aniridia has a nonsense mutation located in the coding region exon 7 of the gene, changing the amino acid glycine (GGA) to a stop codon (UGA). This could potentially result in the formation of non-functional truncated protein with 193 amino acids instead of the functional full-length protein with 423 amino acids. However, due to nonsense-mediated decay it is more likely to result in a loss-of-function allele. The heterozygous *Pax6*^{lacZ/+} mutant

mouse model exhibits a small eye, iris hypoplasia, iridocorneal adhesion and abnormal chamber angle differentiation leading to increase in IOP and develop aniridic glaucoma (Baulmann et al. 2002) similar to the *Pax6*^{Sev/+} phenotype. However, in the *Pax6*^{Sev/+} model, there is also under development of anterior chamber structures and at later stages, corneal opacification, and cataracts (Brigid L. M. Hogan, Elizabeth M. A. Hirst, Horsburgh, & Hetherington, 1988; Kroeber et al., 2010a) making this model more suitable for studying new therapeutic approaches for the aniridic glaucoma.

1.4.2.4 Current treatments

Aniridic patients usually develop glaucoma in late childhood or young adulthood, as progressive anatomical changes occur in the anterior chamber angle. The anterior chamber angle may be underdeveloped independent of whether Schlemm's canal is absent or present. The initial treatment of glaucoma associated with anir. Laser treatment such as Argon laser trabeculoplasty is also performed for patients with aniridic glaucoma. Surgical procedures including goniotomy (Swanner, Walton, & Chen, 2004), trabeculectomy (Adachi et al., 1997; Almousa, Almousa, Lake, & Lake, 2014) and cyclodestructive procedures (Dastiridou et al., 2018) are performed to reduce the severity of the disease in Aniridic glaucoma patients. Furthermore, using glaucoma drainage devices such as a tube shunt or molteno implant surgeries (Arroyave, Scott, Gedde, Parrish, & Feuer, 2003) can be performed to reduce the IOP in the eye. These surgeries are reported to have an approximate 80% of success compared to other surgical procedures. However, these above-mentioned treatment procedures always cause higher rates of associated complications, including cataract formation and often result in further surgical intervention. This is because the aniridic eye is particularly sensitive to trauma associated with surgery which can lead to aniridia fibrosis

syndrome (Tsai et al., 2005) and loss of the eye if the fibrotic membranes are not removed. Therefore, newer treatments that do not involve surgery would be of great benefit to aniridia patients.

1.4.3 Usher syndrome

Usher syndrome is an autosomal recessive disorder causing retinitis pigmentosa (RP) and high frequency sensorineural hearing loss, resulting from abnormalities in the inner ear (Jm et al., 2011; Yan & Liu, 2010). Vision loss is progressive and begins from early childhood. Usher syndrome (USH) is genetically heterogeneous (Whatley et al., 2020) and is the leading genetic cause of combined hearing and vision loss. Around 4 to 17 in 100,000 people are affected by Usher syndrome (Boughman, Vernon, & Shaver, 1983; Kimberling et al., 2010).

1.4.3.1 Symptoms and pathophysiology

Usher syndrome is classified into 3 types based on the severity of the disease including vision loss, vestibular dysfunction, and deafness. USH1 is the most common and severe form of disease where patients experience profound hearing loss and absence of vestibular function, while those affected with Usher syndrome type 2 (USH2) have congenital deafness which is moderate to severe and normal vestibular function. Usher syndrome type 3 (USH3) is more variable in its onset, and manifestations and vestibular functions can range from normal to absent. Thus far, 12 genes have been identified causing USH and each type of USH has been associated with mutations in a specific set of genes (Table 1.3). The USH genes encode structurally and functionally distinct proteins that form bundles in the inner ear and retina that are essential for hearing ability and eyesight (Moosajee, Maria Toms, Waheeda Pagarkar, Mariya, 2020).

1.4.3.2 USH1D - mutation in *CDH23*

Mutation in the *CDH23* (cadherin 23) gene is the second most common form of USH1 after *MYO7A*. About 150 mutations have been identified in the *CDH23* causing USH1D (Azaiez et al., 2018). Mutations in *CDH23* are also found in the patients with non-syndromic deafness (DFNB12) (Schultz et al., 2011; Wagatsuma et al., 2007).

USH type	Locus/ OMIM number	Map Position	Gene name	Protein	Predicted function
USH1	USH1B/276900	11q13.5	<i>MYO7A</i>	Myosin VIIa	Actin-based motor protein
	USH1C/605242	11p15.1	<i>USH1C</i>	Harmonin	PDZ scaffold protein
	USH1D/601067	10q22.1	<i>CDH23</i>	Cadherin 23	Cell adhesion
	USH1F/602083	10q21-q22	<i>PCDH15</i>	Protocadherin15	Cell adhesion
	USH1G/607696	17q24-q25	<i>SANS</i>	SANS	Scaffold protein
	USH1J/614869	15q25.1	<i>CIB2</i>	CIB2	Ca ²⁺ and integrin binding
USH2	USH2A/608400	1q41	<i>USH2A</i>	Usherin	Cell adhesion
	USH2C/605472	5q14.3-q21.3	<i>GPR98</i>	VLGR1	G-protein coupled receptor
	USH2D/611383	9q32	<i>DFNB31</i>	Whirlin	PDZ scaffold protein
USH3	USH3A/276902	3q21-q25	<i>CLRN1</i>	Clarin-1	Auxiliary subunit of ion channels
	USH3B/614504	5q31.3	<i>HARS</i>	Histidyl-tRNA synthetase	Plays a role in axon guidance
	Digenic USH	10q24.31	<i>PDZD7</i>	PDZD7	PDZ scaffold protein

Table 1.3: Known genes causing 3 types of Usher syndrome

Image adapted and modified from (French, Mellough, Chen, & Carvalho, 2020) with licensed under CC BY 4.0.

However, only missense mutations in *CDH23* cause DFNB12, whereas in *USH1D* the most severe phenotype was detected in patients with null mutations more than other types of mutation.

Cadherins belong to large protein family, which contain extracellular calcium-binding domains and are involved in intercellular adhesion. *CDH23* has 69 coding exons spanning more than 300 kb of genomic sequence and the protein sequence has 3,354 amino acids and 27 extracellular cadherin repeats (Bolz et al., 2001).

1.4.3.3 Role of *Cdh23* in the retina and cochlea

In photoreceptors cells, Usher proteins forms a unique complex bundle which are involved in the process of vesicle trafficking near the synaptic region of photoreceptor. In addition, Usher proteins are also involved in the protein trafficking between inner and outer segment of the photoreceptors and important for synapses (Cosgrove & Zallocchi, 2014). The shaker mouse model (*sh-1*) for Usher1B, myosin7a plays an important role for opsin protein trafficking from inner to outer segment of the photoreceptors.(Holme & Steel, 2002; Lopes et al., 2011). Studies have demonstrated that both Usher proteins (*USH1* and *USH2*) interact in the ciliary/periciliary region and basal bodies close to connecting cilium of the photoreceptors and even localized in the synaptic region of the photoreceptors (Cosgrove & Zallocchi, 2014)(Fig. 1.6). Studies from Usher syndrome patients revealed Usher proteins *CDH23* and harmonin forms a complex in the photoreceptor layer of the retina (Siemens et al., 2002). In photoreceptors, the proteins including usherin, *VLGR1*, and *Sans*, are closely related to the periciliary ridge complex, where Golgi vesicles are involved in the transport of rhodopsin during phototransduction cascade (Kremer, van Wijk, Märker, Wolfrum, & Roepman, 2006; Papermaster, 2002). Other *USH1* proteins are confined to various photoreceptor regions like, the outer segment, connecting cilium, inner

segment, and synapse (Mathur & Yang, 2015). Different research groups report different findings regarding the localization of usher proteins in retina. Studies from immunofluorescence and scanning electron microscopy suggest that the calyceal processes present in frog and monkey cone photoreceptors, are laden with Usher type 1 proteins, (Sahly et al., 2012) while in mouse cone photoreceptors, calyceal processes were absent and Usher type I proteins are localized differently in photoreceptors (Cosgrove & Zallocchi, 2014). In *Xenopus tropicalis* Cdh23 is localized to the photoreceptors in the retina (Schietroma et al., 2017) in the region of the connecting cilium at the junction between inner and outer segments as well as within the calyceal processes of the cone photoreceptors in primates (Cosgrove & Zallocchi, 2014; Oshima et al., 2008).

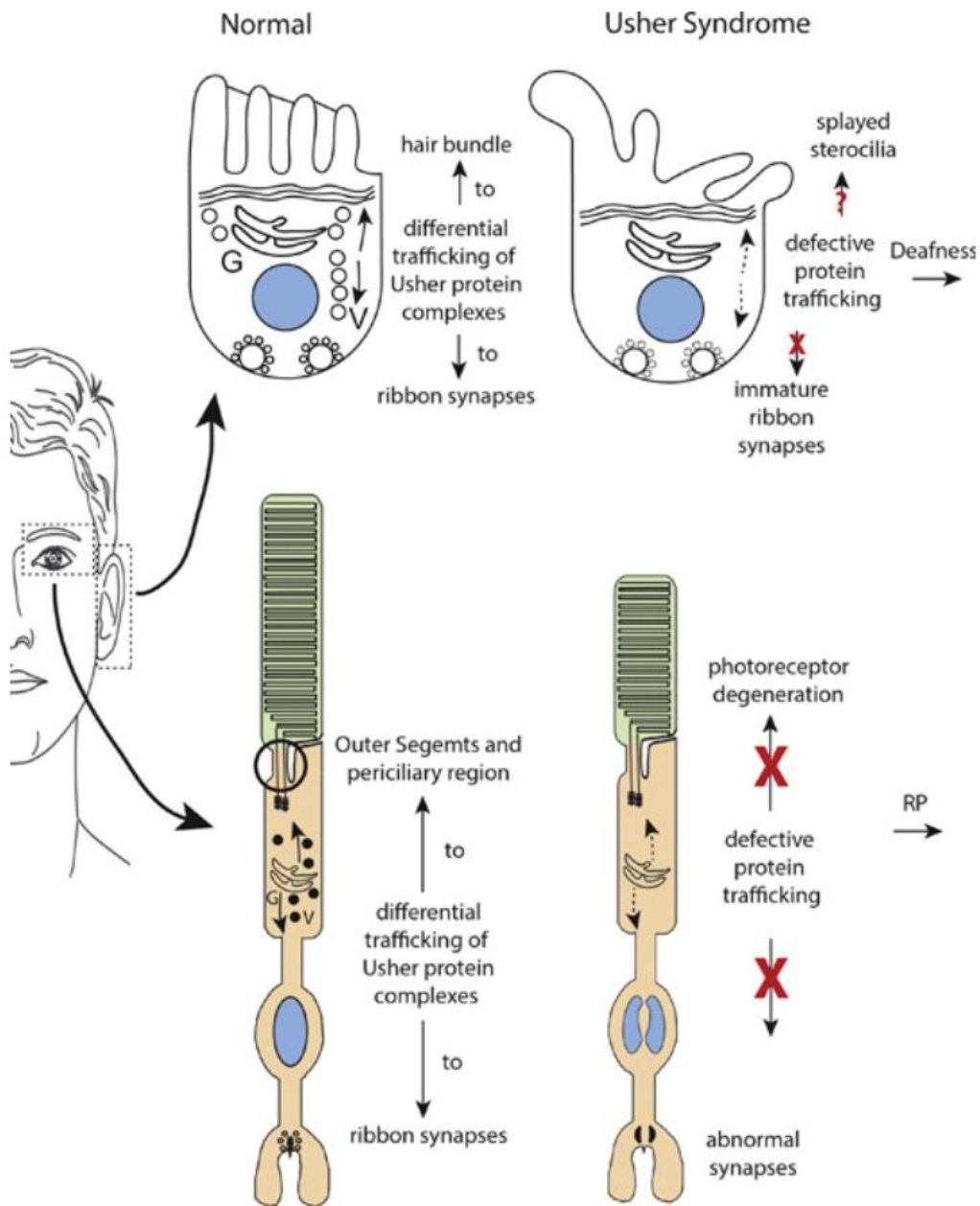


Figure 1.6: Cartoon image representing normal and Usher syndrome phenotypes.
 Image adapted from (Dominic Cosgrove, Marisa Zallochi, 2014) with permission from the Elsevier License # 4858321091656.

Mechanotransduction is the process of conversion of a mechanical stimulus into an electrical signal, which is important for hearing ability and to maintain vestibular balance. Usher proteins are critical in stereocilia development in cochlear hair cells and help to maintain the

connections within the hair bundles (Fig. 1.6) (Cosgrove & Zallochi, 2014). Recent studies suggest that cadherin 23 (CDH23) and protocadherin (PCDH15) are involved in the formation of extracellular filaments of the hair cell bundles by connecting the stereocilia and kinocilium of the hair cell (Fig. 1.7) (U, 2008). These filaments of the tip link of hair cells are involved in the process of mechanotransduction. In auditory inner hair cells, complexes of Usher protein involved in the trafficking of ribbon synapses. Recent studies have been demonstrated that the Usher mutants involved in synaptic dysfunction of both photoreceptors and inner hair cells (Cosgrove & Zallochi, 2014). CDH23 is a structural protein involved in the stereocilia organization in the tip link of hair cells and directly binds to other usher proteins including protocadherin15, harmonin and Myo7A (Adato et al., 2005; Kremer, van Wijk, Märker, Wolfrum, & Roepman, 2006).

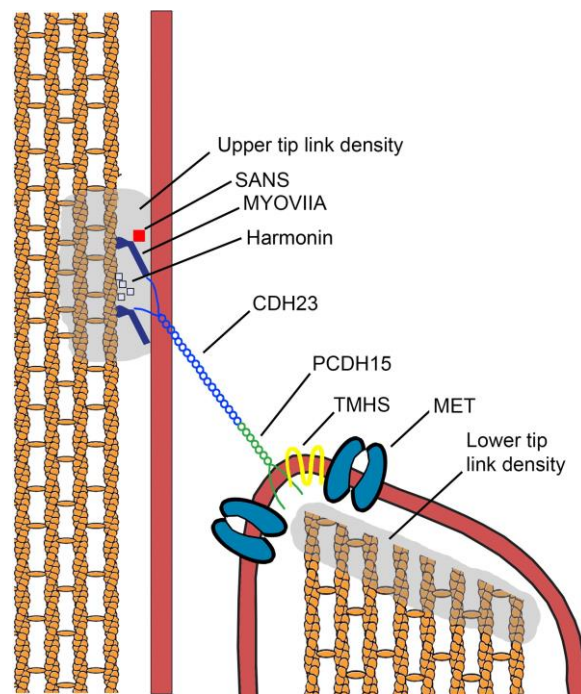


Figure 1.7: Tiplink of the stereocilia in the ear

Image adapted from (Dominic Cosgrove, Marisa Zallochi ,2014) with permission from the Elsevier License #4858370346116.

1.4.3.4 Experimental model: *Cdh23*^{m1btlr-/-} mouse model of USH1D syndrome

To investigate the role of *Cdh23* which is involved in USH1D syndrome, we obtained a *Cdh23* mutant mouse model from Mutagenetix (Beautler lab, UT Southwestern Medical Center, Texas, USA) which was available as a heterozygous frozen sperm allele: *Cdh23*^{m1btlr+/-} with a Y2209X mutation. This nonsense mutation is in the cadherin repeat region of the protein which would either produce truncated protein or no protein due to nonsense-mediated decay. In the homozygous state we would expect the mouse to exhibit circling behavior, but whether a retinal phenotype would be observed is unknown.

1.4.3.5 Current treatments

Currently there is no cure for progressive RP causing vision loss in the Usher syndrome patients. For hearing loss, patients are treated with the use of hearing aids and cochlear implantation. Current knowledge of USH genes in the photoreceptor of retina and vestibular system is very limited. Therapeutic approaches, such as viral-mediated gene replacement, Antisense therapy, translational read-through chemical drugs and genome editing, have been actively explored (Goldmann, T., Overlack, Wolfrum, & Nagel-Wolfrum, 2011; Huang et al., 2017; Kay, Glorioso, & Naldini, 2001; Khan, 2019; Overlack, Goldmann, Wolfrum, & Nagel-Wolfrum, 2012; Samanta et al., 2019), while therapeutic research using various types of stem cells is relatively stagnant for Usher syndrome treatment. Gene replacement of full-length human myosin VIIA by lentiviral vector-based therapy has been shown to rescue melanosome migration and opsin-mislocalization in a *MYO7A*-null mice model for USH1B (Hashimoto et al., 2007). In another study, the efficacy of Ataluren was analysed in both transiently transfected USH2A^{G3142*} HEK293T cells and in patient-derived fibroblasts, which restored USH2A protein

expression (Samanta et al., 2019). Thus potentially, nonsense suppression therapy could work *in vivo* in USH models.

1.4.4 Nonsense-mediated mRNA decay (NMD)

NMD is a cellular surveillance mechanism and quality control process that is present in all eukaryotes from yeast to mammalian cells (Hug, Longman, & Cáceres, 2016). NMD is important during embryonic development to remove any unwanted mRNA in cells and is directly involved in human genetic diseases caused by nonsense mutations. During the normal translation process, pre-mRNA is synthesized during transcription and then undergoes a splicing process to remove intronic regions. However, mRNA which contains a premature termination codon (PTC) or stop codon is degraded by several proteins after the first round of translation. The three core up-frameshift proteins (UPF1, UPF2 and UPF3) along with exon junction complex (EJC) comprising the NMD machinery, bind to the PTCs leading to rapid mRNA degradation. The NMD pathway preferentially degrades mRNA transcripts containing PTCs rather than the normal termination codon, thus decreases the synthesis of truncated proteins with potentially harmful dominant-negative effects. PTCs have been found to be causative in ocular disorders like Aniridia, Usher syndrome, retinal degeneration and in other notable diseases such cystic fibrosis (Linde et al., 2007) and Duchenne muscular dystrophy (McDonald et al., 2017).

In recent years, the mechanisms behind NMD that degrade PTCs have been widely explored (Nguyen, Wilkinson, & Gecz, 2014; Wang & Gregory-Evans, 2015). For example, there are both EJC-dependent and -independent mechanisms that degrade abnormal PTCs (Hug et al., 2016; Scofield, Hong, & Lynch, 2007). Although small molecule drugs such as Ataluren® and Geneticin have been extensively studied for the treatment of various genetic diseases caused by

nonsense mutations, inhibitors of NMD are now being investigated. In two recent studies for Usher syndrome type C (Goldmann, Overlack, Wolfrum, & Nagel-Wolfrum, 2011) and Leber congenital amaurosis (Wang, Shan, Gregory-Evans, & Gregory-Evans, 2020), Amlexanox along with other NMD inhibiting compounds increased the abundance of the nonsense mutation-containing mRNA transcripts (Gonzalez-Hilarion et al., 2012), which were targeted by nonsense-suppression molecules that promoted readthrough at the PTC to produce full-length protein. Over the past decade, several other NMD inhibiting compounds have been studied including 5-azacytidine (Bhuvanagiri et al., 2014), NMDI 1 (Durand et al., 2007) and Pateamine A (Dang et al., 2009). Further studies are required to validate the level of NMD and its related mechanisms for developing effective therapies in ocular diseases linked with nonsense mutations.

1.5 Promising therapies

1.5.1 Mesenchymal stem cells (MSCs) as a promising approach for cell-based therapy

There are currently about 295 clinical trials involving MSC-based therapies listed by the US National Institutes of Health clinical trial database (www.clinicaltrials.gov), which represents the therapeutic applications of MSCs for various diseases. In recent decades, MSC-based therapy is an emerging trend for the field of regenerative medicine. MSCs can be easily obtained from various accessible tissues including peripheral blood, lingual adipose, skin biopsy, bone marrow, and dental tissue, and expanded in appropriate culture conditions efficiently (Ng, Fortino, Pelaez, & Cheung, 2014). MSCs have been shown to have various therapeutic benefits including anti-cell death properties, paracrine effects, neuroprotective properties, immunosuppressive and immunomodulatory properties, and self-migratory activity, making them an excellent therapeutic tool (Hodgkinson, Gomez, Mirotsov, & Dzaou, 2010; Ocansey et al., 2020; Ullah, Subbarao, &

Rho, 2015). Transplantation of humans MSCs into rodent models as well as patients with neurodegenerative disorders, repeatedly reported to migrate towards damaged sites and secrete a broad variety of cell signalling molecules (Wyse, Dunbar, & Rossignol, 2014; Xu, W. & Xu, 2011).

Studies in a rat model of experimental glaucoma has shown encouraging neuroprotective effects upon intravitreal mesenchymal stem cell transplantation (Johnson, T. V. et al., 2010). MSC therapy has demonstrated advanced wound healing capability by promoting secretion of paracrine factors, which regulates host cell inflammation and immune infiltration in corneal surface healing, in *in vivo* animal models and clinical trials (Al-Jaibaji, Swioklo, & Connon, 2019). Another advantage of MSCs is that they can be genetically modified effectively in *ex vivo* and then transplanted into the host. Adipose-derived MSCs were genetically engineered to overexpress human retinoschin-1 and then injected by intravitreally to the retina of the *Rslh* mouse model of X-linked Retinoschisis, which rescued the retinal degeneration (Bashar, A. E., Metcalfe, Viringipurampeer, Yanai, Gregory-Evans, & Gregory-Evans, 2016a). These studies suggest that MSC therapy for other eye diseases may be possible.

Chapter 2: Translational readthrough for genetic eye disorders

Between 5 to 70% of human congenital diseases are caused by in-frame nonsense mutations. Nonsense mutations introduce premature stop codons (UAA, UAG or UGA) in the mRNA leading to a truncated protein or absence of protein due to nonsense-mediated decay. Suppression of nonsense mutations is a therapeutic approach aimed at treating inherited diseases caused by premature in-frame nonsense mutations (PTCs) (Gregory-Evans, Wang, & Gregory-Evans, 2019). The drug Ataluren® helps to readthrough of each of the three nonsense codons with highest efficacy for UGA codons, followed by UAG and UAA (Peltz, Morsy, Welch, & Jacobson, 2013). The small molecule Ataluren® (Translarna™), the first orally available nonsense suppression drug that readthroughs the nonsense mutations, that is in clinical use (Ryan, 2014). In the non-sense suppression therapy Ataluren® interacts with the ribosome of the cell that translates the mRNA to manufacture proteins which enables the translational machinery to overcome the premature nonsense codon, thus allowing the cell to make a full-length functional protein, although at lower than normal levels (Landfeldt, Sejersen, & Tulinius, 2019). This reduced level of normal protein can prevent further disease advancement or in some cases reverse pathology. This specifically works in autosomal recessive conditions, even small increase of full-length functional protein could be sufficient for functional benefit (Samanta et al., 2019). The use of Ataluren® for nonsense suppression therapy has advantages including high-specificity for nonsense readthrough without affecting normal termination codons, and it is oral bioavailability with no to low adverse effects compared to other nonsense suppression drugs (Richardson, Smart, Tracey-White, Webster, & Moosajee, 2017).

In a recent in vitro study of patient with a novel heterozygous mutation of *PAX6*, the nonsense suppression drugs Ataluren® and geneticin were analyzed for their read through

efficiency in the patient's cultured lymphocytes. This treatment rescued the expression of PAX6 protein in patient derived lymphocytes (Liu, X., Zhang, Zhang, Gao, & Qiu, 2020). In another study, PTC and geneticin were able to read through the RP2 mutation in RPE cells derived from patient iPSCs that had X-linked retinitis pigmentosa (Schwarz, Carr, Lane, Moeller, Chen, Aguilà, Nommiste, Muthiah, Kanuga, Wolfrum, Nagel-Wolfrum, da Cruz et al., 2015). In other inherited ocular diseases like Usher syndrome type2A (Neuhaus et al., 2017) and choroideremia (Torriano et al., 2018), disease progression was also rescued by Ataluren® treatment. In our lab, we have effectively stopped disease progression, increased lens size, reversed corneal, and retinal deformity, produced full length functional Pax6 protein (~48kDa), and restored electrical response of the retina of *Pax6*^{sey+/-} mice by topical treatment of START therapy containing Ataluren® (Wang, X. et al., 2017).

2.1.1 Induced pluripotent stem cells (iPSCs) in clinical therapies

Induced pluripotent stem cell (iPSC) technology makes it possible to grow cell types *in vitro* that would otherwise be inaccessible in living patients. iPSCs can self-renew for an indefinite period (Dolmetsch & Geschwind, 2011; Moradi et al., 2019) and all types of differentiated tissues can be generated. The main advantage of the iPSC technology is that these cells can be produced in large numbers using cells taken from the patients, making iPSCs patient specific. The ability to generate patient-specific iPSCs creates unique opportunities for disease modeling and regenerative and transplantation studies and drug discovery. For example, iPSCs are a valuable means for 1) discovery of newly identified disease-causing mutations; 2) studying the disease pathophysiology in relatively remote tissues, such as the retina, that cannot be investigated in living patients; and 3) the rapid testing of new disease and patient-specific molecular therapeutics, which is especially

important for genetically inherited diseases, for which animal models with the disease phenotype do not exist (Rathod, Surendran, Battu, Desai, & Pal, 1988; Wiley et al., 2015).

iPSCs were originally produced from adult fibroblasts (Takahashi & Yamanaka, 2006). Fibroblasts are accessible via less invasive skin biopsy (Foltz & Clegg, 2019), from blood (Staerk et al., 2010), and from urine (Zhou et al., 2011). Cells from either blood or urine can be used in reprogramming to generate iPSCs (Hu et al., 2011; Zhou et al., 2011) which can then be differentiated into any tissue under appropriate culture conditions. Reprogramming of the somatic cells are done using viral vectors and integration-free methods, such as the piggyBac system (Woltjen et al., 2009), Sendai virus (Fusaki, Ban, Nishiyama, Saeki, & Hasegawa, 2009), a minicircle vector (Jia et al., 2010), synthetic mRNA (Warren et al., 2010), recombinant proteins (Kim et al., 2009), and episomal vectors (Okita et al., 2011).

For replacement cell therapy in the eye, candidate retinal cell types include light sensitive photoreceptors (rods and cones), retinal pigment epithelial cells (RPE), and retinal ganglion cells(RGC). The iPSCs can be reprogrammed to generate photoreceptors (Tucker et al., 2013; Yanai et al., 2013) or any retinal cells and these can be transplanted into patients with damaged retina. In the first time, Takahashi's group has conducted human clinical trial of an autologous iPSC derived RPE sheet to treat wet type of age-related macular degeneration (AMD) (Mandai et al., 2017). With the advancement in human iPSC research and the better understanding of differentiation pathways, several research groups have been able to grow cells that express photoreceptor markers (three-dimensional culture techniques) and then transplant these stem cell-derived cells by sub-retinal injection in animal models (Zhu et al., 2018).

2.2 Modes of delivery of therapeutics

2.2.1 Ocular injections versus topical eye drops

The eye is a unique and complex organ both anatomically and physiologically. The eye is more easily accessible and immune-privileged organ, which makes an ideal environment for studying and developing novel therapies for various genetic eye diseases. Efficient development of drug delivery systems for the treatment of eye diseases has been challenging. Drug delivery to the ocular tissues is directly linked with static and dynamic characteristics of the outer corneal barrier. Over the last two decades, novel ocular drug delivery systems have been developed including emulsions, ointments, hydrogels, nanomaterials, liposomes, intraocular implants, and microneedles. Moreover, these delivery systems are generally safe and maintain drug bioavailability in the desired targeted sites. One of most common methods for the treatment of anterior chamber eye pathology is non-invasive topical eye drop instillation. The routes of drug administration for the treatment of posterior eye diseases are sub-retinal, intravitreal and systemic injections to the patients. For example, cell and gene-based therapeutics have been tested for the treatment of anterior segment and retinal pathologies, where genetic materials can be delivered to targeted cells or tissues by viral and non-viral vector-based systems.

2.2.2 Vectors

Vectors are delivery vehicles which contain a transgene to be delivered to the targeted cell or tissue. Vectors are used in the gene and cell-based therapies to deliver a particular gene to overcome the defect in the tissue and to express the normal protein. Vectors can either be viral or non-viral systems.

2.2.2.1 Viral vectors

Several types of viral vectors have been in use for decades in animal studies including adenoviral-associated vectors (AAV), lentiviral vectors and retroviral vectors (Hashimoto et al., 2007; Kay et al., 2001; Lundstrom, 2018). Most commonly they are used in a gene augmentation approach to produce new protein in recessive disease. These vectors can enter the cell and produce the transgene under its own promoter control. Most viral vectors are replication-deficient, generated by removing most of the viral genes, making room for foreign genes to be inserted. The ideal viral vectors for gene therapy need to be easily purified into high titers and exhibit prolonged gene expression with minimal side effects.

2.2.2.2 Non-viral systems

Numerous non-viral systems have been used as carriers for gene editing and gene augmentation therapies including expression vectors (plasmids), nanoparticles, liposomes, CRISPR/Cas9 system and antisense oligonucleotides. Expression vectors contain a promoter region, a transgene containing start and termination codon, and antibiotic resistance gene giving the ability to switch the gene expression on and off.

2.2.2.3 Efficiency and limitations

In past two decades, viral vectors have emerged as safe and effective gene delivery systems, because of their well-defined biology, genetic stability, high gene transduction efficiency, and large scale production capacity. However, retroviral-based gene delivery can trigger inflammatory response, cause genotoxicity and are considered as unsafe for clinical practice (Biasco, Rothe, Büning, & Schambach, 2018; Montini et al., 2009; Nienhuis, Dunbar, & Sorrentino, 2006). On the

other hand, non-viral systems are safe and can accommodate large transgene insertion. One of the disadvantages of non-viral system such as nanoparticles and polymers is the lack of self-replicating capacity, and they are less permeable to cells. Therefore, multiple injections would be needed to deliver the transgene.

Although recent advances in viral and non-viral delivery systems for gene therapy have emerged, some limitations still need to be overcome: 1) appropriate delivery to the targeted cells and to avoid neighboring cells; 2) steady and continuous transgenic expression leading to functional benefits in the targeted tissues; 3) avoiding unwanted local and systemic toxic responses (Conley, Cai, & Naash, 2008). Almost all approaches are applicable for the treatment of ocular diseases, thus the cell type to be targeted and the type of study will determine the respective approach to use. Preclinical studies are used to determine the most efficacious delivery approach, ocular tissue specificity, biostability and safety of gene delivery systems for the treatment of various ocular diseases. In my studies, I decided to use MSCs as a carrier an expression vector to deliver our target gene to the diseased site.

Chapter 3: Therapeutic strategies for the treatment of anterior chamber abnormalities

3.1 Chapter Introduction

The PAX6 transcription factor is highly evolutionarily conserved gene and critical to the development of ocular and neurosensory organs during embryogenesis (Simpson & Price, 2002). Mutations in the *PAX6* gene cause aniridia, a rare genetic panocular condition affecting various region of the eye including cornea, anterior chamber, iris, lens, retina, fovea and optic nerve (Lee et al., 2008; Nelson, Spaeth, Nowinski, Margo, & Jackson, 1984; Netland, Scott, Boyle, & Lauderdale, 2011). Although between 5-70% of aniridic patients suffer from glaucoma as an adult, approximately 50% of them develop glaucoma during adolescence or in the early years of life (Brauner et al., 2008). Aniridic juvenile glaucoma is caused by developmental aberrations in the anterior chamber angle of the eye which obstructs the aqueous humor outflow to the trabecular meshwork and Schlemm's canal, a structure which drains the aqueous humor to the episcleral vessels of the eye (Grant, W. M. & Walton, 1974). Both medical and surgical procedures are used to overcome the anterior chamber aberrations in the aniridic patients, however over time they become less effective at reducing intraocular pressure. This leads to optic nerve damage and subsequently vision loss. The haploinsufficient *Pax6*^{Sey/+} mouse eye is caused by a naturally occurring G194X nonsense mutation, (Hill, 1991) which leads to defects in anterior chamber morphogenesis, providing a suitable model to test new therapies for glaucoma aimed at targeting the TM and SC tissues (Baulmann et al., 2002).

3.1.1 Therapeutic strategies for the treatment of anterior chamber abnormalities

Once maximum medical therapies no longer control increased intraocular therapy, several surgical procedures including trabeculectomy (Lee et al., 2008) and KPro surgery (Nascimento e Silva et al., 2019) are available to treat glaucoma. However, these interventions often lead to further complications such as aniridic fibrotic syndrome and further vigorous management and monitoring of the patients. In an attempt to overcome these late-stage problems, we proposed two strategies, a cell-based protein delivery approach using genetically modified mesenchymal stem cells and an RNA therapy using a small molecule compound.

3.1.1.1 Specific hypotheses

- The delivery the *Tgfb2*-expressing mesenchymal stem cells to the iridocorneal angle will induce the formation of the trabecular meshwork and Schlemm's canal in the haploinsufficient *Pax6*^{Sev/+} mouse.
- Nonsense suppression by pre- and postnatal delivery of the small molecule drug Ataluren® will rescue the iridocorneal angle defects in the haploinsufficient *Pax6*^{Sev/+} mouse eye.

3.1.1.2 Rationale

The anterior chamber dysgenesis in aniridia patients is caused by abnormal differentiation of trabecular meshwork and absence of Schlemm's canal (Margo, 1983). In the *Pax6*^{Sev/+} mouse model, similar pathology affects the formation of the trabecular meshwork and Schlemm's canal (Baulmann et al., 2002). The first therapeutic approach to be tested is based on the knowledge that in wildtype mice, the Pax6 signal from the lens epithelium induces the production and secretion of Tgfβ2 (Kroeber et al., 2010). This growth factor migrates to the iridocorneal angle to drives the

formation of trabecular meshwork and Schlemm's canal. Since the formation of these anterior segment structures occurs postnatally from P4–P21 (Smith, R. S., Zabaleta, Savinova, & John, 2001), the delivery of external Tgfb β 2 protein maybe able to improve ocular development, compensating for the lack of Pax6 activity. Mesenchymal stem cells (MSCs) that are genetically engineered to secrete proteins can promote cell survival due to their innate homing and adhesion to normal or diseased tissues (Ocansey et al., 2020). In addition, MSCs also secrete various growth factors which can activate endogenous repair mechanisms (Labrador-Velandia et al., 2016). For example, bone marrow stromal cells injected into a chronic glaucoma mouse model resulted in elevation of ciliary neurotrophic factor and basic fibroblast growth factor from the transplanted cells, which correlated with a reduction in retinal ganglion cell death (Yu, Tanabe, Dezawa, Ishikawa, & Yoshimura, 2006). Therefore, we hypothesized that Tgfb β 2-expressing MSCs could improve the development of anterior segment structures in the *Pax6*^{Sev/+} mouse eye. The second therapeutic approach of RNA-mediated nonsense suppression has been used in a variety of pre-clinical disease models and clinical trials including Duchenne muscular dystrophy, (McDonald et al., 2017) cystic fibrosis (Du, M. et al., 2008) and several ocular phenotypes (Guerin et al., 2008). This approach relies on producing approximately 5-20% increased levels of mRNA and subsequent protein that can improve or rescue the disease phenotypes. Nonsense suppression has been previously used in our lab to rescue the retinal, lens and corneal ocular defects in the *Pax6*^{Sev/+} mouse which carries a nonsense mutation (Wang et al. 2014). However, the effects on trabecular meshwork and Schlemm canal development were not assessed. Thus, in this study, we hypothesized that postnatal nonsense suppression using Ataluren® could rescue the anterior segment defects in the *Pax6*^{Sev/+} mouse eye.

3.1.1.3 Experimental plan

The experimental outline for testing the cell-based therapy is outlined below:

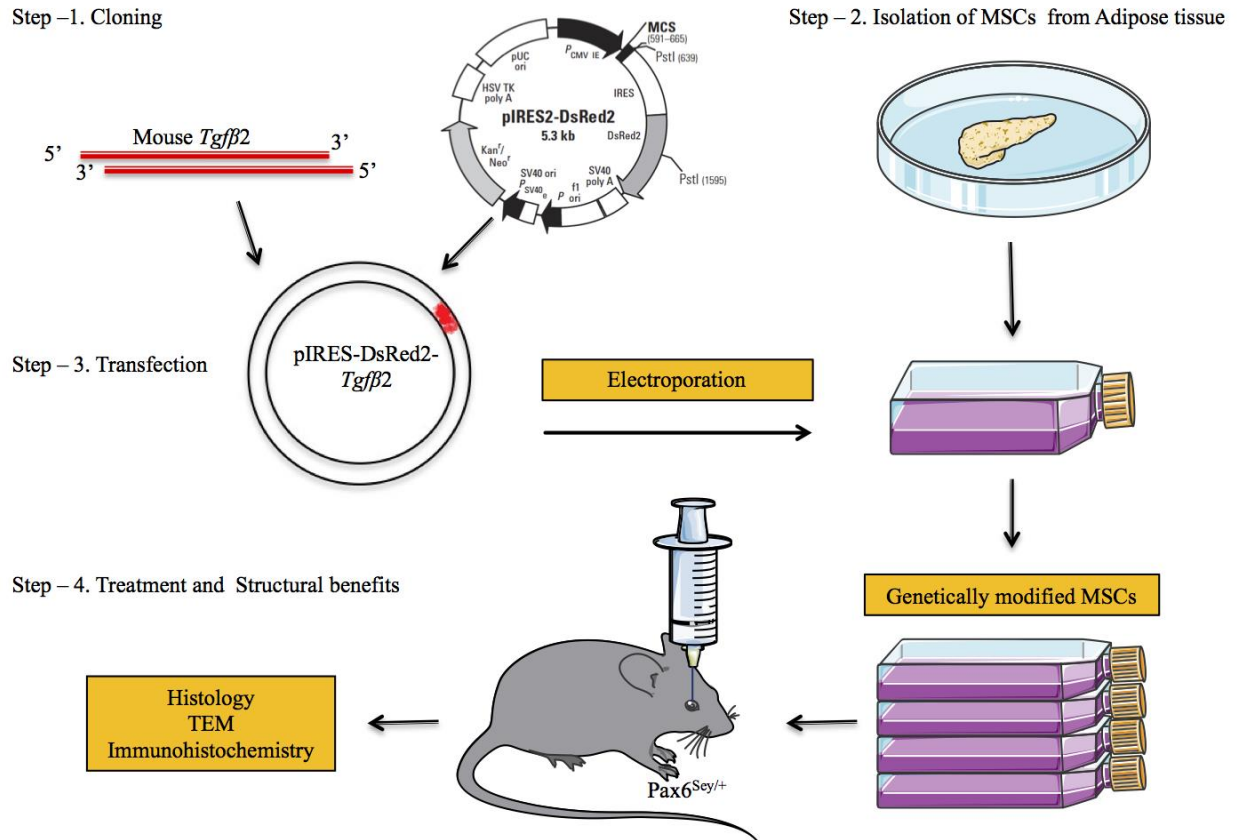


Figure 3.1: Overview of the cell-based gene therapy approach.

Step1: Cloning of *Tgfb2* cDNA into pIRES expression vector. Step 2: Isolation of MSCs from adipose tissue of the mice. Step 3: Transfection of MSCs with pIRES vector by electroporation. Step 4: Ocular injection and structural benefits were studied.

The experimental outline for testing RNA suppression is outlined below:

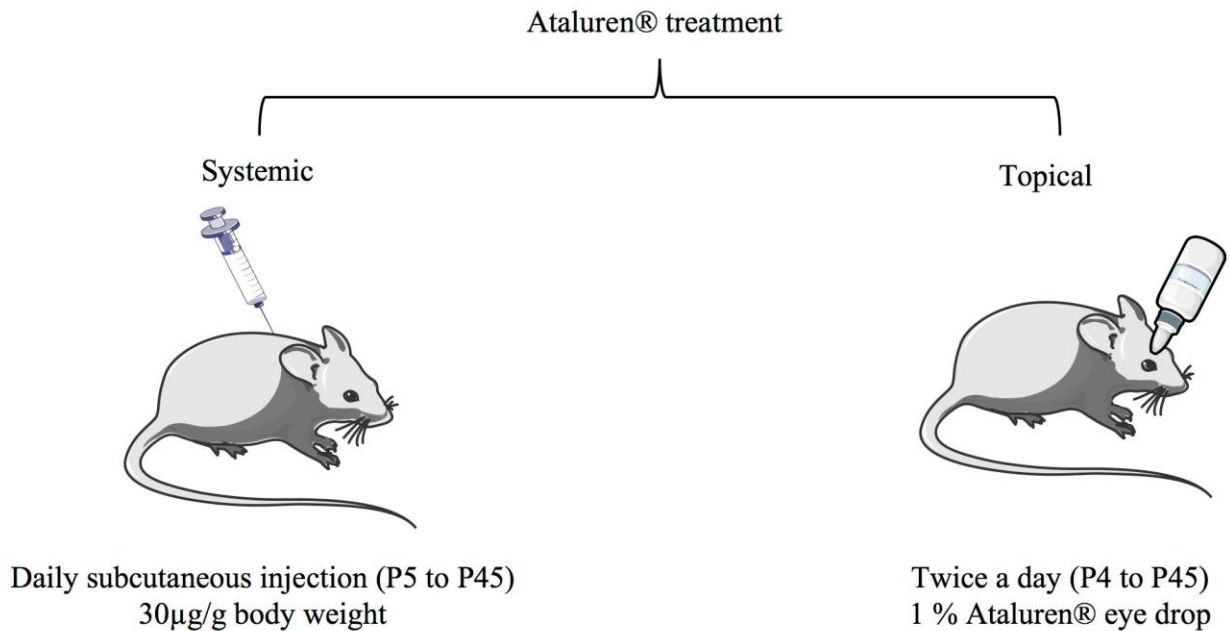


Figure 3.2 : Overview of Ataluren® treatment.

In systemic treatment the mouse treated with daily subcutaneous injection of 1% Ataluren® suspension from P4 to P45. In topical treatment, the Ataluren® eye drops were instilled twice a day from P4 to p45.

3.2 Methods

3.2.1 Animal housing and husbandry

This study was carried out in accordance with protocols compliant with the Canadian Council on Animal Care (CCAC) and with the approval of the local Animal Care Committee (ACC) at the University of British Columbia, Vancouver, Canada. Heterozygous *Pax6*^{Sey/+} mice were obtained from Veronica van Heyningen, Human Genome Centre, Edinburgh, UK. All mice were bred and housed/maintained on a 12-hr light/dark cycle and had easy access for water and food *ad libitum*. Equal number of male and female mice were used.

3.2.2 Genotyping of *Pax6*^{Sey/+} mouse

The *Pax6*^{Sey/+} mouse mutant has a heterozygous mutation caused by a G: T transversion which replaces the glycine at codon 194 (GGA) with a TGA stop codon. *Pax6*^{Sey/-} offspring were identified by genotyping of genomic DNA extracted from either tail or ear trephine punches using the REDEExtract-N-Amp Tissue PCR kit (Sigma, Oakville, ON, Canada). Each 25 μ L PCR reaction contained 1 X PCR master mix (Promega, Wisconsin, United States), 250 nM of forward and reverse primers and 4 μ L tissue lysate. PCR was amplified with the following cycles: first cycle: 95°C, 3 min; 55°C, 1 min; 72°C, 1 min, and then for 35 cycles of 1 min at 95°C, 40 seconds at 55°C, and 40 seconds at 72°C. Primers for amplifying the *Pax6*^{Sey/+} mutation were as follows: forward SP1 (annealing to *Sey* allele): 5'-GAGAACACCAACTCCATCAGTTCTAAGT-3'; forward SP2 (annealing to wildtype allele): 5'-AGCAACAGGAAGGAGGGGGAACGAACACCAACTCCATCAGTTCTTACG-3'; reverse MC130 for both PCR reactions: 5'-CTTTCTCCAGAGCCTCAATCTG-3'. PCR amplified DNA was analyzed on a 3% TBE agarose gel (see Appendix A.1). The wildtype *Pax6* allele produces a 148 bp SP2/MC130 band and the *Pax6*^{Sey} allele generates a 129 bp SP1/MC130 band (Collinson, Hill, & West, 2000)

3.2.3 Cell-based gene therapy

3.2.3.1 Cloning of *Tgfb2* cDNA

Full length mouse *Tgfb2* cDNA was amplified by PCR from a commercially available plasmid (Sino Biological, Wayne, PA, USA) using a forward primer designed with a *Bgl* II restriction site and the ATG start codon 5'-GGAAGATCTTCCGAACATGCACTACTGTGTGCTG-3' and a reverse primer 5'-

CCGGAATTCTTAGCTGCATTTACAAGACTTG-3` containing an *EcoRI* site and the termination codon. This cDNA gene was subcloned directionally into the pIRES-DsRed2 bicistronic vector under the control of the CMV promoter (Takara Bio USA Inc., Mountain View, CA, USA), which constitutively expresses *Tgfb2* and the DsRed gene in transfected cells. The construct containing the transgene was validated by restriction digestion analysis and performing gel electrophoresis subsequently (Appendix A.2).

3.2.3.2 Isolation and expansion of MSCs from adipose tissue

Isolation of the mouse MSCs and expansion were performed as previously described with minor modification (Bashar, Abu Emran et al., 2013). Briefly, primary mouse MSCs were isolated from inguinal adipose tissue of two-month-old C57BL/6 mice. The tissue was aseptically dissected and gently washed with cell culture grade 1X Dulbecco's phosphate buffered saline (DPBS, Life Technologies, Burlington, ON, Canada), and then minced with sterile surgical scalpel in 3 mL of 1 mg/mL Collagenase type 1 (Sigma, Oakville, ON, Canada) in DPBS, and incubated for 1hr at 37°C. The digested tissue was filtered through a 40µ cell strainer, and the filtrate was centrifuged at 1200 rpm for 10 mins at room temperature. The cell pellet was resuspended in 3ml of MesenCult MSC Basal Medium (Stemcell Technologies, Vancouver, BC, Canada) supplemented with 10% fetal bovine serum (FBS), 1% glutamine and 1% penicillin/streptomycin (all from ThermoFisher Scientific, Waltham, MA, USA). The cells were counted by tryphan blue method using hematocytometer. About 1000 Cells were seeded on 6-well plates and allowed to expand at 37°C with 5% CO₂. After the cells reached 90% confluency, they were subcultured by trypsinization (0.05% w/v Trypsin-EDTA: ThermoFisher, Scientific, Waltham, MA, USA) for 3 minutes at 37°C and MSC basal growth medium was added to stop the trypsinization and centrifuged for 5 minutes

at 1200 rpm. The cell pellet was suspended in 10ml of MSC basal medium and transferred to a 75 cm flask and incubated at 37°C for further culturing. Cells of early passages were used in all experiments. Identity of the cells as MSCs was confirmed by testing their differentiation ability into adipocytes (MesenCult Adipogenic Stimulatory kit from Stem Cell Technologies, Vancouver, BC, Canada) or osteoblasts (MesenCult Osteogenic Stimulatory kit from Stem Cell Technologies, Vancouver, BC, Canada) according to manufacturer's instructions. Adipocytes and osteoblasts were visualized with Oil-Red-O or Alizarin Red staining (both from MilliporeSigma, Oakville, ON, Canada), respectively.

3.2.3.3 Transfection of MSCs with *Tgfb2*-containing expression vector

The bi-cistronic expression vector pIRES-DsRed2-*Tgfb2* driven by the CMV promoter has a neomycin resistance gene which was utilized for the selection of transfected MSCs containing the *Tgfb2* gene. Flasks containing 100% confluent MSCs were trypsinized, centrifuged for 5 minutes at 1200 rpm and collected. These cells were washed with DPBS and re-centrifuged as above to remove any trypsin enzyme and the cells were counted using a hemacytometer. Approximately 100µg of *Tgfb2*-containing expression vector was resuspended with 1 million cells in 300 µL of Gene Pulser® electroporation buffer (Bio-Rad, Mississauga, ON, Canada) and transferred to 0.4 mm cuvette. A Gene Pulser Xcell System (Bio-Rad, Mississauga, ON, Canada) was used to generate a square wave pulse of 220 V for 25 ms for electroporation of cells (Appendix A.3). The cells were then quickly transferred to a 6 well plate containing 2mL of Mesencult MSC Basal growth media and placed in the incubator at 37°C/5% CO₂ for 24 hrs. The growth medium containing 200 µg/mL of G418 antibiotic (sigma, Etobicoke, ON, Canada). The selection medium was replaced every 2 days for 2 to 3 weeks to allow for stable transfection. The cells were imaged

using a Zeiss LSM 510 Meta laser scanning confocal microscope (Zeiss, Toronto, Canada) to evaluate the expression of DsRed-Tgfb β 2 proteins.

3.2.3.4 Anterior chamber ocular injection

Tgfb β 2-expressing MSCs were labelled with 20 μ M CellTrace far red DDAO-SE (ThermoFisher Scientific, Waltham, MA, USA) and then resuspended in DPBS. The 5-day old *Pax6*^{Sev/+} mouse pups were anesthetized using isoflurane gas and were placed under a stereomicroscope on a heating pad. Their future eyelids were separated carefully using a sterile 30-gauge needle and the pupils were dilated with 1% tropicamide (Bausch and Lomb, Rochester, NY, USA). By using a disposable syringe with 31-gauge needle as a scalpel, the tip was used to carefully penetrate the cornea and then a single lateral incision was made. This procedure was done between the apex of cornea and limbus to minimize reflux of the MSCS during injection out of the anterior chamber of the eye. Tear-gel (Alcon, Fort Worth, TX, USA) was applied to the cornea throughout the surgery to keep it moist. A 2 μ L suspension (50,000 cells/ μ L) of *Tgfb β 2*-expressing MSCs was transplanted into the right eye and the left eye was the uninjected control. Another cohort of mice were used as sham/vector controls injected with modified MSCs containing pIRES-DsRed2 vector without *Tgfb β 2*. After injection, mouse pups were then allowed to recover on a heating pad and the mouse eyes were treated with proparacaine analgesic drops, tobramycin (0.3%) ophthalmic antibiotic ointment, and hydrated with tear gel (all from Alcon, Fort Worth, TX, USA). The location of transplanted cells was identified by the cell tracer and expression of Tgfb β 2 protein.

3.2.4 Pharmaceutical therapy

3.2.4.1 Ataluren® preparation for topical eye drops and systemic injection

A once daily subcutaneous injection of a suspension of 1% Ataluren® (Selleckchem, Houston, TX, USA) was given to pregnant *Pax6^{Sev/+}* dams from E12.5 and to their offspring from P4 onwards and control groups that were sham treated. For topical delivery, one eye received twice-daily instillation of a 1% START therapy eye drop containing 1% Ataluren® (Appendix A.4) from P4 onwards after the eyelids had been separated with a sharp 30-gauge needle and the other eye with suspension omitting Ataluren® (Gregory-Evans et al., 2014).

3.2.5 Histology

Enucleated eyes were punctured using a needle and the tissue were fixed with EM grade 2.5% aqueous glutaraldehyde in 0.1M sodium cacodylate buffer fixative (Electron microscopy Sciences, Hatfield, PA) for 1 hour. For histology, eye sections (5 µm thick) were stained with hematoxylin and eosin (Appendix A.5). Images were obtained using an Aperio ScanScope digital scanning system (Leica Imagescope, Buffalo Grove, USA).

3.2.6 Immunohistochemistry

For immunostaining, fixed eyes were perfused in 30% sucrose solution at 4°C for overnight. The processed tissues were mounted with optimal cutting temperature medium (OCT) (Tissue-Tek; Torrance, CA, USA) and transferred to -80 °C. Prior to sectioning, the samples were transferred to -20°C. 10-12µ thick cryosections were incubated at 4°C in a humidified chamber for overnight with appropriate primary antibodies: Tgfb2 rabbit polyclonal (Abcam; catalog# ab66045; 1:200); Pax6 rabbit polyclonal (Biolegend; catalog# 901301; 1:500); F-actin mouse

monoclonal (Abcam; catalog# ab205; 1:200); PDGFR α goat polyclonal (R&D; catalog# AF1062; 1:500); Prox1 rabbit polyclonal (MyBiosource; catalog # 2542828; 1:300). After the slides were washed 4 times with PBST they were incubated for 1 hr at room temperature (RT) with the appropriate secondary antibody: AlexaFluor® 488 goat anti-rabbit IgG or Alexafluor® 594 goat anti-mouse IgG (ThermoFisher; catalog#11008; 1:200). The slides were counterstained with DAPI Fluoromount-G® medium (SouthernBiotech, Birmingham, AL, USA) for nuclei. Confocal images were imaged using a Zeiss LSM 510 Meta laser scanning confocal microscope (Zeiss Canada, Toronto, Canada).

3.2.7 Transmission electron microscopy (TEM)

Eyes were enucleated and fixed with 0.1 M sodium cacodylate buffer (pH 7.4) containing 1% glutaraldehyde. To preserve lipids, dissected eyes were post-fixed for 1 hr with 1% osmium tetroxide in 0.1 M cacodylate buffer pH 7.4 and then washed in 0.1M cacodylate buffer for 1 hr. Tissues were dehydrated with graded ethanol (30%, 50%, 70%, 95%, and 100%). Then samples were gradually infiltrated with Spurr resin (Ted Pella, Redding, CA, USA) until the samples were embedded in 100% Spurr resin. Samples were incubated overnight at 60°C to induce polymerization. Ultra-thin sections of 70 nm thickness were mounted on copper grids coated with formvar and stained with 2% uranyl acetate and lead citrate for contrast. Images were obtained by transmission electronmicroscopy (100 kV: model H600, Hitachi, Tokyo, Japan).

3.2.8 Western blot

The anterior segment of the eye was carefully dissected and homogenized by sonication in PBS supplemented with protease/phosphatase inhibitor cocktail (Cell Signalling, Beverly, MA,

USA). For cultured MSCs, protein lysis buffer (10 mM Tris base, pH 7.4, 150 mM NaCl, 1 mM EDTA, 1 mM EGTA, 1% Triton-X-100, 0.5% NP-40, protease/phosphatase inhibitor cocktail) was added directly to the culture plate and the lysed cells were scraped off. Total protein concentration was measured using the DC protein assay (Bio-Rad, Hercules, CA, USA). For western blots proteins samples (25 µg) were mixed with sample buffer, boiled for 5 to 10 min at 95°C. The protein lysates were separated by SDS-polyacrylamide gel electrophoresis, and then transferred to Immobilon-FL membrane (MilliporeSigma, Etobicoke, ON, Canada). Membranes were blocked in 5% non-fat milk powder in PBS for 1 hr at RT and incubated overnight at 4 °C with appropriate primary antibodies diluted with 5% non-fat milk powder in PBS/0.1% Tween-20 (PBST): Tgfβ2 rabbit polyclonal (Abcam; catalog #ab66045; 1:200); Pax6 rabbit polyclonal (Biolegend; catalog# 901301; 1:500); PDGFRα goat polyclonal (R&D; catalog# AF1062; 1:500); LMX1b rabbit polyclonal (Sigma; catalog# 3501024; 1:500) Foxc1 goat polyclonal (Novus Biologicals, Littleton, CO, USA) in blocking buffer. Following 5 washes in PBST, the membranes were incubated with an appropriate fluorescent secondary antibody (IRDye 800 or IRDye 680) for 1 hr at RT. The membranes were then washed five times for 5 mins in PBST and protein bands were visualized and imaged using a Li-COR Odyssey Imaging System (Mandel Scientific, Guelph, ON, Canada). The band intensities relative to loading control (β-actin) were analyzed by NIH ImageJ software. Western blots were repeated three times using tissues from independent animals (N=3) for each treated group.

3.2.9 Enzyme-linked immunosorbent assay (ELISA)

For ELISA, culture medium or tissue lysates were centrifuged at 10,000 x g for 10 mins to remove debris and the supernatant used to quantify the expression level of Tgfβ2, Pitx2 and

Foxc1 proteins using commercially available kits according to manufacturer's instructions (MyBiosource, San Diego CA, USA). All ELISAs were conducted in two independent experiments in triplicate (N=6).

3.2.10 Statistical analysis

The significance of the differences between the treated and untreated groups were analyzed by unpaired 2-tailed Student's *t* test. A P value of less than 0.05 was considered statistically significant. All values were presented as the mean \pm standard error of the mean (SEM).

3.3 Results

3.3.1 Anterior segment morphogenesis in the Pax6^{Sey/+} mouse eye

The anterior segment of the normal mouse eye develops postnatally requiring Pax6 activity and is functionally mature by postnatal day P21. The anterior segment of the eye consists of the cornea, iris, ciliary body and drainage structures trabecular meshwork and Schlemm's canal. Aqueous humor fluid that is secreted by the ciliary body flows narrowly between the lens and iris, into the anterior chamber and drains out through the trabecular meshwork and Schlemm's canal. At P5 ocular mesenchyma is densely packed at the anterior chamber angle and it differentiates into trabecular cells from P6 to P10 (Fig. 2.3 A). Unlike wildtype mice, the Pax6^{Sey/+} mouse eye exhibits an underdeveloped anterior chamber region from P5 with the iris adhered to the corneal endothelium blocking the fluid outflow (Fig. 2.3 A, D) and a compact aggregated mass of cells was present. At P21 in the wildtype eye, morphogenesis of trabecular meshwork was complete with abundant extracellular matrix (ECM) and inter-trabecular spaces being observed. However, the drainage canal structures were undeveloped in the Pax6^{Sey/+} eye and there is no anterior

chamber angle (Fig. 2.3 B, E). In the *Pax6*^{Sev/+} adult at P45 there was a reduced number of ciliary body processes and their folding was impaired (Fig. 2.3 C, F). Furthermore, the corneal epithelium was hypoplastic, the trabecular meshwork beams were absent and Schlemm's canal was either very small or absent. The underdevelopment of the *Pax6*^{Sev/+} eye was also reflected in it being microphthalmic (small). Electronmicroscopy revealed the absence of postnatal mesenchymal condensation in the mutant eye at P5, which normally denotes the beginning of trabecular meshwork morphogenesis (Fig. 2.3 G). By P21 the trabecular beams and Schlemm's canal were formed in the wildtype eye, however, disorganized trabecular meshwork and lack of an obvious Schlemm's canal was observed in the *Pax6*^{Sev/+} eye. (Fig.2.3 H). In place of Schlemm's canal were giant vacuoles at the corneal stroma/ciliary body interface by light microscopy (Fig. 2.3 H). When these anterior chamber sections were imaged under TEM these gaps and vacuoles were seen in place of Schlemm's canal in the *Pax6*^{Sev/+} mouse eye. These features that have been characterized in the anterior segment of the *Pax6*^{Sev/+} eye allows for testing of possible therapies to see if improvements in the abnormal development are possible.

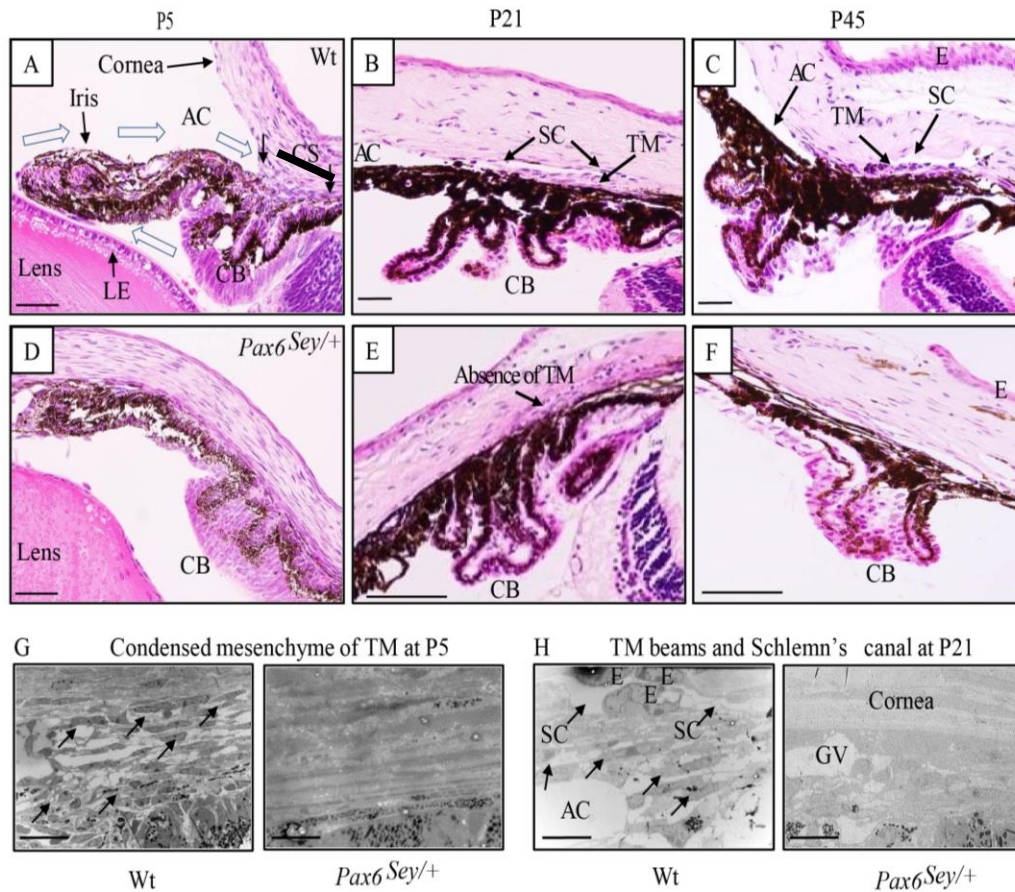


Figure 3.3: Ocular anterior segment morphogenesis *Pax6^{Sey/+}* mouse eye.

(A) At P5 the wildtype (Wt) trabecular meshwork anlage is observed as condensed mesenchyme (beneath thick black line between arrows) separating the corneal stroma (CS) and the ciliary body (CB). The iris is typically positioned adjacent to the lens epithelium (LE). The open arrows indicate the future flow of fluid from the CB, between the iris and lens, towards the anterior chamber angle (AC) and into the drainage canal. (B) By P21 the narrow drainage channel known as Schlemm's canal (SC) is visible (between arrows) and beneath it lies the mature trabecular meshwork beams (TM). The processes of the CB are more developed and highly pigmented. (C) At P45 the anterior chamber is fully remodeled and the corneal epithelium (E) is several cells thick. (D) *Pax6^{Sey/+}* mouse eye at P5. The hypoplastic iris is adhered to the cornea so there is no AC. Only a few LE cells are present at the surface of the lens. (E) CB processes begin to develop, but the TM and SC posterior to the CB are underdeveloped (arrow). (F) At P45 the TM beams are absent, there are large vacuoles in the corneal stroma adjacent to the CB, the CB processes are underdeveloped lacking pigmentation, and the corneal epithelium (E) is only 1 cell thick. Size bar in A and D = 50 μm ; B, C, E and F = 25 μm (NB: *Pax6^{Sey/+}* eye is smaller). (G) TEM showing condensed mesenchyme (white arrows) at the beginning of TM formation in Wt, but not in *Pax6^{Sey/+}*. (H) Well organized trabecular beams (white arrows) and endothelial cells (E) lining Schlemm's canal (SC) in Wt. TM and SC are hypoplastic and giant vacuoles (GV) are present between the CB and corneal stroma in *Pax6^{Sey/+}* eyes. Size bar = 500nm

3.3.2 Comparative localization of Pax6 and Tgfb2 in the anterior chamber region

Since the *Tgfb2* gene is a direct downstream target of Pax6 in the developing lens and iris, the localization of both proteins was compared in the developing anterior segment tissues of wildtype and *Pax6*^{Sev/+} eyes (Fig. 2.4 A). High levels of Pax6 protein were localized to the non-pigmented epithelium of the developing ciliary processes, whereas reduced levels of expression were seen in *Pax6*^{Sev/+} mouse eye. F-actin was localized to the vasculature inside the ciliary processes and in the corneal stroma, but this greatly reduced in the underdeveloped *Pax6*^{Sev/+} eye. Tgfb2 was localized to the lens epithelium, corneal epithelium, non-pigmented ciliary epithelium, and retina in wildtype eyes. In contrast greatly reduced expression of Tgfb2 was observed in all anterior segment tissues of the *Pax6*^{Sev/+} eye. These results further support the notion that Pax6 is driving directly or indirectly the expression of Tgfb2 in the anterior segment. We also quantitated protein expression in wildtype and *Pax6*^{Sev/+} anterior chamber tissue by western blot (Fig. 2.4 B, E). Pax6 and Tgfb2 were reduced to 43% and 13% of wildtype levels, respectively. We therefore hypothesized that delivery of exogenous Tgfb2, thereby bypassing the *Pax6* mutation, might be able to improve ciliary body, trabecular meshwork and Schlemm's canal development in the *Pax6* haploinsufficient eye.

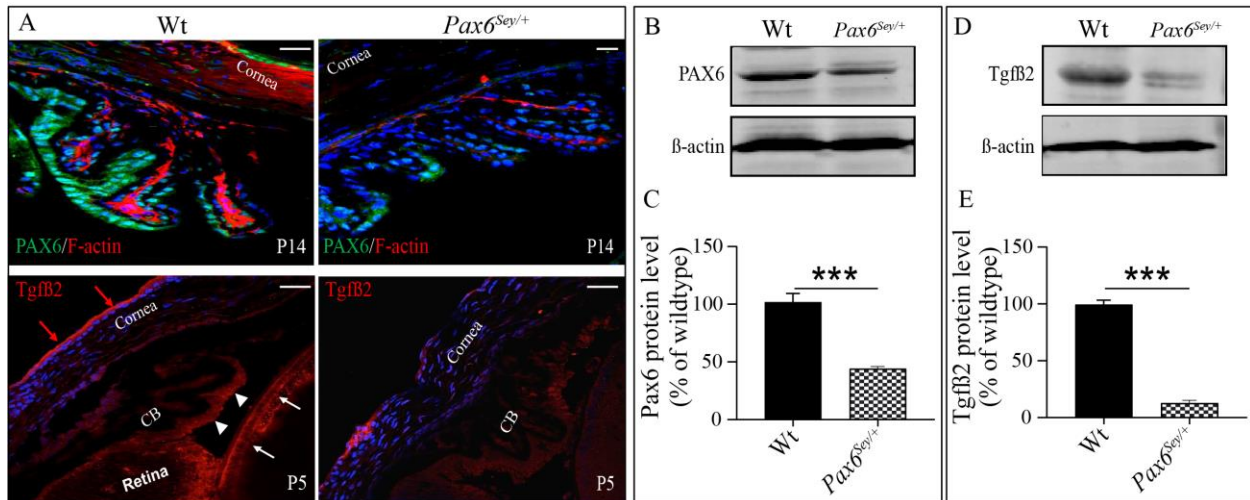


Figure 3.4 : Localization of Pax6 and Tgfb2 in the anterior segment.

(A) Upper panels: High levels of Pax6 (green) were localized to the non-pigmented ciliary epithelium and corneal epithelium in wildtype (Wt) eyes compared to low levels in *Pax6^{Sey/+}* eyes at P14. F-actin (red) localized to the vasculature inside the ciliary processes and in the corneal stroma. Size bar = 10 μm. Lower panels: High levels of Tgfb2 in the non-pigmented ciliary epithelium (white arrowheads), lens epithelium (white arrows), corneal epithelium (red arrows) and retina compared to low levels in *Pax6^{Sey/+}* eyes at P5. The corneal stroma appears thicker in the mutant eyes at P5. Nuclei were counterstained with DAPI. Size bar = 25 μm. (B) Western blot comparing Pax6 in Wt and *Pax6^{Sey/+}* anterior chamber tissue with β-actin loading control. (D) Western blot comparing Tgfb2 in Wt and *Pax6^{Sey/+}* anterior chamber tissue with β-actin loading control. Quantification of western blots for Pax6 (C), and Tgfb2 (E). Data plotted as mean ± SEM (N = 3), and statistical significance was determined using the student *t*-test, ***P < 0.001.

3.3.3 Characterization of genetically modified MSCs expressing Tgfb2 protein

To deliver Tgfb2 to the eye, we chose an *ex vivo* gene therapy approach using mesenchymal stem cells (MSCs) to secrete the protein as this method had been previously used to successfully deliver retinoschisin to the retina (Bashar, A. E., Metcalfe, Viringipurampeer, Yanai, Gregory-Evans, & Gregory-Evans, 2016b). Primary cultures of MSCs from wildtype mice were prepared from adipose tissue. To confirm their correct identity, primary cells were differentiated into adipocytes and osteocytes (Fig. 2.5). Adipocytes were characterized by Oil-Red-O staining in the cell cultures, whereas osteocytes had very strong Alizarin Red stained cytoplasm.

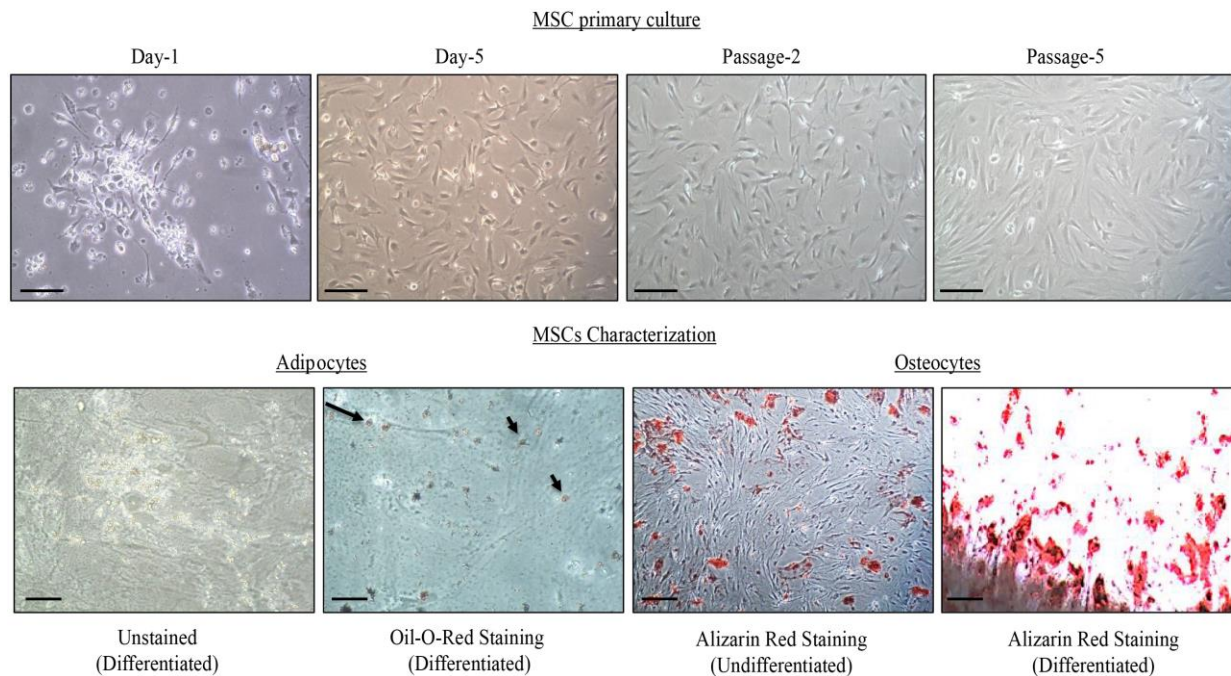


Figure 3.5: Characterization of MSCs from adipose tissue

Upper panels: cells from mouse inguinal adipose tissue were cultured to Passage 5 and then differentiated into either adipocytes or osteocytes (lower panels). Differentiated adipocytes stain red with Oil-Red-O stain (arrows) whereas differentiated osteocytes display strong cytoplasmic Alizarin Red staining.

The expression of $Tg\beta 2$ was further studied by cellular and biochemical analyses in the transfected MSCs. Passage 5 primary MSCs were electroporated with a bicystronic mammalian expression vector engineered to express $Tg\beta 2$ (pIRES-DsRed2- $Tg\beta 2$). In untransfected MSCs there was no DsRed2 expression, the tracer confirming the presence of the expression vector, however we noted low levels of $Tg\beta 2$ in the nuclei of MSCs (Fig. 2.6 A). In contrast MSCs that received the pIRES-DsRed2- $Tg\beta 2$ vector exhibited perinuclear DsRed2 expression and high levels of cytoplasmic $Tg\beta 2$ protein expression (Fig. 2.6 A). Expression of $Pdgfra$ (a marker for MSCs) was expressed in both untransfected and transfected MSCs. ELISA quantification revealed that transfected MSCs secreted approximately 24ng $Tg\beta 2$ /million cells per day compared to

vehicle control cells (Fig. 2.6 B). Western blot analysis revealed a relative increase in the active Tgf β 2 protein (25 kDa) in transfected cells compared to vehicle control cells (Fig. 2.6 C) mirroring the cell expression data. Tgf β 2-expressing MSCs were then injected into the anterior chamber of a wildtype mouse eye to confirm the expression of Tgf β 2 protein in the anterior chamber of the eye (Fig. 2.6 D). Endogenous Tgf β 2 was also detected in the ciliary body as would be expected.

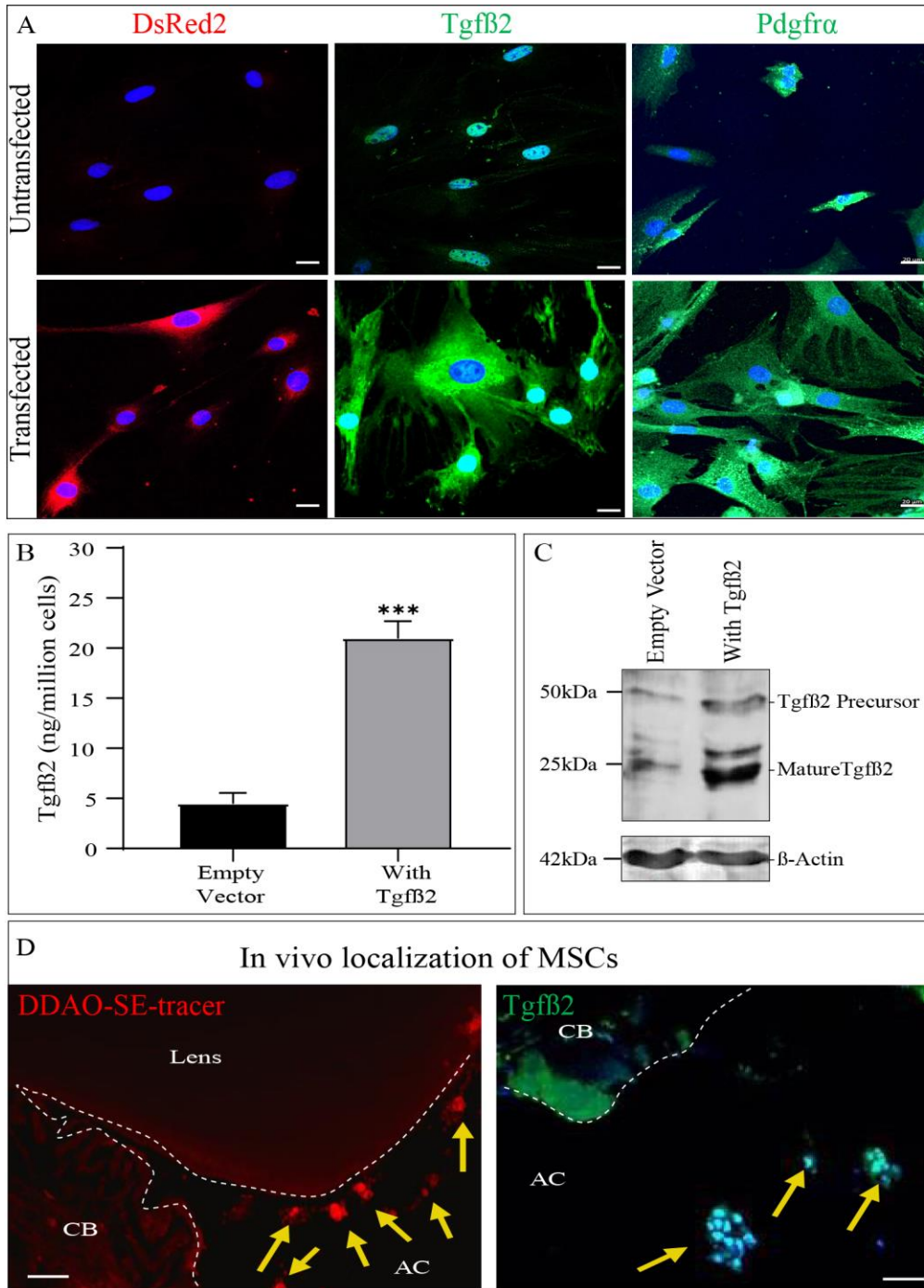


Figure 3.6: Characterization of genetically modified *Tgfb2*-expressing MSCs

(A) Left panels: comparison of DsRed2 expression in untransfected and transfected MSCs. Middle panels: untransfected cells express low levels of Tgfb2 protein (green) in the nucleus whereas transfected cells have high levels of cytoplasmic Tgfb2 protein expression. Right panels: Both transfected and untransfected MSCs express the Pdgfra which is a positive marker for MSCs. Cells counterstained with DAPI. Size Bar= 20µm. (B) ELISA quantitation of Tgfb2 protein

secreted in the culture medium from MSCs transfected with DsRed2-*Tgfb2* compared to cells transfected with an empty vector. (C) Western blot showing upregulation of precursor and mature Tgfb2 protein in cells transfected with DsRed2-*Tgfb2* expression vector compared to empty vector. (D) Left panel; location of *Tgfb2*-expressing MSCs (yellow arrows) 10 days after injection into the anterior chamber (AC) of the mouse eye. The lens and ciliary body (CB) are outlined with a dotted line. A red DDAO-SE tracer detects the location of the MSCs. Right panel; Tgfb2 localization was detected in the injected MSCs (yellow arrows). Cells were counterstained with DAPI. Size bar = 50µm

3.3.4 Outcomes of cell-based delivery of Tgfb2 and non-suppression therapy to the

Pax6^{Sev/+} eye

3.3.4.1 Structural benefits

The effect of a single injection of 50,000 Tgfb2-expressing MSCs into the anterior chamber of the *Pax6*^{Sev/+} eye at P5 was assessed by histology, TEM and immunohistochemistry at P21 (Fig. 2.7). In cell-based treatment group Schlemm's canal was developed and trabecular beams and cell arrangement could be identified, whereas eyes treated with MSCs containing an empty vector had neither aqueous humor draining structures by histology and TEM. The iris appeared to be mature, however, the ciliary body fronds were less well-developed compared to the wildtype eye. In comparison, topical administration of Ataluren® START therapy twice daily also resulted in both Schlemm's canal and trabecular meshwork structures. In addition, there was a mature ciliary body and iris structure and ECM components and in vehicle control groups, accumulation of ECM components was observed. Using the systemic Ataluren® treatment protocol, the ocular drainage structure development was not improved. Immunolabelling with Prox1 which is specific for Schlemm's canal (Park et al., 2014) revealed the presence of Schlemm's canal in wildtype eye and in the treatment groups, whereas it was absent in the vehicle controls of each treatment group. Prox 1 is a transcription factor which is up-regulated during SC development since it is regulator for the development of lymphatic system.

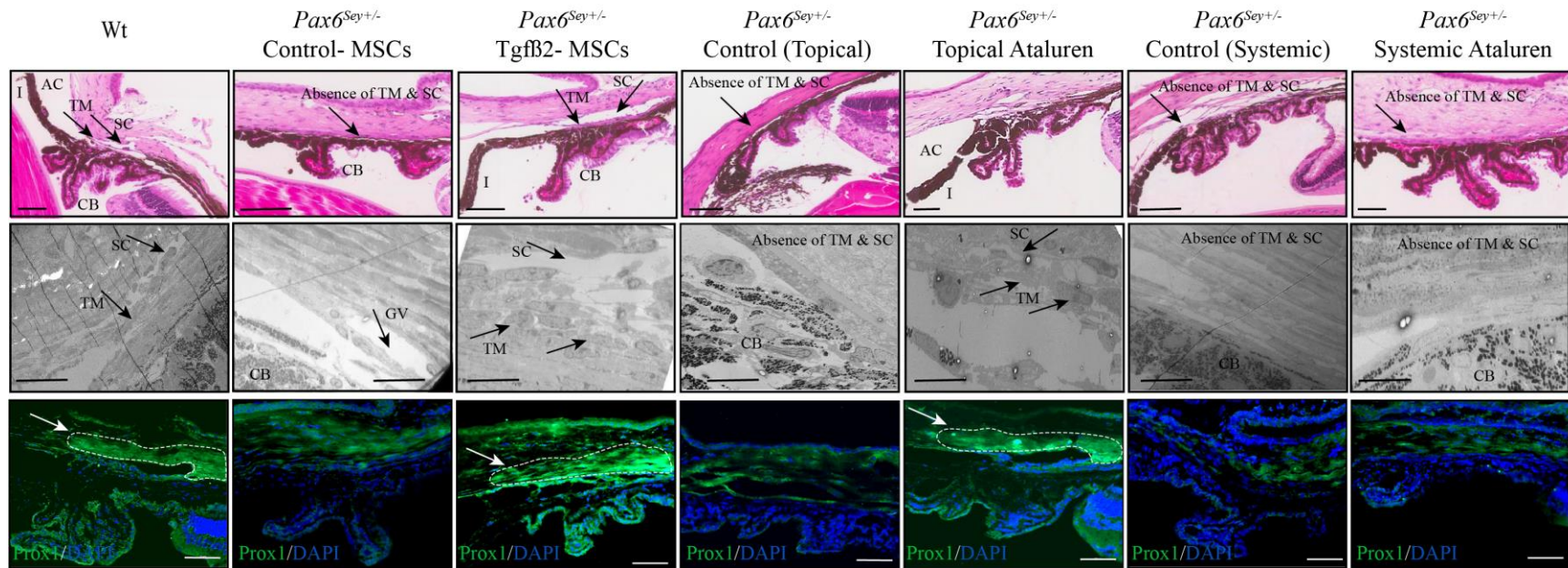


Figure 3.7: Efficacy of cell-based delivery compared to nonsense suppression therapy at P21.

Upper panels: H and E staining of anterior segment structures in wildtype (Wt), and $Pax6^{Sey+/-}$ eyes treated with either Tgf β 2-MSCs, topical or systemic Ataluren® in comparison to controls. TM, trabecular meshwork; SC, Schlemm's canal; CB, ciliary body; AC, anterior chamber angle; I, iris. Size bar = 50 μ m. Middle panels: TEM images of the corresponding TM and SC structures in the different treatment groups. GV = giant vacuole. Size bar in all panels = 5 μ m.

Lower panels: Immunolabelling of Prox1 (green) in the endothelial cells lining Schlemm's canal (white dotted lines). Cell nuclei counterstained with DAPI. Size bar = 50 μ m.

3.3.4.2 Quantification of anterior segment proteins in the eye

Since we observed structural changes to the eye with the different treatment groups, we analyzed the expression of anterior segment proteins by western blot. The topical treatment revealed increase in the level of Pax6 protein (Fig 2.8 A) and the bar graph quantifies the change in Pax6 expression (Fig 2.8 B). Treatment with topical Ataluren® resulted in Pax6 protein at 83.67% of wildtype levels ($P<0.01$, $N=3$). Furthermore, we also wanted to validate the Tgfβ2 protein expression levels in the different treatment groups. By western blot increased amounts of Tgfβ2 protein were detected in eyes treated with Tgfβ2-MSCs and topical Ataluren® treatment (Fig. 2.8 C). In MSC control treated eyes Tgfβ2 expression was approximately 21.3% of wildtype ($P<0.01$, $N=3$), whereas eyes treated with Tgfβ2-MSCs resulted in a significant increase in Tgfβ2 expression to 69.3% of wildtype levels ($P<0.01$, $N=3$) (Fig. 2.8 D). When eyes were treated with topical Ataluren®, levels of Tgfβ2 increased to 80% of wildtype levels ($P<0.05$, $N=3$), whereas systemic delivery of Ataluren® did not have any significant effect on Tgfβ2 protein levels.

To confirm that Tgfβ2 protein was active the expression of phosphorylated SMAD2 (pSMAD2) was assessed as it is a downstream target of TGFβ receptor-activated signalling (Massagué, Seoane, & Wotton, 2005). In MSC control treated eyes pSmad2 was expressed at 62% of wildtype levels ($P<0.05$, $N=3$), However in eyes treated with Tgfβ2-MSCs pSmad2 levels were increased to 90% of wildtype levels ($P<0.05$, $N=3$). Similarly, eyes treated with topical Ataluren® showed a significant increase in pSmad2 expression ($P<0.05$, $N=3$) (Fig. 2.8 E,F)

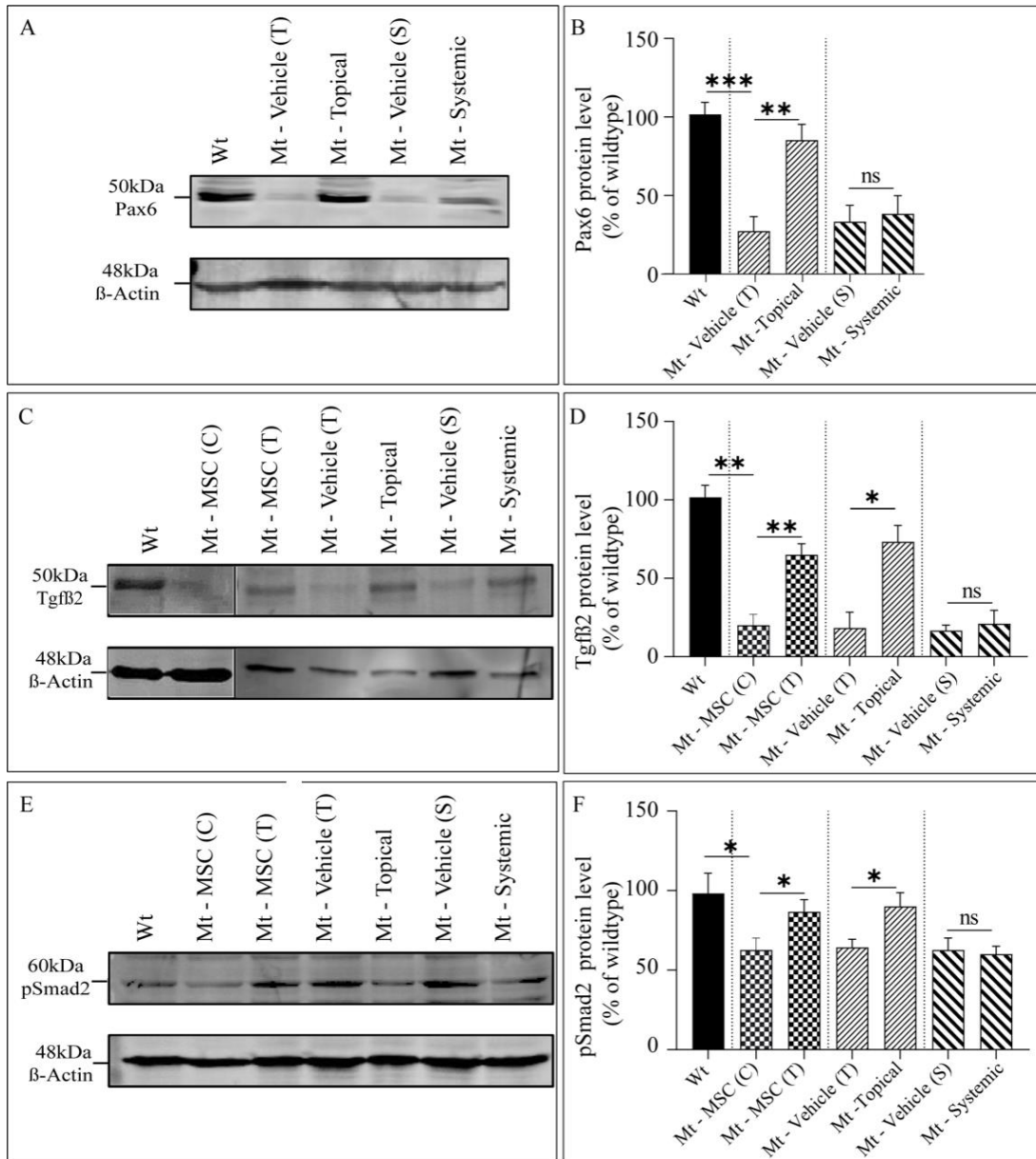


Figure 3.8: Protein expression analysis in treated *Pax6*^{Sey/+} mutant mouse eye tissue lysates
 Treatment groups for all images were: Wildtype, Wt; mutant treated with control MSCs, Mt-MSC (C); mutant treated with Tgfb2-MSCs, Mt-MSC (T); mutant treated with topical vehicle control, Mt-Vehicle (T); mutant treated with topical Ataluren®, Mt-Topical; mutant treated with systemic vehicle control, Mt-Vehicle (S); mutant treated with systemic Ataluren®, Mt-Systemic. Western blots of Pax6 (A), Tgfb2 (C) and pSmad2 (E). β-Actin used as loading control. Quantification of western blots for Pax6 (B), Tgfb2 (D) and pSmad2 (F). Data plotted as mean ± SEM (N = 3), and statistical significance was determined using the Student *t*-test, *P < 0.05, **P < 0.01, ***P < 0.001; n s = not significant.

3.3.4.3 Analysis of other proteins in the development of anterior chamber angle

Foxc1 is another downstream target of Pax6 and absence of Foxc1 is known to cause severe anterior segment dysgenesis (Mears et al., 1998). Therefore, we analysed the levels of Foxc1 protein in the anterior segment in the different treatment groups. Western blotting revealed an 84% reduction in Foxc1 protein in *Pax6*^{Sev/+} mutant eyes, whereas treatment with Tgfβ2-MSCs or topical Ataluren® increased levels of Foxc1 to 67.8% and 66.1% of wildtype, respectively (Fig. 2.9 A). Since the cornea is specifically affected in *Foxc1* mutants, changes in Foxc1 levels were measured by ELISA in the *Pax6*^{Sev/+} mutant cornea in the different treatment groups (Fig 2.9 B). In *Pax6*^{Sev/+} cornea, Foxc1 levels were decreased by 64.3% compared to wildtype (P<0.0001; N=6). Treatment with Tgfβ2-MSCs increased Foxc1 by 45.9% (P<0.05, N=6), whereas Ataluren® therapy significantly increased the levels of Foxc1 by 51.8% (P<0.0001, N=6).

We also tested for changes in Pitx2 protein expression as it is also important in anterior segment development and interacts specifically with Foxc1 (Berry et al., 2006). ELISA revealed that Pitx2 was decreased by 44.6% in *Pax6*^{Sev/+} corneal tissue compared to wildtype (Fig. 2.9 C; P<0.0001, N=6). Tgfβ2-MSCs increased Pitx2 protein levels by about 33.7% (P<0.001, N=6) and Ataluren® treatment raised Pitx2 levels by about 40.1% (P<0.0001, N=6) to almost wildtype levels. There was also a small (19.4%) but significant change in Pitx2 with systemic Ataluren® treatment (P<0.001, N=6).

In *Pax6*^{Sev/+} anterior chamber Tgfβ2 protein was reduced by about 49.8% compared to wildtype eyes (Fig. 2.9. D; P<0.001, N=6). Treatment with Tgfβ2-secreting MSCs resulted in a 61.2% increase in Tgfβ2 to above wildtype levels (P<0.0001, N=6). A similar 49.2% increase was evident in eyes treated with topical Ataluren® (P<0.0001, N=6). Systemic Ataluren® did not significantly affect the level of Tgfβ2 protein levels.

Finally, we studied the transcription factor Lmx1b which is important for the development of anterior chamber angle of the eye during early embryonic stage. In adults, haploinsufficiency of Lmx1b causes increase the intraocular pressure(Liu & Johnson, 2010; Pressman, Chen, & Johnson, 2000). The amount of Lmx1b protein in the *Pax6^{Sey/+}* mouse anterior chamber was reduced by 70% compared to wildtype eyes (Fig. 2.9 A). Treatment with MSCs or Ataluren® increased Lmx1b expression to 54% and 56%, respectively.

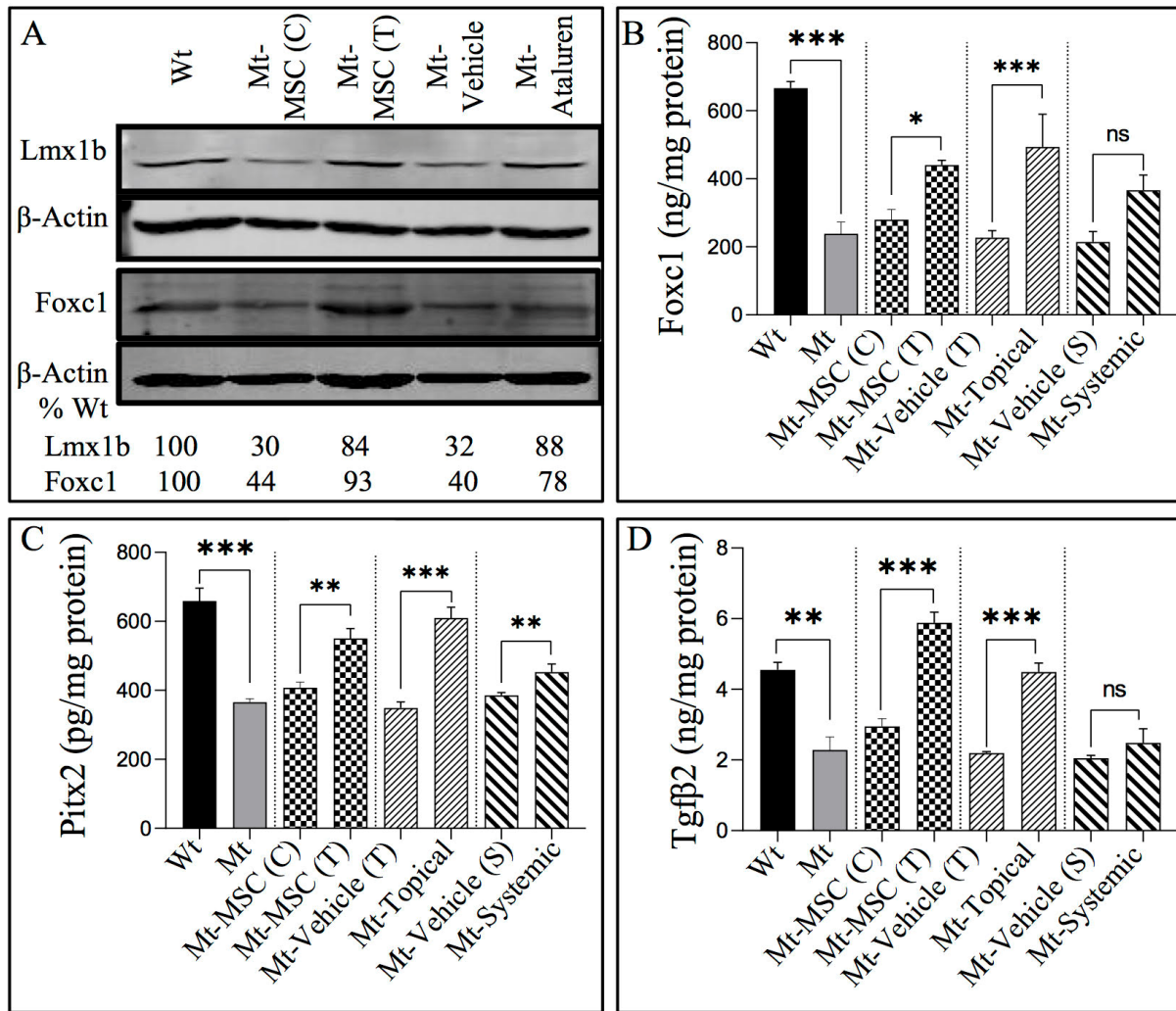


Figure 3.9: Analysis of other proteins in the development of anterior chamber angle

(A) Representative western blot showing increased Lmx1b and Foxc1 proteins in anterior segment lysates when mice were treated with Tgfb2-secreting MSCs (Mt-MSCs(T)) or by nonsense

suppression using Ataluren® therapy (Mt-Ataluren). β -Actin was used as a loading control. Densitometry was used to compare the level of Lmx1b and Foxc1 compared to wildtype (100%). Treatment groups for panels B-D were: Wildtype, Wt; mutant treated with control MSCs, Mt-MSC (C); mutant treated with Tgf β 2-MSCs, Mt-MSC (T); mutant treated with topical vehicle control, Mt-Vehicle (T); mutant treated with topical Ataluren®, Mt-Topical; mutant treated with systemic vehicle control, Mt-Vehicle (S); mutant treated with systemic Ataluren®, Mt-Systemic. (B) ELISA quantitation of Foxc1 in corneal tissue. (C) ELISA quantitation of Pitx2 in corneal tissue. (D) ELISA quantitation of Tgf β 2 in corneal tissue. Data presented as mean SEM. * $P < 0.05$, ** $P < 0.001$, *** $P < 0.0001$ (N=6).

3.4 Discussion

Anterior chamber abnormalities are one of several pathophysiology's observed in Aniridia patients. These individuals develop glaucoma in their early childhood which is caused by abnormalities in the development of ocular drainage structures. Under normal conditions intraocular pressure (IOP) is generated by resistance to the passage of aqueous humor produced by the ciliary body that flows through the trabecular meshwork and into Schlemm's canal. If the outflow is reduced either by a rigidity in the contractile tissue of the outflow pathway or developmental aberrations to these structures, then IOP will increase above normal leading to damage to the optic nerve. The histopathological analysis of the eyes of two children with aniridia syndrome has provided the supportive evidence for abnormal trabecular meshwork differentiation and the complete absence of Schlemm's canal (Grant & Walton, 1974) which prompted this study.

In the normal mouse eye, both trabecular meshwork and Schlemm's canal develop postnatally from P5 and are functionally mature by P21. This provided a window of opportunity to treat the anterior chamber defects. The trabecular meshwork originates from the neural crest-derived periocular mesenchyme (POM) cells that migrate to the eye (Gage, P. J., Rhoades, Prucka, & Hjalt, 2005), whereas Schlemm's canal is of mesodermal origin derived from blood vessels that enter the eye at the junction between the cornea and sclera (Cvekl & Tamm, 2004). A potential

way by which Pax6 acts indirectly on neural crest-derived mesenchyme in the eye could be by altering the secretion of lens-derived signaling molecules (Baulmann et al., 2002). The development of the trabecular meshwork and Schlemm's canal requires a low and transient expression of Pax6 on the mesenchymal cells during early postnatal days (Smith et al., 2001). This low level of expression is considered important for the expression of signaling molecules by Pax6 which helps in the differentiation of trabecular meshwork (Baulmann et al., 2002). Differentiation of migrating neural crest cells is regulated by dosage-sensitive transcription factors including Foxc1 (Gage et al., 2005) and Pitx2 (Evans & Gage, 2005), and mutations in the respective genes are associated with glaucoma and other iridocorneal defects in humans (Alward et al., 1996; Mears et al., 1998; Strungaru, Dinu, & Walter, 2007). In *Foxc1*^{+/-} haploinsufficient mice, POM development is abnormal resulting in a small or absent Schlemm's canal and hypoplastic trabecular meshwork (Smith, R. S. et al., 2000). In haploinsufficient *Pitx2*^{+/-} mice, anterior segment defects include an undeveloped ciliary body and iridocorneal synechiae (iris stump) which block the outflow pathway leading to increased IOP (Chen, L. S. & Gage, 2016). The mechanisms by which haploinsufficiency of these transcription factors leads to these defects is incompletely understood because their activity is required at different times and in different cells, during development and postnatal maturation of the outflow pathway (Gage, Philip J. & Zacharias, 2009).

At E12 the POM cells migrate into the space between the lens and surface ectoderm, which then mature by a process of mesenchyme-epithelial transition (MET) into the corneal endothelium via inductive cues initiated from the lens epithelium (Beebe & Coats, 2000; Reneker, Silversides, Xu, & Overbeek, 2000; Zhang, Y., Overbeek, & Govindarajan, 2007). Abnormal formation of the corneal endothelium results in anterior segment defects such as iridocorneal synechiae (Gage & Zacharias, 2009). It has been demonstrated that initiation of MET involves Tgfβ2 directly

downregulating both *Foxc1* and *Pitx2* in the POM (Silla, Naidoo, Kidson, & Sommer, 2014). This suggests that in conditions of reduced Tgf β 2 (i.e. *Pax6*^{Sev/+} haploinsufficiency) that MET may not be initiated correctly leading to abnormal corneal endothelium differentiation and the subsequent iridocorneal synechiae. By E16.5, expression of *Foxc1* is restricted to the region of the future trabecular meshwork, where it is required for trabecular meshwork formation (Kidson, Kume, Deng, Winfrey, & Hogan, 1999). In mice that are deficient in the Tgf β 2 receptor the trabecular meshwork and ciliary body do not develop supporting the role of Tgf β 2 in this process (Ittner et al., 2005).

In the developing iridocorneal angle and in mature tissue, FoxC1 and Pitx2 are required for establishing angiogenic privilege and for preserving corneal transparency by regulating vascular development (Chen & Gage, 2016; Gage, Philip J., Kuang, & Zacharias, 2014; Seo et al., 2012). In aniridia, corneal keratopathy manifests as a VEGF-dependent neovascularization into the transparent corneal stroma (Ambati et al., et al 2006), thickening of the central cornea, appearance of goblet cells, corneal erosion and opacities in the cornea (Lee et al., 2008). Thus, since Foxc1 is reduced in adult mouse *Pax6*^{Sev/+} cornea, then this could account for the corneal deficits associated with vascular overgrowth in aniridic corneal keratopathy.

Lmx1 is another important factor which is responsible for anterior chamber development. Lmx1 is expressed in the POM during development and then in adult tissues in the trabecular meshwork, corneal stroma and anterior iris stroma. *Lmx1* mice die soon after birth however, the eyes lack a ciliary body, have a thin cornea and abnormal iris (Chen, H. et al., 1998). However, using a conditional *Lmx1* allele and a Cre recombinase that is active in neural crest cells, it has been demonstrated that Lmx1 is necessary for the development of trabecular meshwork and for preventing corneal neovascularization in the adult mouse (Liu, P. & Johnson, 2010). Thus, since

Lmx1 is reduced in the adult *Pax6*^{Sev/+} anterior segment it may be associated with maintaining corneal transparency as well as contributing to abnormalities of the trabecular meshwork. Then identity of the downstream targets of the Lmx1 transcription factor remain to be determined.

In the adult lens epithelium transcription of *Tgfβ2* is under the direct control of Pax6 (Wolf et al., 2009). Tgfβ2 protein is secreted by the lens into the aqueous humor where it acts as an immunosuppressant (Cousins, McCabe, Danielpour, & Streilein, 1991) and is involved in the turnover of the extracellular matrix proteins in the trabecular meshwork (Fuchshofer & Tamm, 2009). For example, heparan sulfate is expressed in the extracellular matrix of the iridocorneal angle and on the surface of trabecular meshwork cells (Tawara, Varner, & Hollyfield, 1989). Mice that are deficient in heparin sulfate have decreased Tgfβ2 expression in the POM, with a concomitant down-regulation of *Foxc1* and *Pitx2* expression and adhesion of the lens to the cornea (Iwao et al., 2009), a phenotype also observed in *Pax6*^{Sev/+} and *Tgfβ2*-deficient mice (Saika et al., 2001) The heparin sulfate-deficient mice also have raised IOP similar to mice with conditional loss of Pax6 in the cornea and lens, associated with optic nerve damage and subsequent glaucoma (Kroeber et al., 2010). These observations are in support of our data suggesting that cell-based delivery of exogenous Tgfβ2 protein can rescue the anterior segment abnormalities in the *Pax6*^{Sev/+} haploinsufficient mouse eye via changes in Foxc1/Pitx2 expression levels during the early postnatal period.

Long-term over expression of Tgfβ2 in the aqueous humor and trabecular meshwork cells is associated with raised intraocular pressure leading to primary open-angle glaucoma (POAG) (Agarwal, Daher, & Agarwal, 2015; Tripathi, Li, Chan, & Tripathi, 1994). The cause of elevated Tgfβ2 in POAG is not known, however excess Tgfβ2 stimulates connective tissue growth factor (CTGF) to increase the synthesis of fibrillar extracellular matrix (ECM) components in the TM

(Junglas, Yu, Welge-Lüssen, Tamm, & Fuchshofer, 2009). In addition, there is an increase in contractility of the TM actin cytoskeleton (Junglas et al., 2012). Together these changes are thought to lead to an overall stiffening of the outflow tissue and an increase in IOP (Braunger, Fuchshofer, & Tamm, 2015). Thus, it is possible that if the amount of Tgfβ2 provided by the cell-based delivery to the *Pax6*^{Sev/+} mouse eye went above normal levels, than damage to the newly formed TM could occur in the longer term. However, it should be noted that MSCs only survive for about 6 weeks so repeat injections would be required to maintain the correct amount of Tgfβ2, and IOP could be monitored serially to determine if there were any changes with treatment.

In comparison to *ex vivo* delivery of a downstream target of Pax6 (i.e., Tgfβ2) into the eye, we examined the effect of RNA nonsense suppression using the drug Ataluren® to override the underlying nonsense mutation in *Pax6* and thereby produce Tgfβ2 endogenously. This RNA approach has been tested in a variety of diseases (Du et al., 2008; McDonald et al., 2017; Welch et al., 2007) and in animal models of ocular conditions such as coloboma and retinitis pigmentosa (Guerin et al., 2008; Moosajee, Mariya, Gregory-Evans, Ellis, Seabra, & Gregory-Evans, 2008). We have previously used this approach postnatally in the *Pax6*^{Sev/+} mouse which showed reversal of tissue damage to the retina and corneal epithelium, but did not perform an in depth analysis of the effect of treatment on the anterior chamber outflow structures. Topical eye drops containing Ataluren® (START therapy) resulted in formation of Schlemm's canal and TM beams, very similar to the Tgfβ2 therapy. Systemic treatment however did not improve the outflow pathway structures which correlated with little or no change in the levels of Tgfβ2, Foxc1 and Pitx2. Since the central cornea is lacking a blood supply, it is unlikely that Ataluren® could reach the *Pax6* expressing tissues at a high enough concentration to induce nonsense suppression.

In conclusion, both cell-based delivery of exogenous Tgfβ2 and START therapy to produce endogenous Tgfβ2 were able to rescue the outflow pathway structures. Treatment with Tgfβ2- MSCs partially rescued the ocular drainage structures such as beams of trabecular meshwork cells and Schelmn's canal. Furthermore, the decreased expression of Foxc1 and Pitx2 in the postnatal anterior segment and cornea of the *Pax6*^{Sev/+} eye was reversed by this treatment, suggesting they are either direct or indirect targets of Tgfβ2 signalling. In addition, we compared this cell-based delivery of Tgfβ2 to directly treating the underlying mutation in *Pax6* using an RNA nonsense suppression therapy. Similar improvements in the anterior segment tissues and changes in protein expression were also observed with nonsense suppression. Thus, START therapy would be the approach of choice for aniridia patients with *PAX6* nonsense mutations whereas *TGFβ2* therapy would be an approach to use in all other types of *PAX6* mutation. The outcome of such novel treatment strategies could provide effective long-term therapeutic benefits that may be able to replace the inadequate medical and surgical procedures for aniridic glaucoma.

Chapter 4: Nonsense suppression therapy in an animal model of Usher 1D syndrome

4.1 Chapter introduction

Usher 1D syndrome (USH1D; OMIM # 601067) is characterized by severe hearing impairment and progressive vision loss in the form of retinitis pigmentosa. This syndrome is inherited in an autosomal recessive pattern and is caused by mutations of the cadherin 23 (*CDH23*) gene. Profound hearing loss is present in early infancy and progressive vision impairment is apparent within the first decade of life (Okano et al., 2019). *CDH23* is the structural protein present in the cilia of the photoreceptors of the retina and stereocilia of the cochlea. There are no treatments available for the vision loss, however, cochlear implants have been useful for maintaining some hearing capacity (Mathur & Yang, 2015). Due to the large size of the *CDH23* cDNA (10 Kb), traditional gene augmentation is not possible using validated gene therapy vectors for the retina (e.g. adeno-associated viruses), therefore other pre-clinical therapies need to be considered.

4.1.1 Nonsense suppression therapy for USH1D syndrome

Based on our experience with nonsense suppression we considered testing this approach for the USH1D phenotype. Since this approach is systemic, both the eye and hearing defects can be targeted. Previously, nonsense suppression had been evaluated and found to be successful for Usher 1C syndrome (mutations in the *USH1C* gene coding for Harmonin) in *in vitro* and in *ex vivo* retinal explants (Goldmann, Tobias et al., 2012). However, it was not tested *in vivo* as there was

no naturally occurring nonsense mutant allele. Thus, the effect of nonsense suppression on hearing loss and retinal dysfunction could not be evaluated.

4.1.1.1 Specific hypothesis

- Nonsense suppression by pre- and postnatal delivery of the small molecule drug Ataluren® will rescue the ocular and hearing deficits in the *Cdh23*^{m1btlr^{-/-}} mouse carrying a nonsense mutation.

4.1.1.2 Rationale

Unfortunately, most of the current mouse models of Usher syndrome, including USH1D, do not have the retinal degeneration phenotype (Slijkerman et al., 2015) so testing retinal therapies has been hampered. However, a previous analysis of null *Cdh23* mutant mice alleles suggested that despite no evidence of retinal degeneration by histological analysis there is retinal dysfunction (Libby, Richard T., Kitamoto, Holme, Williams, & Steel, 2003). In this study one allele had a 20% reduction in a- and b-waves of the ERG, and another allele had faster implicit times for both a- and b-waves. Of the 10 *Cdh23* alleles that have been studied none of them had a nonsense mutation. We searched through a number of mouse repositories of genetic mutants: The Jackson Laboratory (<https://www.jax.org/>); Mutant Mouse Resource Research Centers (<https://www.mmrc.org/>); Canadian Mutant Mouse Repository (<http://www.cmmr.ca/>); and Mutagenetix (<https://mutagenetix.utsouthwestern.edu/>). One allele generated at Mutagenetix was identified and available as a heterozygous frozen sperm allele: *Cdh23*^{m1btlr^{+/-}} with a Y2209X mutation. Therefore, the line was regenerated at Mutagenetix and we obtained the heterozygous line for investigation.

4.1.1.3 Experimental design

The *Cdh23*^{m1btr+/-} mouse line carrying a heterozygous Y2209X (A>T transition) was in-crossed to produce homozygous test mice. Mice were initially assessed by electroretinography (ERG) at P45 and P90 to determine if abnormal electroretinographic responses are present. Two drug treatment protocols (prenatal and postnatal) were carried out: (1) prenatal: time-mated pregnant mice received daily subcutaneous injections of 30 µg/g Ataluren® and then offspring received the same daily injections from P4 to P90; (2) postnatal: mice from P4-P120 received daily injections of 30 µg/g Ataluren®. ERGs were measured at P45, P90 and P120. Mice were then euthanized to obtain retinal and cochlear tissue to determine the protein concentration of Cdh23. In addition, immunohistochemistry was performed to examine the effect of nonsense suppression on the mutant stereocilia phenotype and retinal photoreceptors. We further analyzed the structural benefit by transmission electron microscopy (TEM) for retinal photoreceptors.

4.2 Methods

3.2.1. Animal husbandry and breeding

This study was carried out in accordance with protocols compliant with the Canadian Council on Animal Care (CCAC) and with the approval of the local Animal Care Committee (ACC) at the University of British Columbia, Vancouver, Canada. Heterozygous *Cdh23*^{m1btr+/-} mice were obtained from Mutagenetix, Beutler Lab, UT Southwestern Medical Center. All mice were bred and maintained on a 12-h light/dark cycle and had easy access for water and food *ad libitum*. Equal number of male and female mice were used. Mating of heterozygous pairs of mice were used to generate homozygous offspring.

3.2.2. Genotyping of *Cdh23*^{m1btlr/-} mice

Homozygous *Cdh23* mutant offspring were identified by genotyping. DNA from an ear sample was aseptically collected using ear punches and DNA was extracted by the NaOH method as described previously (Truett et al., 2000). Extracted DNA was amplified by PCR using the following specific primers for *Cdh23*: Forward primer: 5'-GCTAGAGCACAGCCACCTTC-3' and reverse primer: 5'-CCCGAGTTCCTCAACCCTAT-3'. Amplified products were digested with *BaeI* restriction enzyme (New England Biolabs, Massachusetts, USA) at 25°C for 8 hours followed by heat inactivation at 65°C and separated by 3% agarose gel electrophoresis. The homozygous mutant does not have the *BaeI* restriction digestion site so will not produce fragments whereas the wildtype has 2 sites and heterozygous 3 restriction sites. Primers to determine the status of other potential null mutations in the *Cdh23*^{m1btlr/-} strain are listed in Table 3.1.

Gene	Mutant site	Primer used for sequencing	Covering chromosome region	PCR size (bp)
<i>Aggf1</i>	Chr13: 95,371,656 T>A	Forward 5'-TGTTCCAGACGCCTTTACC-3' Reverse 5'CTTGACTTGTGAATGCTGAA AAAGG-3'	Chr13: 95371262- 95371800	539
<i>Carmil3</i>	Chr14: 55,502,435 T > C	Forward 5'-GCCAACTGGGAAGTTTGGG-3' Reverse 5'-TCCCTTCCCTCTTTCCTCC-3'	Chr14: 55502249- 55502732	484
<i>Tiprl</i>	Chr1: 165,222,523 A > G	Forward 5'-CCTCTTCTGACCTCCAATGAC3' Reverse 5'-CAAATGTGAATACCGATGCTATGC-3'	Chr1: 165222193- 165222759	567
<i>Txndc16</i>	Chr14: 45,165,361 T > A	Forward 5'-TGGGTGGCTTCTTTAGACGA-3' Reverse 5'-AAAAGCAATTGTGCATTTTCA-3'	Chr14: 45165217- 45165459	243

Table 4.1: Primers for other null mutations in *Cdh23*^{m1btlr/-} Y2207X mouse strain

3.2.3 Systemic injection of Ataluren® in *Cdh23^{m1btlr-/-}* mice

A once daily subcutaneous injection of a suspension of 1% Ataluren® (Selleckchem, Houston, TX, USA) was given to pregnant *Cdh23^{m1btlr+/-}* dams beginning at E12.5 and then to their offspring from P4 onwards as previously described (Wang et al., 2017). The control group of mice were sham injected with normal saline or sterile PBS.

4.2.1.1 Immunohistochemistry

The protocol for cryosection immunohistochemistry is as described in section 2.2.6. Primary antibodies used in this study and their dilution factor were: rabbit polyclonal antibody to human Cadherin 23 (1:500; Catalog #: C354296, Lifespan Biosciences, Seattle, USA); rabbit polyclonal antibody to mouse Recoverin (1:1000; Catalog #:5585, Millipore-Sigma, Etobicoke, Canada); mouse monoclonal antibody to mouse visual Arrestin (1:300; Catalog #: 5580, Millipore Sigma, Etobicoke, Canada); mouse monoclonal antibody to Rhodopsin (1:500; Catalog #: ab5417, Abcam, Toronto, Canada). The secondary antibodies used were conjugated Alexa Fluor® 594 goat anti-mouse IgG (Fisher Scientific Ottawa, ON, Canada; A-11005, 1:200, IHC), Alexa Fluor® 488 goat anti-mouse IgG (Fisher Scientific Ottawa, ON, Canada; A-11001, 1:200, IHC), Alexa Fluor® 488 goat anti-rabbit IgG (Fisher Scientific Ottawa, ON, Canada; A-11008, 1:200, IHC), Alexa Fluor® 594 goat anti-rabbit IgG (Fisher Scientific Ottawa, ON, Canada; A-11012, 1:200, IHC); DAPI was used to counterstain nuclei. Images were obtained using scanning confocal microscopy. For each staining experiment a negative control was performed to test nonspecific staining. Tissue sections were stained with secondary antibodies with no primary antibody.

4.2.1.2 Electrorretinography

For ERG analysis, the mice to be tested were dark adapted for overnight. Electrorretinograms were recorded at P45, P90 and P120 in Wild type and treated *Cdh23^{m1bitr/-}* groups. Mice were anesthetized with xylazine (4 mg/kg, Rompun, Bayer Healthcare) and ketamine (70 mg/kg, Vetalar, Bioniche Animal Health) and kept on a heating pad to maintain the body temperature at 37°C. The corneas were anesthetized by topically with 0.5% proparacaine hydrochloride (Bausch and Lomb, Rochester, NY, USA) and the pupils were dilated with 2.5% phenylephrine and 1% atropine. To maintain corneal hydration in the animals a drop of 2% hydroxy-propyl-methylcellulose was placed on the cornea. Electrical responses of the retina were recorded using an Espion V5 Electrorretinogram Console plus ColorDome (Diagnosys LLC, Lowell, MA, USA) with corneal gold foiled electrodes. Scotopic (rod function) and photopic ERGs (mixed rod and cone function) were carried out using white flashes of intensity 2.25 cd.s/m² and 3.0 cd.s/ m² respectively. Furthermore, cone functional response were recorded by 30Hz flicker with white light flashes of 2.25 cd.s/m². The ERGs were recorded by averaging 15 recordings taken for rod responses and averages of 50 for 30Hz flicker cone responses. Average amplitudes of rod and cone functional responses are presented as means \pm SEM.

4.2.1.3 Statistics

For ERG analyses, the significance of the differences between the treated and untreated groups were analyzed by unpaired 2-tailed Student's *t* test. A P value of less than 0.05 was considered statistically significant. All values were presented as the mean \pm standard error of the mean (SEM).

4.3 Results

4.3.1 Preclinical model of USH1D

Before being able to test the hypothesis we first had to characterize the *Cdh23*^{m1btlr+/-} mutant mouse model obtained from Mutagenetix (Beutler lab, UT Southwestern Medical Center and, Texas, USA). Since this mutant was generated by ENU mutagenesis where multiple mutations occur, whole exome sequencing at Mutagenetix was carried out to reveal all coding sequence mutations. The breeding strategy performed at Mutagenetix was as follows: The ENU mutant mice were bred with C57BL/6 to produce the G0 generation and then crossed again with C57BL/6 to obtain generation G1. Sperm was then stored until recovered for us by Mutagenetix. This line was regenerated at Mutagenetix and the heterozygous line was sent to us. In our animal facility, we have backcrossed the mice ourselves through 4 generations to C57BL/6.

4.3.2 Assessment of incidental mutations in the *Cdh23*^{m1btlr+/-} mouse

Whole exome sequencing had revealed 62 other gene mutations in the *Cdh23*^{m1btlr+/-} mutant that could potentially contribute to the homozygous phenotype if they were recessively inherited as well. None of the heterozygous mutations caused an apparent phenotype in mice. The majority of mutations (58/62) were missense mutations of which 15/58 were classified as benign, 9/58 possibly damaging, and 34/58 probably damaging, and none of them would not respond to Ataluren® therapy. However, 4 of the mutations (in *Aggf1*, *Carmil3*, *Tiprl* and *Txndc16*) were potentially null alleles that could respond to Ataluren® therapy. Therefore, the status of these 4 mutations in the homozygous *Cdh23*^{m1btlr-/-} mice were assessed by Sanger sequencing.

In the *Aggf1* gene there is a T>A change (position 13: 95,371,656 [genome assembly GRCm38.p6]) resulting in the creation of a new splice-site acceptor that results in a premature stop codon after the addition of 4 new amino acids (Fig. 3.1). If translated, this would result in a truncated protein of 75 amino acids (*Aggf1* protein is 711 amino acids in length). However, it is likely to be degraded by nonsense-mediated decay resulting in no protein product.


```

Query: None Query ID: lcl|Query_61245 Length: 537
>Mus musculus BAC clone RP23-330F6 from 13, complete sequence
Sequence ID: AC133188.4 Length: 201730
Range 1: 156704 to 157240

Score:992 bits(537), Expect:0.0,
Identities:537/537(100%), Gaps:0/537(0%), Strand: Plus/Plus

Query 1      TGTTCAGACGCCTTTACCTCTGACTGAGAACCTGACTCAAGCAACAAGAACAGAATAC 60
Sbjct 156704 TGTTCAGACGCCTTTACCTCTGACTGAGAACCTGACTCAAGCAACAAGAACAGAATAC 156763

Query 61     TTAGTGAGCACTGAAAACATACAAAAGCATTAAATAAGTTAGAAATTATAATACATCCC 120
Sbjct 156764 TTAGTGAGCACTGAAAACATACAAAAGCATTAAATAAGTTAGAAATTATAATACATCCC 156823

Query 121    TATTTTGCCACCCAAAAATTGACAAAAAAGTGATATAGACAGAAATCTGTATTATCAGAT 180
Sbjct 156824 TATTTTGCCACCCAAAAATTGACAAAAAAGTGATATAGACAGAAATCTGTATTATCAGAT 156883

Query 181    TCCTCCTATTTTCATATTTTGTCTGTATTATTTTAAAGAAACACTACACCCATGTGTCA 240
Sbjct 156884 TCCTCCTATTTTCATATTTTGTCTGTATTATTTTAAAGAAACACTACACCCATGTGTCA 156943

Query 241    TGAATGTTCCGAGGGTACTAGTGCAACTATACTGAGTACCTGAAATCGCCCAAGGAGCTT 300
Sbjct 156944 TGAATGTTCCGAGGGTACTAGTGCAACTATACTGAGTACCTGAAATCGCCCAAGGAGCTT 157003

Query 301    GGCTCTCTGTCTGTACTTCTACATCAGACTTCGGATTATCTTCATTTTTCCACAATGGA 360
Sbjct 157004 GGCTCTCTGTCTGTACTTCTACATCAGACTTCGGATTATCTTCATTTTTCCACAATGGA 157063

Query 361    GTATTTTACTAAGTTCTTCTACCTGAAAGGAAACAGAGCTTTAGGAAAAATAACCATAAA 420
Sbjct 157064 GTATTTTACTAAGTTCTTCTACCTGAAAGGAAACAGAGCTTTAGGAAAAATAACCATAAA 157123

Query 421    GCAACTCAGTAATACACAACCCCTCCACCATCCTCAGAACATTGCAGGCACCTTATCTTGGT 480
Sbjct 157124 GCAACTCAGTAATACACAACCCCTCCACCATCCTCAGAACATTGCAGGCACCTTATCTTGGT 157183

Query 481    AGAACTTTTAGACCTGTACCCAAAGCATCTGGCTCCTTTTTCAGCATTACAAGTCA 537
Sbjct 157184 AGAACTTTTAGACCTGTACCCAAAGCATCTGGCTCCTTTTTCAGCATTACAAGTCA 157240

```

Figure 4.2: Sequence analysis of *Aggf1* in *Cdh23^{m1btr/-}* Y2207X mouse strain.

The Query sequence (*Aggf1*) is from *Cdh23^{m1btr/-}* mouse; the reference sequence (Sbjct) is the from a wildtype mouse BAC clone. Green boxes: primer sequences used for sequencing. Red box, location of expected mutation site.

In mice a homozygous *Aggf1* mutation is embryonic lethal at E8.5 (Zhang T et al, 2016) and since the *Cdh23^{m1btlr/-}* mice survive, this mutation is unlikely to be a factor in our model. In addition nonsense suppression treatment does not start until E12.5, so this would have no effect on an embryonic lethal mutation at E8.5. Sanger sequencing was used to confirm the status of this *Aggf1* mutation in the *Cdh23^{m1btlr/-}* mice, revealing that the mice were homozygous for the wildtype T allele (Fig. 3.2), so the mutation would have no phenotypic effects.

In the *Carmil3* gene there is a T>C change (position 14: 55,502,435 [genome assembly GRCm38.p6]) in the splice-site donor sequence of exon 31. This results in loss of splicing and instead, the addition of 51 new amino acids before a premature stop codon occurs. (Fig. 3.3) Postnatal CRISPR targeting of *Carmil3* in mouse pups at P0 caused a reduction in dendritic protrusions during spinogenesis at P14, suggesting an involvement in synapse formation (Spence et al. 2019). No knockout mouse mutants for *Carmil3* have been published so phenotypic information is not available. No causative mutations have been identified in the human mutation databases (ClinVar, 1000 genomes), although high levels of CARMIL3 protein is associated with breast and prostate cancer metastasis (Wang, H. et al., 2020). It is therefore unclear what effect this mutation might have in the *Cdh23^{m1btlr/-}* mice but could have some effect on brain development. Sanger sequencing was used to confirm the status of this *Carmil3* mutation in the *Cdh23^{m1btlr/-}* mice, revealing that the mice were homozygous for the wildtype T allele (Fig. 3.4), thus the mutation would have no phenotypic effects.

In the *Tiprl* gene there is an A>G change (position 1: 165,222,523 [genome assembly GRCm38.p6]) in a splice donor which is considered an alternative donor isoform/cryptic donor. The DNA change at this site still results in a cryptic donor. However, if the new donor sequence is skipped then another 20 amino acids would be added before a stop codon is encountered (Fig. 3.5). There are no mouse models available for *Tiprl* phenotype analysis. The Tiprl protein is ubiquitously expressed with a role in autophagy (Johnson, C. E. & Tee, 2017). No causative mutations have been identified in the human mutation databases (ClinVar, 1000 genomes), however, upregulation of TIPRL induces autophagy and thereby potentiates lung cancer survival (Jeon et al., 2019). Therefore, the effect that *Tiprl* mutation would have in the *Cdh23^{m1btlr-/-}* mice is unclear. Sequencing of the *Tiprl* mutation in the *Cdh23^{m1btlr-/-}* mice revealed that the mice were homozygous for the wildtype allele (Fig. 3.6), thus it would have no effect on the phenotype.


```

Query: None Query ID: lcl|Query_34721 Length: 536
>Mus musculus targeted KO-first, conditional ready, lacZ-tagged mutant allele Tiprl:
Sequence ID: JN957690.1 Length: 38809
Range 1: 28244 to 28774

Score:974 bits(527), Expect:0.0,
Identities:530/531(99%), Gaps:1/531(0%), Strand: Plus/Minus

Query 7      AGTGCATGAAAGCAA-CGTTCAACAACATAAAATAAAATACCTAAAGCATCCATCCAACA 65
Sbjct 28774  AGTGCATGAAAGCAAACGTTCAACAACATAAAATAAAATACCTAAAGCATCCATCCAACA 28715

Query 66     TGCTACCTGCAGATTCTACAAATATCATTTTAAATTATGAACATAAAAAATTAAGTCACAG 125
Sbjct 28714  TGCTACCTGCAGATTCTACAAATATCATTTTAAATTATGAACATAAAAAATTAAGTCACAG 28655

Query 126    TTTTCATTCAGTCAAGTTGAATAATAAGCAAATAACCAAAGATGCTGGACAGGTATATT 185
Sbjct 28654  TTTTCATTCAGTCAAGTTGAATAATAAGCAAATAACCAAAGATGCTGGACAGGTATATT 28595

Query 186    TTTAAAAAGACTAAATATCATTGTTTCTGGTAAATGTCACAAAGCTGTGCTGTAGACTTA 245
Sbjct 28594  TTTAAAAAGACTAAATATCATTGTTTCTGGTAAATGTCACAAAGCTGTGCTGTAGACTTA 28535

Query 246    AACCTTACAAGGCATCACACCAGCCGCTGGTGAGAATGGAGGATTAATTTGAGTACTCAC 305
Sbjct 28534  AACCTTACAAGGCATCACACCAGCCGCTGGTGAGAATGGAGGATTAATTTGAGTACTCAC 28475

Query 306    AATTTTCACACTCAGGCTGGAAACACCATGATCATGCAATTCATCTTCAAACAGGAGAAC 365
Sbjct 28474  AATTTTCACACTCAGGCTGGAAACACCATGATCATGCAATTCATCTTCAAACAGGAGAAC 28415

Query 366    TTCTTCAAAAAATTAATCTGTTCTCTGGCTTTCAATTTTTCTGTATCTATATGATCTGT 425
Sbjct 28414  TTCTTCAAAAAATTAATCTGTTCTCTGGCTTTCAATTTTTCTGTATCTATATGATCTGT 28355

Query 426    TGTAGGTACAACCTGAAATACACAATTTTAAATGACGACTTTCAATGAAAAGCACTAGAG 485
Sbjct 28354  TGTAGGTACAACCTGAAATACACAATTTTAAATGACGACTTTCAATGAAAAGCACTAGAG 28295

Query 486    TTGCAAGAAAGTTTGATCATTTCCTTTGCATAGCATCGGTATTACATTTG 536
Sbjct 28294  TTGCAAGAAAGTTTGATCATTTCCTTTGCATAGCATCGGTATTACATTTG 28244

```

Figure 4.6: Sequence analysis of *Tiprl* in *Cdh23^{m1btlr/-}* Y2207X mouse strain.

Query sequence (*Tiprl*) is from *Cdh23^{m1btlr/-}* mouse; the reference sequence (Sbjct) is the from the wildtype mouse sequence. Green boxes: primer sequences used for sequencing. Red box: location of expected mutation site

There is a T>A change (position 14: 45,165,361 [genome assembly GRCm38.p6]) resulting in an in-frame nonsense mutation (R101X) in a variant transcript of the *Txndc16* gene (Fig. 3.7). The main *Txndc16* transcript on the forward DNA strand encodes 822 amino acids. The *Txndc16* variant transcript on the reverse strand encodes only 119 amino acids because the 5' sequence is incomplete. Thus, it is questionable as to whether it has any relevance in the *Cdh23^{m1btlr-/-}* mice. The main Txndc16 protein is a ubiquitously expressed glycoprotein in the endoplasmic reticulum. No live mice are available to assess the phenotype and no mutations have been identified in the human gene. Little is known about the function of the protein, although it is an antigen marker for meningiomas (Harz et al., 2014). If the variant transcript is made then Ataluren® is predicted to read through it.

Gene	Mutation	Predicted or known effect	Expression	Mouse phenotype	Human phenotype	Refs
<i>Txndc16</i>	R101X T>A	Probably null	Ubiquitous, ER glycoprotein	Mouse strain archived, no phenotype information	No mutations identified. Benign brain tumor antigen	Harz C et al., 2014

```

Query: None Query ID: lcl|Query_11081 Length: 212

>Mus musculus BAC clone RP23-248E1 from chromosome 14, complete sequence
Sequence ID: AC154575.2 Length: 210912
Range 1: 188715 to 188925

Score:377 bits(204), Expect:9e-101,
Identities:209/211(99%), Gaps:1/211(0%), Strand: Plus/Plus

Query 3      TTAttttttttttC-AAAGGGACTCCATGGATGTTAACATTCCCTCAGCACGCTAATGTG 61
            |||
Sbjct 188715 TTATTTTATTTTCAAAGGGACTCCATGGATGTTAACATTCCCTCAGCACGCTAATGTG 188774

Query 62      GCCTTCAGAAGAGCAGAGAAGGTTAGTCATTTTACACACTGGTCTGTAATTTACCTCTT 121
            |||
Sbjct 188775 GCCTTCAGAAGAGCAGAGAAGGTTAGTCATTTTACACACTGGTCTGTAATTTACCTCTT 188834

Query 122     TGAGCTAAAGTAGTCCATGTGGACTAAAGTATTACATGTTTACTATTAGAAAGATCTTTA 181
            |||
Sbjct 188835 TGAGCTAAAGTAGTCCATGTGGACTAAAGTATTACATGTTTACTATTAGAAAGATCTTTA 188894

Query 182     AATTATCATTTGAAAAATGCACAATTGCTTTT 212
            |||
Sbjct 188895 AATTATCATTTGAAAAATGCACAATTGCTTTT 188925

```

Figure 4.7: Effect of mutation of *Txndc16* in *Cdh23^{m1btlr/-}* Y2207X mouse strain.

The *Tyndc16* has an in-frame nonsense mutation in a variant transcript. Query sequence (*Txndc16*) is from *Cdh23^{m1btlr/-}* mouse; the reference sequence (Sbjct) is the from a mouse BAC clone. Green boxes: primer sequences used for sequencing. Red box: location of mutation

4.3.3 Reduced body weight in homozygous *Cdh23^{m1btlr/-}* mice

Both male and female homozygous *Cdh23^{m1btlr/-}* mice were consistently smaller compared to sex-matched heterozygous littermates (Fig. 3.8A). The body weight of female homozygous mice was significantly lower than the male homozygous mice (Fig 3.8B). There were no differences in the body weight of heterozygous littermates when compared to wild type mice.

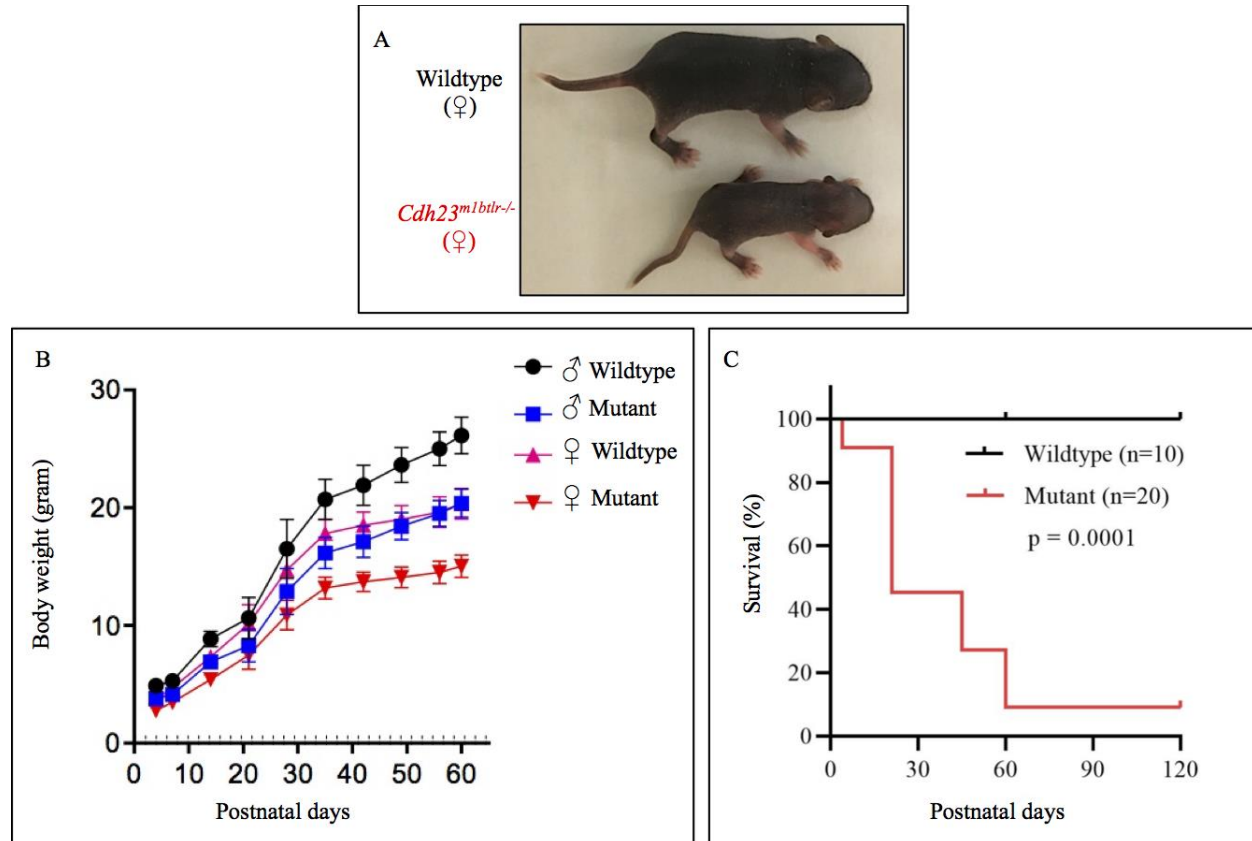


Figure 4.8: Lifespan of homozygous *Cdh23^{m1btlr/-}* mice.

(A) Representative images of wildtype and *Cdh23^{m1btlr/-}* homozygous mice (B) Body weight plot over time comparing male and female homozygous age-matched *Cdh23^{m1btlr/-}* mice and wildtype mice. (C) Kaplan-Meier Mantel-Cox survival curve plotted against of wildtype and *Cdh23^{m1btlr/-}* homozygous mice ($p < 0.0001$ wildtype N= 10; Mutant N=20)

4.3.4 Decreased survival rates in *Cdh23^{m1btlr/-}* homozygous mice

Survival differences started to appear compared to wildtype and homozygous *Cdh23^{m1btlr/-}* mice at around the first week of birth. About 10% and 40% of *Cdh23^{m1btlr/-}* mice did

not survive within 1 and 3 weeks of postnatal days, respectively (Fig. 3.8C). By P45 approximately 80% of homozygous mice were dead and 95% homozygous mice were dead by P60 (WT vs. homozygous *Cdh23^{m1btlr/-}* mice, Kaplan-Meier Mantel-Cox: $p < 0.0001$) (Fig 3.8C).

4.3.5 Sequencing of *Cdh23^{m1btlr/-}* with Y2207X mutation

To confirm the nonsense mutation in the *Cdh23* gene in the *Cdh23^{m1btlr/-}* Y2207X mouse strain Sanger sequencing was performed. Using NCBI BLAST tool, we confirmed the presence of A>T base change leads to a stop codon on the reverse strand (Fig. 3.9).

```

Query: None Query ID: lcl|Query_54843 Length: 223

>Mus musculus strain C57BL/6J chromosome 10 clone rp23-362c8, complete sequence
Sequence ID: AC079818.56 Length: 238658
Range 1: 6366 to 6588

Score:407 bits(220), Expect:1e-109,
Identities:222/223(99%), Gaps:0/223(0%), Strand: Plus/Plus

Query 1      GCTAGAGCACAGCCACCTTGTACCTGTATTGATATTCACAGCAAAGGCGTCTTCCTGGT  60
              |||
Sbjct 6366   GCTAGAGCACAGCCACCTTGTACCTGTATTGATATTCACAGCAAAGGCGTCTTCCTGGT  6425

Query 61     CAGGCACCAGGCGGTTCGGTGTTCATCCTTGCCACGATGCTGATGATGCTTACTCCAGTT  120
              |||
Sbjct 6426   CAGGCACCAGGCGGTTCGGTGTTCATCCTTGCCACGATGCTGATGATGCTTACTCCAGTT  6485

Query 121    TGGGGTTGAGGTCGAGATCGATGGCGGTGACATTGGCAATGATGGTGCCTGGCTCTGCGG  180
              |||
Sbjct 6486   TGGGGTTGAGGTCGAGATCGATGGCGGTGACATTGGCAATGATGGTGCCTGGCTCTGCGG  6545

Query 181    ATTCCAGCACGCTCACTGTCTGGATAGGGTTGAGGAACTCGGG  223
              |||
Sbjct 6546   ATTCCAGCACGCTCACTGTCTGGATAGGGTTGAGGAACTCGGG  6588
  
```

Figure 4.9: *Cdh23* BLAST result for *Cdh23^{m1btlr/-}* mice.

Query sequence (*Cdh23*) is from *Cdh23^{m1btlr/-}* mouse; the reference sequence (Sbjct) is the from a mouse BAC clone. Green boxes: primer sequences used for sequencing. Red box: location of mutation site (converting ATA to ATT [TAA stop codon] on the reverse strand).

4.3.6 PCR genotyping of the mice

For genotyping of mice we took advantage of a *BaeI* restriction enzyme site that cuts the wildtype DNA fragment (+/+) into two bands of 127 bp and 96 bp, whereas DNA from mice that

were homozygous for the mutation (-/-) was not cut by *Bae*I. A 223 bp PCR product was amplified from DNA extracted from ear clippings of *Cdh23^{m1btlr-/-}* mice and analyzed by restriction digestion (Fig. 3.10) DNA from mice that were heterozygous (+/-) for the *Cdh23* mutation produced in three bands upon restriction digest (223 bp, 127 bp and 96bp).

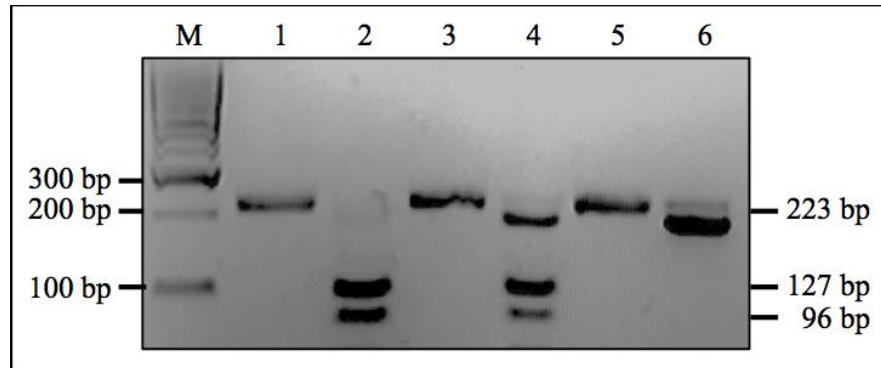


Figure 4.10: Representative image of genotyping of *Cdh23^{m1btlr-/-}* mice by restriction digestion analysis:

Lane M, Marker; Lane 1, undigested PCR product from wildtype DNA; Lane 2, digested wildtype PCR product; Lane 3, undigested PCR product from *Cdh23^{m1btlr+/-}* DNA; Lane 4, digested *Cdh23^{m1btlr+/-}* PCR product; Lane 5, undigested PCR product from *Cdh23^{m1btlr-/-}* DNA; Lane 6, digested *Cdh23^{m1btlr-/-}* PCR product.

4.3.7 Immunohistochemistry in retinal and cochlear *Cdh23^{m1btlr-/-}* tissue sections

Most homozygous nonsense mutations would result in absence of protein due to mRNA nonsense-mediate decay. Therefore, the location of Cdh23 protein in *Cdh23^{m1btlr-/-}* mouse retina was compared to wildtype controls. Expression of Cdh23 protein was localized to the connecting cilium located between the inner and outer segments of the photoreceptors, whereas Cdh23 protein was undetectable in the homozygous *Cdh23^{m1btlr-/-}* mutant retina (Fig. 3.11A). In the cochlea, Cdh23 is a structural protein that is involved in organizing the alignment of the stereocilia in the inner and outer hairs. Wholemount cochlea was stained for Cdh23 and Myo7A and the results

demonstrated abnormalities in the inner and outer hair cell arrangement in the mutant *Cdh23^{m1btlr/-}* as compared with wildtype mouse cochlear sections (Fig 3.11B). In wildtype cochlea there are three rows of outer hair cells and one row of inner hair cells that are labelled with both Cdh23 and Myo7a, whereas this structural arrangement is disrupted in the *Cdh23^{m1btlr/-}* cochlea.

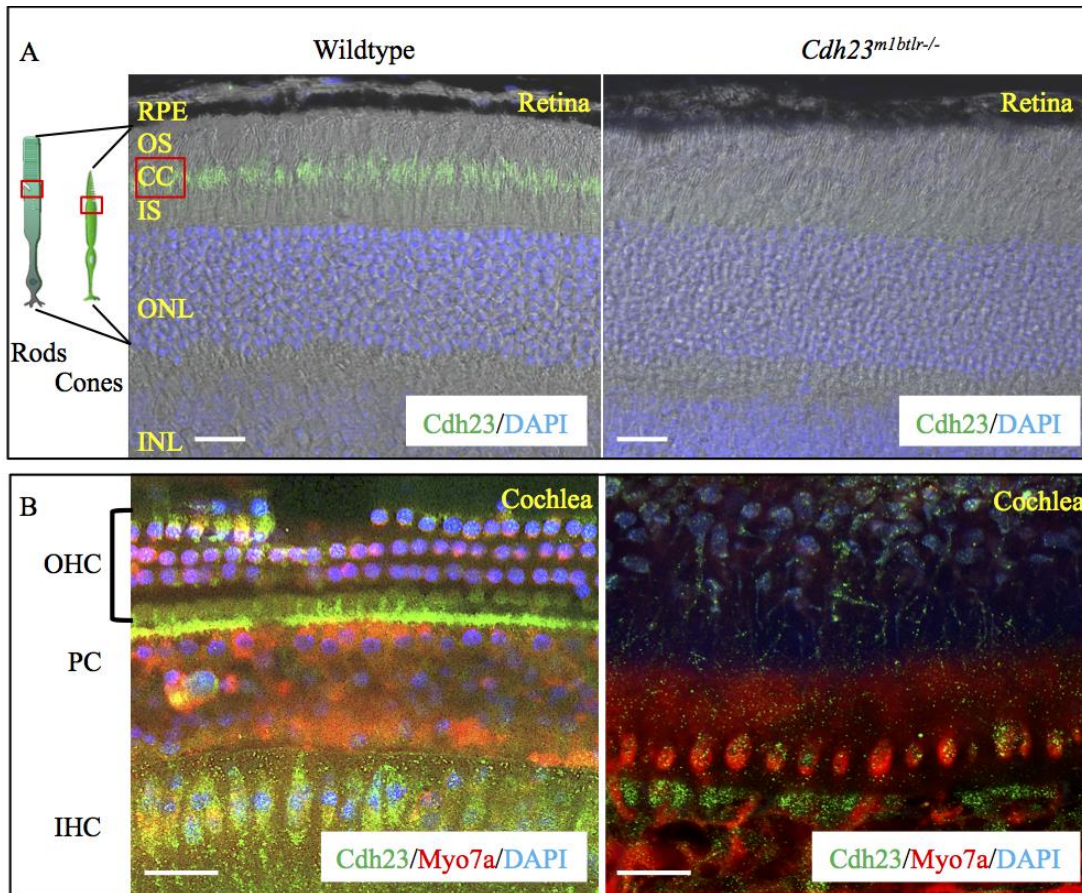


Figure 4.11: Immunohistochemical staining of retinal and cochlear sections.

(A) Representative image of retinal sections from wildtype and mutant *Cdh23^{m1btlr/-}* mice. Cdh23 antibody (green) labels the connecting cilium (CC) of the photoreceptors in wildtype but not *Cdh23^{m1btlr/-}* retina. RPE, retinal pigment epithelium; OS, outer segments; IS, inner segments; ONL, outer nuclear layer; INL, inner nuclear layer. Nuclei stained with DAPI. Scale bar = 50µm
 (B) Representative image of cochlear sections from wildtype and mutant *Cdh23^{m1btlr/-}* mice. Cdh23 (green) and Myo7A (red) label the outer (OHC) and inner hair cells (IHC) in wildtype but not *Cdh23^{m1btlr/-}* cochlea. PC, Pillar cells. Nuclei stained with DAPI. Scale bar = 20µm

4.3.8 Ataluren® treatment corrects the abnormal photoreceptor protein translocation

The *Cdh23^{m1btlr-/-}* mutant mice were treated with a daily subcutaneous injection of a 1% Ataluren® suspension and results were analyzed at P120 by immunohistochemistry. Ataluren® treatment rescued the expression of Cdh23 protein in the connecting cilium of the photoreceptors (Fig. 3.12A-C). Since the connecting cilium is involved in the trafficking of photoreceptor proteins during visual transduction, we investigated the localization of rhodopsin, arrestin, α -transducin and recoverin before and after treatment with Ataluren®. When light passes through the retina, the arrestin protein present in the inner segment of the photoreceptor translocates to the outer segment (Whelan & McGinnis, 1988). In the *Cdh23^{m1btlr-/-}* mutant retina arrestin is located in both inner and outer segments, whereas arrestin is only in the outer segments in wildtype retina (Fig. 3.12 D-E). When *Cdh23^{m1btlr-/-}* mice were treated with Ataluren® the normal trafficking of arrestin to the outer segments was corrected (Fig. 3.12 F). Similarly, in the *Cdh23^{m1btlr-/-}* retina rhodopsin was mis-localized in the inner segments of the photoreceptors, however, Ataluren® treatment rescued this mis-localization defect (Fig. 3.12 G-I).

Two other proteins that translocate in response to light are α -transducin and recoverin, but in the opposite direction from outer segment in the dark to inner segment and outer plexiform layer in the light (Strissel et al., 2005; Zhang, H. et al., 2003). In dark-adapted retinas of wildtype mice α -transducin was observed in the outer segments whereas in the *Cdh23^{m1btlr-/-}* retina, α -transducin was observed in the outer segments, inner segments and outer plexiform layer as would be expected in light conditions (Fig. 3.12 J-K). Treatment with Ataluren® resulted in correct localization of α -transducin to the outer segments (Fig. 3.12 L).

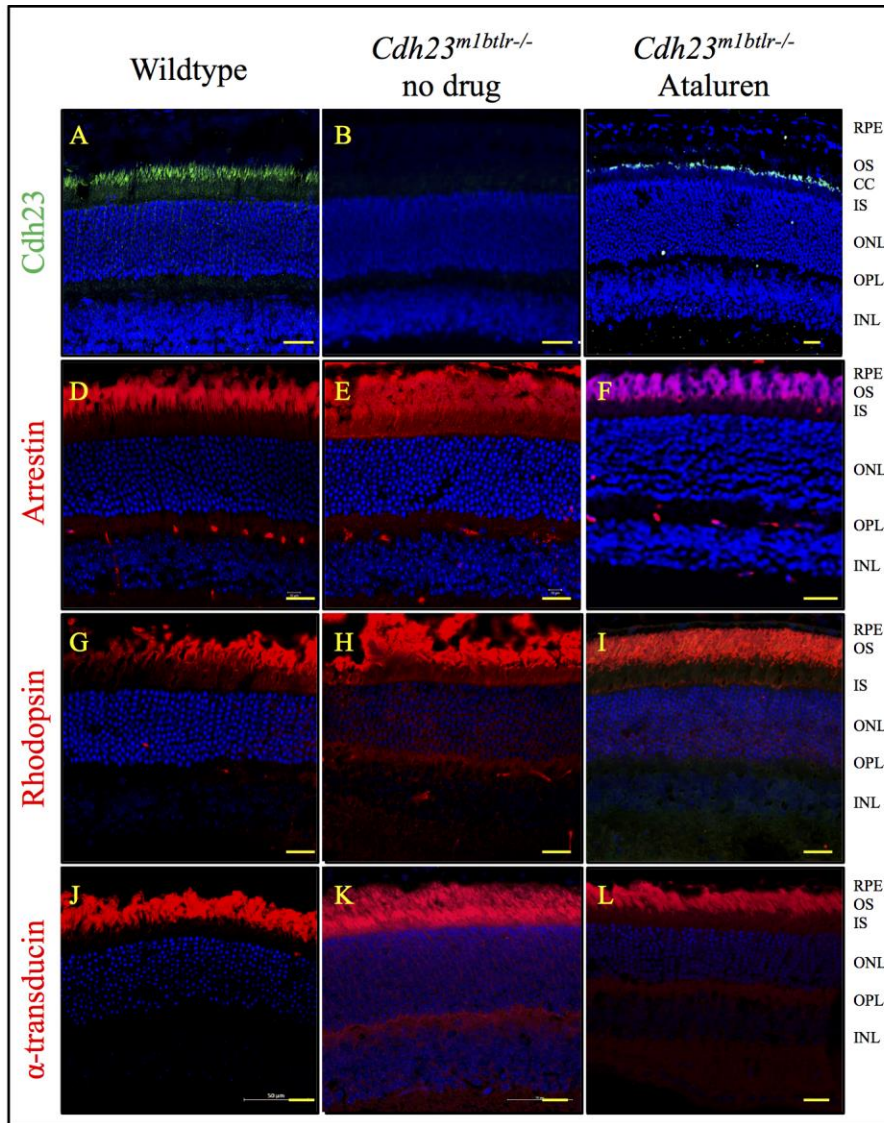


Figure 4.12: Light-induced translocation of retinal proteins in wildtype and *Cdh23*^{m1btlr-/-} mice.

Localization of Cdh23 in (A) wildtype, (B) untreated *Cdh23*^{m1btlr-/-} and (C) Ataluren®-treated *Cdh23*^{m1btlr-/-} retina under light conditions. Localization of Arrestin in (D) wildtype, (E) untreated *Cdh23*^{m1btlr-/-} and (F) Ataluren®-treated *Cdh23*^{m1btlr-/-} retina under light conditions. Localization of Rhodopsin in (G) wildtype, (H) untreated *Cdh23*^{m1btlr-/-} and (I) Ataluren®-treated *Cdh23*^{m1btlr-/-} retina under light conditions. Localization of α-transducin in dark-adapted (J) wildtype, (K) untreated *Cdh23*^{m1btlr-/-} and (L) Ataluren®-treated *Cdh23*^{m1btlr-/-} retina. Size bar in all images = 50µm. RPE, retinal pigment epithelium; OS, outer segment; CC, connecting cilium; IS, inner segment; ONL, outer nuclear layer; OPL, outer plexiform layer; INL, inner nuclear layer.

4.3.9 Photoreceptor synaptic terminal protein expression in *Cdh23^{m1btlr-/-}* retina

In some Usher genotypes the photoreceptor synapses are affected. For example, in Usher type 3A syndrome caused by homozygous mutations in the Clarin-1 (*CLRN1*) gene, progressive vision and hearing loss occur (Joensuu et al., 2001). In the retina Clarin-1 expression is restricted to photoreceptor synapses and the base of the connecting cilium (Zallocki et al., 2009) and *Clrn1* knockout mice have impaired vision due to synaptic transmission defects (Tian, G., Lee, Ropelewski, & Imanishi, 2016). Furthermore, ERGs studies demonstrated decrease in the functional response of the retina and reduction in the photoreceptor synapses in myosin VIIa-deficient *shaker-1* mouse, a model for usher syndrome 1B (Libby, R. T. & Steel, 2001). To examine photoreceptor synapses in *Cdh23^{m1btlr-/-}* mice we used immunohistochemistry to localize the protein Ribeye, the main component of ribbon synapse (tom Dieck et al., 2005). In wildtype retina Ribeye was localized to the outer plexiform layer (OPL) where the photoreceptor synapses are located, and to the inner nuclear layer (Fig. 3.13A). In the *Cdh23^{m1btlr-/-}* retina similar labelling was observed in the OPL with reduced inner nuclear layer labelling (Fig. 3.13B). It has been reported that Cdh23 is also expressed in the OPL as it co-localizes with Harmonin in the synaptic terminals (Reiners et al., 2003). In wildtype retina Cdh23 is detected in the OPL and is absent in *Cdh23^{m1btlr-/-}* retina (Fig. 3.13C).

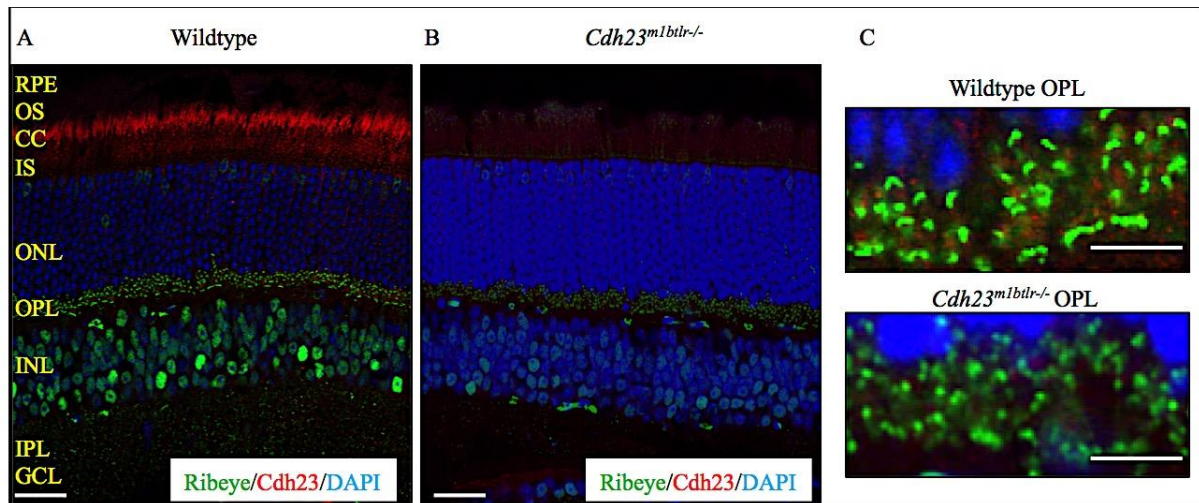


Figure 4.13: Synaptic ribbons in the retinal photoreceptors.

(A) Representative image of Ribeye (green) expression in the outer plexiform layer (OPL) and inner nuclear layer (INL) of the retina in wildtype mouse. Localization of Cdh23 (red) in connecting cilium (CC). White box denotes area of higher magnification in (C). (B) Representative image of Ribeye and Cdh23 expression in *Cdh23^{m1btlr-/-}* mutant retina. White box denotes area of higher magnification in (C). RPE, retinal pigment epithelium; OS, outer segments; IS, inner segments; ONL, outer nuclear layer; IPL, inner plexiform layer; GCL, ganglion cell layer. Scale bar = 50µm. (C) Higher magnification of OPL labelling of Cdh23 in wildtype and *Cdh23^{m1btlr-/-}* retina. Size bar = 10µm.

4.3.10 Ataluren® treatment reverses functional responses.

To test whether Ataluren® treatment improved functional electrical response, we studied the benefits of Ataluren® treatment on electroretinographic responses (ERG) in wildtype and *Cdh23^{m1btlr-/-}* mutant mice. The b-wave amplitude represents the response of rod photoreceptors to a light stimulus. In wildtype mice at P90 the maximum b-wave amplitude was 225 µV whereas in the *Cdh23^{m1btlr-/-}* heterozygous mice, the b-wave was significantly smaller at around 200 µV (Fig. 3.14B-C). *Cdh23^{m1btlr-/-}* mutants did not survive long enough to record an ERG. In *Cdh23^{m1btlr-/-}* mutants treated up to P45, there was no recordable b-wave (Fig. 3.14 D). However, by P90 a significant b-wave amplitude of about 150 µV (N=3, P<0.001) was observed in treated *Cdh23^{m1btlr-/-}* mutants (Fig. 3.14 E). Similarly, at P120 (N=2) a maximum b-wave of 150 µV was also recorded (Fig. 3.14 F).

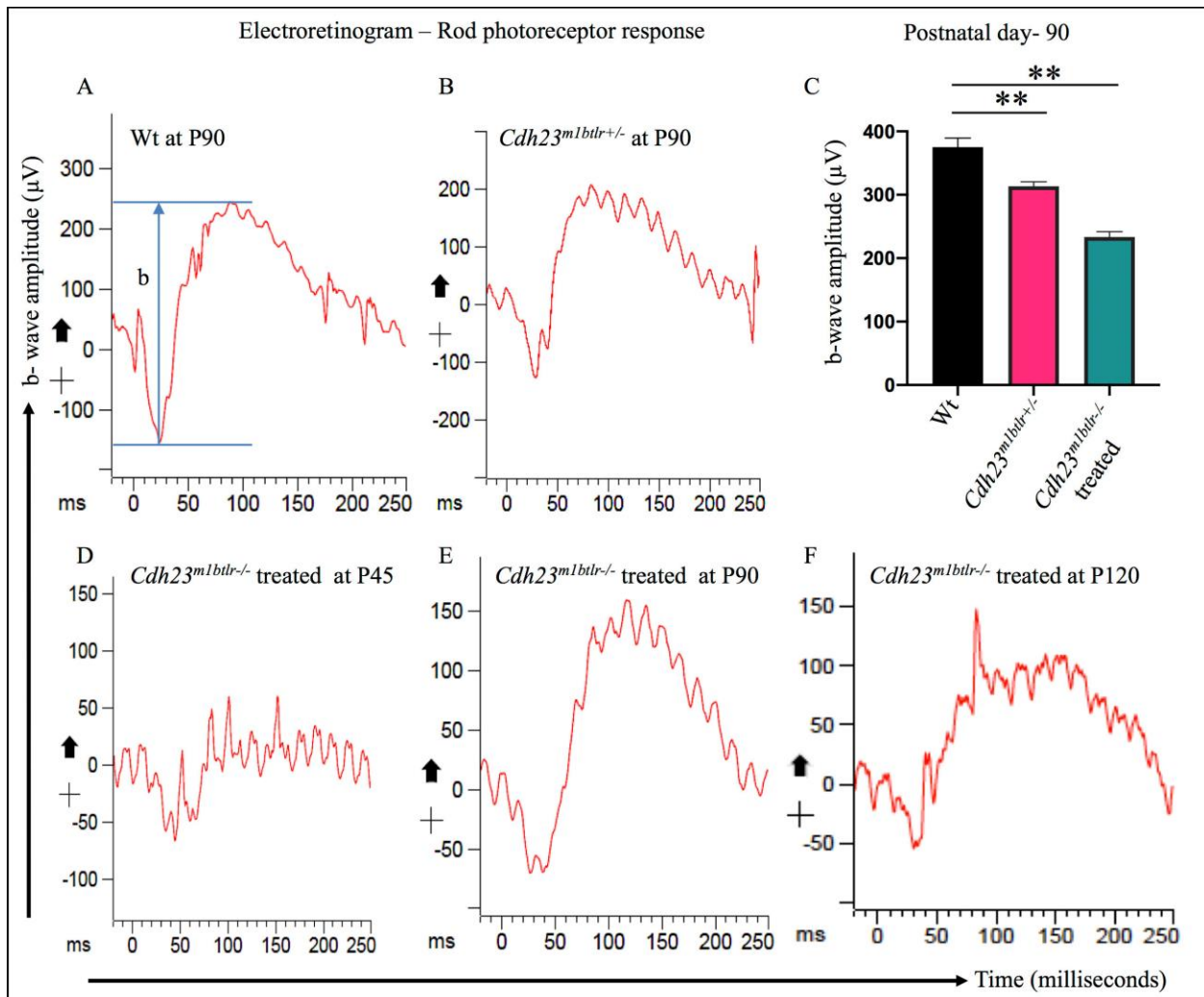


Figure 4.14: Representative scotopic ERG recordings with Ataluren® Therapy.

(A) Vehicle-treated wildtype (Wt) b-wave (arrow) recording at P90. (B) vehicle-treated heterozygous *Cdh23^{mbtr+/-}* recording at P90. (C) b-wave amplitude plots for Wt, *Cdh23^{mbtr+/-}* and Ataluren®-treated homozygous *Cdh23^{mbtr-/-}* mutants. Significance was determined by an unpaired 2-tailed Student's *t* test. N=3, **P < 0.001. ERG recordings in Ataluren®-treated *Cdh23^{mbtr-/-}* mice at P45 (D), P90 (E) and P120 (F).

The 30 Hz flicker recording was also measured as this represents the cone response to light. In the vehicle-treated wildtype and heterozygous *Cdh23^{mbtr+/-}* mice, the average 30 Hz flicker maximum amplitude responses were 51.6 µV and 36.6µV, respectively, (Fig. 3.15A-B) indicating that the

cone responses in the heterozygotes was significantly smaller than in wildtype mice ($P < 0.05, N = 3$) (Fig. 13.15 C). In homozygous $Cdh23^{m1btlr/-}$ mutants treated up to P45 there was no recordable 30 Hz flicker response (Fig. 3.15 D), whereas a repetitive, but smaller and delayed flicker began to emerge at P90 (Fig. 3.15E: 26.6 μV [65 msec implicit time] versus 51.6 μV [30 msec] in wildtypes animals). A similar delayed 30 Hz flicker of 25 μV (65 msec) was present at P120 in Ataluren®-treated $Cdh23^{m1btlr/-}$ mutants (Fig. 3.15F).

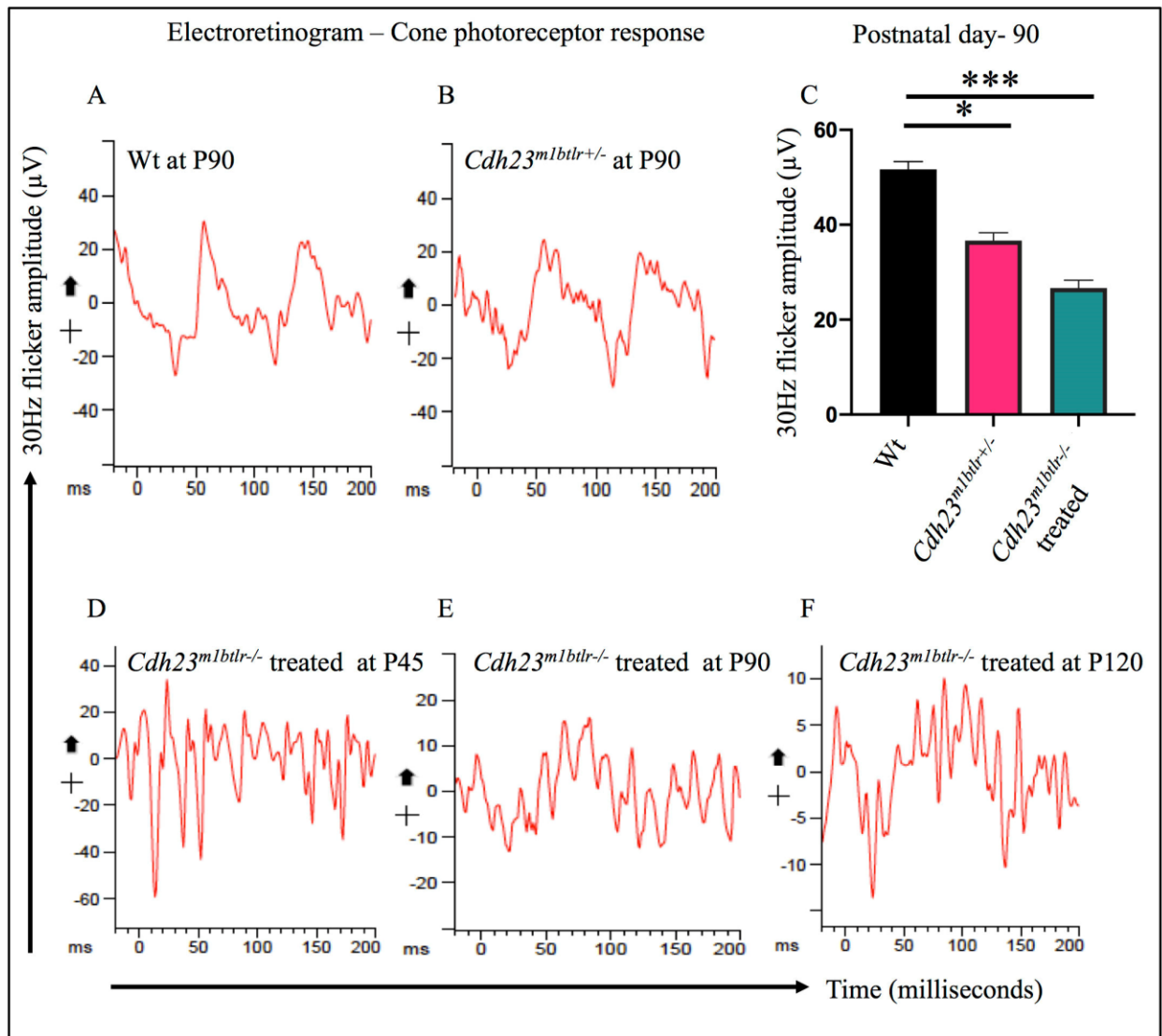


Figure 4.15: Representative 30Hz flicker ERG recordings with Ataluren® Therapy.

(A) vehicle-treated wildtype and (B) vehicle-treated heterozygote *Cdh23^{m1btlr+/-}* responses at P90. (C) 30 Hz amplitude plots for Wt, *Cdh23^{+/-}* and Ataluren®-treated homozygous *Cdh23^{-/-}* mutants. Amplitude and implicit times measured from trough to peak. Significance was determined by an unpaired 2-tailed Student's *t* test. (***)*P* < 0.001; **P* < 0.05; N=3). 30 Hz recordings in Ataluren®-treated *Cdh23^{-/-}* mice at P45 (D), P90 (E) and P120 (F).

4.3.11 Transmission electron microscopy analysis of retinal photoreceptors

Ultrathin plastic sections were used to study retinal photoreceptor ultrastructure in the vehicle-treated wildtype and Ataluren®-treated homozygous *Cdh23^{m1btlr-/-}* mice at P120. In wildtype mice, the outer segments are tightly packed with stacks of photoreceptor disks attached to the connecting cilium (Fig. 3.16 A-B). In Ataluren®-treated *Cdh23^{m1btlr-/-}* mice, the packing density of photoreceptor outer segments appeared to be reduced (Fig. 3.16 C), however, the outer segments were packed with stacked photoreceptor disks attached to the connecting cilium (Fig. 3.16 D). Micrographs for untreated homozygous *Cdh23^{m1btlr-/-}* mutants were not available for comparison as they did not survive to P120.

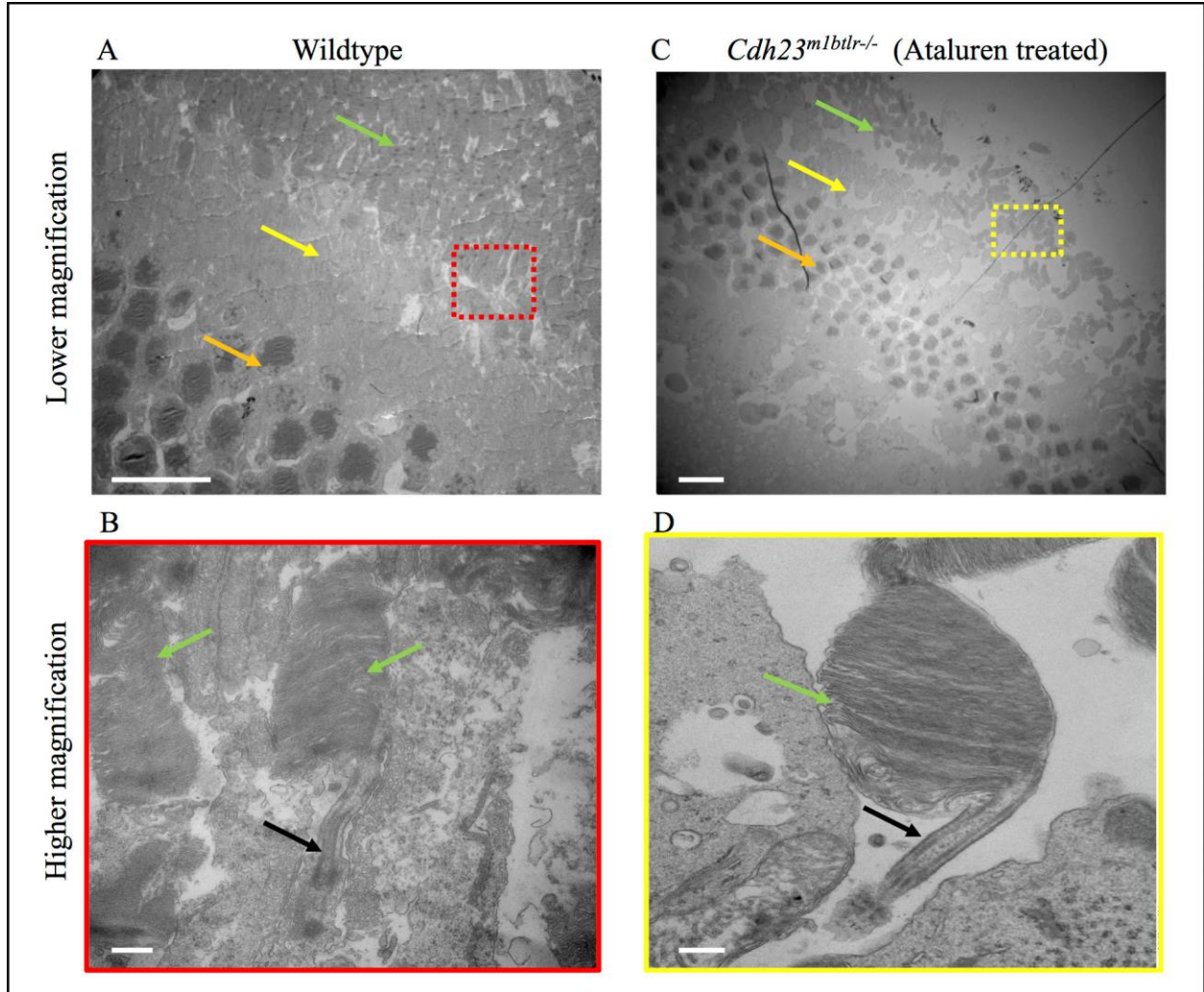


Figure 4.16: Electronmicrographs of retinal photoreceptors at P120.

(A,C) Representative images of the photoreceptor organization in the retina of wildtype and *Cdh23^{m1btlr-/-}* mice. Green arrow, outer segments; yellow arrow, inner segments; orange arrow, inner nuclear layer. Size bar = 10µm. Coloured boxes denoted where the images in B and D are taken from. (B,D) Representative image of the photoreceptor outer segment showing organized photoreceptor disks (green arrow) and connecting cilium (black arrow). Size bar = 500nm.

4.3.12 Real-time circling behavioral after Ataluren® treatment

The untreated homozygous *Cdh23^{m1btlr-/-}* mice exhibited the severe circling behavior during their entire lifetime and were very agitated when handled. In comparison, the Ataluren®-treated

Cdh23^{m1btlr/-} mice displayed much less circling activity and remained calm when handled. Over a 20 sec period, the untreated homozygous *Cdh23^{m1btlr/-}* at P40 circled about 12 times whereas the Ataluren®-treated *Cdh23^{m1btlr/-}* at P120 mice circled only 2 times (Fig. 3.17). Direct comparison at P120 was not possible as the untreated mice do not survive to this timepoint. Further studies are necessary to determine if hearing impairment is rescued in the Ataluren®-treated *Cdh23^{m1btlr/-}* mice.

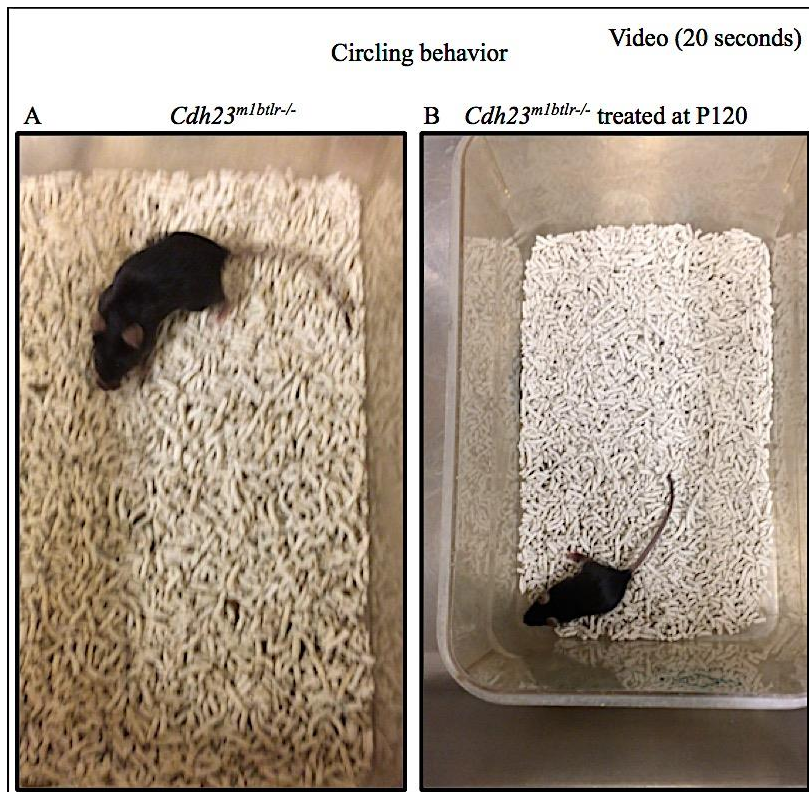


Figure 4.17: Circling behavior.

(A) Video of circling in untreated mouse at P40. (B) video of circling behaviour in Ataluren®-treated *Cdh23^{m1btlr/-}* mouse at P120.

4.4 Discussion

Usher syndrome (USH) is a complex genetic disease causing ciliopathy, hearing loss, early onset of retinitis pigmentosa (RP) and vestibular dysfunction. USH1D is the most severe form of this inherited syndrome. Due to the large size of the *CDH23* gene typical gene augmentation therapies are not possible. Therefore, we tested the hypothesis that nonsense suppression therapy could rescue the ocular and hearing deficits in a mouse model of USH1D. First, we characterized a new mouse model of USH1D (*Cdh23^{m1btlr/-}*) that had an in-frame nonsense mutation in *Cdh23*. Phenotypically, the *Cdh23^{m1btlr/-}* were significantly smaller than wildtype mice, they exhibited a severe circling behavior and did not survive past 60 days of age. Structural abnormalities were observed in the outer and inner hair cells of the cochlea that accounts for this circling behavior. As in most other mouse models of Usher syndrome we observed no structural abnormalities in the *Cdh23^{m1btlr/-}* retina (Slijkerman et al., 2015). However, we found abnormalities in light-induced trafficking of phototransduction proteins including rhodopsin, arrestin, α -transducin and recoverin. When *Cdh23^{m1btlr/-}* mice were treated with Ataluren® *Cdh23* protein was expressed in the connecting cilium, the trafficking defects were rescued, electrical response to light showed substantial improvement, the circling behavior was reduced and the mice survived to P120, doubling their lifespan. These data show for the first time that nonsense suppression in a mouse model of USH1D is able to rescue the major phenotypic features observed in the homozygous *Cdh23^{m1btlr/-}* mutant mice.

The trafficking abnormalities we observed could be the underlying cause of the defects found in the functional ERG testing in both rod and cone systems in the *Cdh23^{m1btlr/-}* mutant mice. Light-dependent movement of arrestin and α -transducin within 30 minutes of light-onset, is the functional mechanism by which the sensitivity of rods to different levels of light is thought to be

modulated (McGinnis, Whelan, & Donoso, 1992). Furthermore, translocation of α -transducin may have a neuroprotective role by reducing metabolic stress in rods when exposed to bright light conditions (Slepak & Hurley, 2008), which could in turn affect rod response to light. Other reports suggest that defects in protein translocation could increase the susceptibility to photoreceptor degeneration and thus affect the electrical responses of the photoreceptors (Kong et al., 2006).

Trafficking defects in rhodopsin and α -transducin have been reported in two other mouse models of Usher syndrome. In *shaker1* mice (USH1B model), mutations of the *Myo7a* gene cause delayed α -transducin translocation and mis-localization of rhodopsin to the inner segments of photoreceptors (Peng, Zallocchi, Wang, Delimont, & Cosgrove, 2011). These mice were found to be susceptible to light-induced retinal degeneration. However, sub-retinal injection of lentiviral vectors expressing wildtype *Myo7a* into *shaker1* mice rescued the trafficking defect and protected the mice from light-induced retinal degeneration (Peng et al., 2011). This provided evidence that the trafficking defect and the retinal degeneration were functionally linked. Similar defective trafficking of α -transducin and mis-localization of rhodopsin, as well as light-induced retinal degeneration, was observed in *whirler* mice (USH2D model) caused by mutation of the *Whrn* gene (Tian, M. et al., 2014). It can be argued that since mis-localization of rhodopsin is evident in other retinal degeneration models (Concepcion, Mendez, & Chen, 2002; Green, Menz, LaVail, & Flannery, 2000), then the light-induced retinal degeneration in *shaker1* and *whirler* mice is due to rhodopsin mis-localization rather than the α -transducin trafficking defect. Contrary to this, prolonged activation of the phototransduction cascade has been associated with photoreceptor degeneration in α -transducin and arrestin mutants (Brill et al., 2007; Xu, J. et al., 1997). It would

be interesting to determine if exposure of *Cdh23^{mlbtr/-}* mutant mice to prolonged bright light would also result in a light-induced retinal degeneration.

The lack of retinal degeneration in most mouse models of Usher syndrome has hampered deciphering the pathophysiological mechanism causing photoreceptor cell death. There are three different isoforms of Cadherin-23 protein, and the longest form is not expressed in mouse photoreceptors, whereas it is present in the ciliary region of primate photoreceptors, which may explain the lack of retinal phenotype in this mouse model (Lagziel et al., 2009). This is consistent with a report by Williams and co-workers who found that the largest harmonin isoforms were not expressed in the mouse retina (Williams et al., 2009) implying that the mouse USH1C model is not a good model to study the retinal phenotype. An additional explanation is that mouse photoreceptors do not have calyceal processes (Fig. 3.18) unlike human, monkey and frog retina (Cosgrove & Zallocchi, 2014).

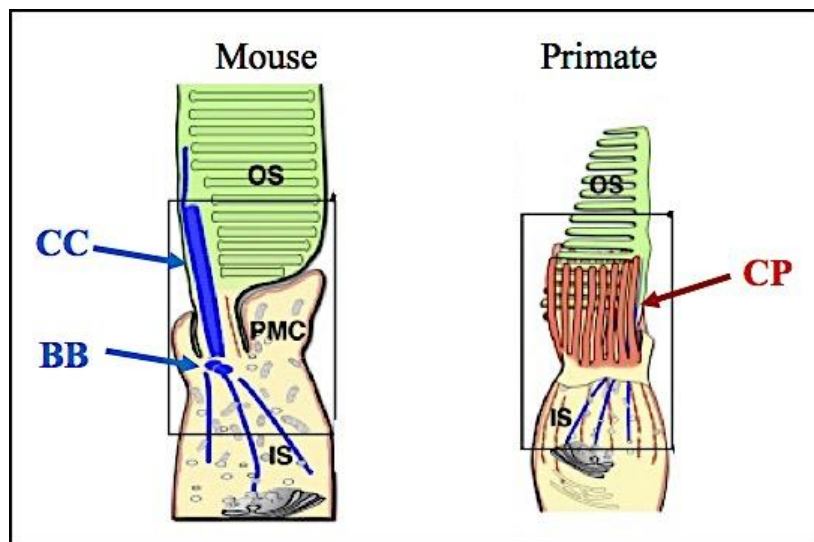


Figure 4.18: Finger-like calyceal processes in primate photoreceptors.

In the mouse rod photoreceptor the outer segment (OS) is connected to the inner segment (IS) by the connecting cilium (CC). PMC, periciliary complex. BB, basal body. In primate cones and rods microvillous structures, known as calyceal processes (CP) protrude from the apical region of the

IS encasing the base of the OS (Adapted from Sahly I. et al, 2012 licensed under CC- BY- NC-SA 3.0).

The long isoform of Cadherin-23, as well as Protocadherin-15 and Harmonin proteins are all expressed in the calyceal processes in primate and *Xenopus laevis* photoreceptors (Sahly et al., 2012) and are thought to provide a structural support mechanism similar to the tip-link structure in hair cells involved in mechanotransduction (Kazmierczak et al., 2007). Recently, it was shown that the calyceal processes are involved in regulating the size of rod disks and cone lamellae during daily photoreceptor renewal in *Xenopus tropicalis* (Schietroma et al., 2017). It was found that *cdh23* and *pcdh15* morphants had bulging disks and abnormal photoreceptor alignment, with reduced a- and b-wave amplitudes in the ERG confirming the role of these proteins in photoreceptor function. Based on these observations and new technologies such as gene editing, it may be possible to engineer an in-frame nonsense mutation into *Xenopus* to test the effectiveness of nonsense suppression drugs on repairing defects in disk morphogenesis.

Chapter 5: Nonsense suppression therapy in human iPSC-derived 3D retinal organoids

5.1 Chapter introduction

Usher syndrome type 1D manifests in two children in our study family. Genetic testing has revealed two heterozygous DNA variants in the Cadherin 23 (*CDH23*) gene: Arg1437X (the base change is C>T, a previously reported nonsense mutation in exon 35 and Thr2454Thr G>A, a presumed cryptic splicing mutation in exon 52 that has been previously reported and rarely seen in the general population (0.01%). Each parent is a *CDH23* mutation carrier. The mother has the nonsense mutation TGA, which has good readthrough efficacy for nonsense suppression and the father carries the splicing mutation. Based on earlier publications from our laboratory showing that nonsense suppression (START therapy) can reverse disease as seen in aniridia (Wang et al., 2017), nonsense suppression would be predicted to work well on this mutation.

To test the effect of nonsense suppression in this family we proposed to make retinal organoids from the children and an unaffected control. Nonsense suppression has been used in human cell lines (Peltz et al., 2013; Samanta et al., 2019) and retinal organoids (Schwarz, Carr, Lane, Moeller, Chen, Aguilà, Nommiste, Muthiah, Kanuga, Wolfrum, Nagel-Wolfrum, Cruz et al., 2015) indicating that defects in human photoreceptors can respond to nonsense suppression.

5.1.1 Specific hypothesis

- Incubation of patient retinal organoids with the small molecule drug Ataluren® will drive read-through of the nonsense mutation allele restoring *CDH23* protein expression.

5.1.2 Rationale

Since mouse *Cdh23* models have a modest retinal dysfunction and no retinal degeneration, a better model to test a new therapeutic would be a human retinal cell line, retinal explants or even better still 3D retinal organoids, closely recapitulating the developing neuroretina (Wahlin et al., 2017). The neuroretina is a complex nine-layered structure and it is technically challenging to culture individual photoreceptors for more than a few hours as they do not survive (Gaudin, Forster, Sahel, Dreyfus, & Hicks, 1996). The major advance in being able to derive retinal organoids from induced pluripotent stem cells (iPSCs) reprogrammed from patients' blood or skin cells, has opened new opportunities for testing novel therapies. In addition, positive therapeutic results in retinal organoids would be important data to support ethical approval for a clinical trial. Therefore, we took the approach of testing nonsense suppression in retinal organoids. The one caveat with this technology is that the differentiation of iPSCs to produce fully formed photoreceptors takes up to 200 days (Sridhar et al., 2020) along the timeline of human gestation.

5.1.3 Experimental design

Briefly, blood samples were collected from the subjects to isolate the peripheral blood mononuclear cells (PBMCs). The isolated PMBCs were sent for reprogramming into iPSCs at the Centre for Commercialization of Regenerative Medicine in Toronto, Canada. Reprogramming into iPSCs occurs through transduction using four Yamanaka transcription factors: OCT4, SOX2, KLF4, and C-MYC (OSKM) (Takahashi & Yamanaka, 2006). Then the iPSCs were differentiated into 3D retinal eyecups. After initial differentiation, the eyecups were treated with 10µg/ml Ataluren® along with differentiation media every 2 days. At day 120 and day 150 the eye cups

were processed and analyzed for the presence of CDH23 protein and other photoreceptors protein markers by western blot and immunocytochemistry.

5.2 Methods

5.2.1 Culture, maintenance, and characterization of patient-derived iPSCs

Patient peripheral blood was collected in a BD Vacutainer tube (Thermo Fisher) and processed within two hours of collection. Mononuclear cells were isolated using the SepMate kit (STEMCELL Technologies, Vancouver, Canada) according to the manufacturer's protocol. Briefly, blood samples were diluted 1:1 with PBS containing 2% fetal bovine serum (FBS; Thermo Fisher, Waltham, MA, USA) and slowly added to a SepMate tube that was preloaded with 3.5ml density gradient medium (Lymphoprep; STEMCELL Technologies). Tubes were centrifuged for 10 min at 1,200 xg in a swing-out bucket rotor with the brake on. The top layer was poured off into a clean 15 ml tube (Thermo Fisher, Waltham, MA, USA) and 3 ml of PBS/2%FBS was added to it. The tubes were then centrifuged for 8 min. at 300x g at RT and the pellet was resuspended in 10ml PBS/2%FBS. The centrifugation and resuspension of the cell pellet was repeated one more time and finally the tubes were centrifuged, and the cell pellet was resuspended in 900µl FBS followed by drop-wise addition of 100µl DMSO. The latter cell suspensions were transferred into cryovials (Nalgene, Rochester, NY,USA), placed in a cryo-container and stored at -80°C for 24-48 hours, after which they were sent to the Centre for Commercialization of Regenerative Medicine (CCRM; Toronto) for reprogramming. Two vials from two clones of each iPSC line were fully characterized at the CCRM, to confirm pluripotency and chromosomal integrity. The cells were shipped back to our laboratory on dry ice and one vial of each cell line was immediately thawed and expanded, both for generating backup vials and for differentiation.

5.2.2 Differentiation of 3D retinal organoid derived from patient iPSCs

iPSCs derived from peripheral blood mononuclear cells from a healthy individual and from individuals with hereditary retinal degeneration were maintained in a 20% O₂/5% CO₂ incubator at 37°C, expanded in Essential 8 media (E8; Thermo Fisher) on Matrigel (Corning, New York, USA) coated 6-well dishes (Thermo Fisher) and passaged as clumps using Gentle Cell Dissociation Media (STEMCELL Technologies). For organoid formation, iPSCs were dissociated into single cells using TrypLE Express Enzyme (Thermo Fisher). The cell suspension was centrifuged at 200 xg for 3 min and the resulting cell pellet was resuspended in 3D differentiation medium containing 10% FBS, 20% Knockout serum replacement (KOSR), 1% Non-Essential Amino Acids, 1% NaPyruvate, 0.1mM β-mercaptoethanol in high-glucose containing DMEM (all from Thermo Fisher), supplemented with 20mM ROCK inhibitor (STEMCELL Technologies) and 3mM IWR1e (Cayman Chemical, Michigan, USA). Live cells were counted and adjusted to a concentration of 1x10⁶ cells in 10ml of 3D differentiation medium (supplemented as above) followed by distribution into Ultra-Low Attachment Spheroid 96-well Microplate (Corning,.) at 10,000 cells per well (100 μl per well). Two days later, 100 μl of the same media, supplemented with 1% Matrigel, was added to each well. On days six and ten, 100 μl of media was removed from each well and 100 μl fresh 3D media (including ROCK inhibitor, IWR1e and Matrigel) was added. On day 12, spheres were carefully transferred to an Ultra-Low Attachment 24-well plate (Corning; 4 spheres per well) and the media was replaced with fresh 3D differentiation medium containing only 1% Matrigel. On days 14 and 16, media was replaced with 3D differentiation medium containing 1% Matrigel, 3mM CHIR99021 (the GSK3β inhibitor) (Miltenyi Biotec, Bergisch Gladbach, Germany) and 100nM SAG (smoothened agonist) (Enzo Life Sciences, New York, Canada). On day 18 the media was changed to neural retina (NR) medium (DMEM: F12,

1% N2 supplement, Glutamax; Thermo Fisher) and from then on spheres were fed three times a week with NR media. On days 30-40 media was supplemented with 10 mM of the γ -secretase inhibitor DAPT, to enhance photoreceptor generation, and feeding continued three times a week until organoid harvest.

5.2.3 Quantitative polymerase chain reaction (qPCR)

To identify the pluripotency potential of patient-derived iPSCs, total RNA was isolated from undifferentiated and differentiated iPSCs using the Aurum™ Total RNA Mini Kit (Bio-Rad Laboratories) according to the manufacturer's instructions. For cDNA synthesis, 1mg of total RNA was reverse transcribed using the QuantiTect Reverse Transcription Kit (Qiagen) and relative gene expression for NANOG and SOX2 were quantified using appropriate TaqMan primer and labelled probe protocol with ViiA 7 Real-Time PCR system (Applied Biosystems, Foster, CA) as previously reported (Viringipurampeer et al., 2016). Briefly, all reactions were done using the TaqMan Universal Master Mix (2X), FAM-labeled TaqMan Gene Expression assays were used for all the genes of interest, and VIC-labeled TaqMan endogenous positive control GAPDH and 4ng of cDNA. Thermocycling parameters were as follows: 2 min at 50°C, 10 min at 95 °C, 40 cycles of 15 s at 95 °C, plus 1 min at 60 °C. PCR data were analysed by the comparative CT method as previously reported (Schmittgen & Livak, 2008). Each reaction was performed four times, and each sample was partitioned into three aliquots for measurement.

5.2.4 Western blotting

Retinal organoids were collected by centrifugation and lysed in 100 μ L protein lysis buffer (10 mM Tris base, pH 7.4, 150 mM NaCl, 1 mM EDTA, 1 mM EGTA, 1% Triton X-100, 0.5% NP-40, protease/phosphatase inhibitor cocktail (Cell Signalling, Beverly, MA). The lysates were subjected to three freeze-thaw cycles after which they were centrifuged for 2 minutes at 15,000 rpm at 4°C and the supernatant was collected in ice-cold fresh tube. Protein concentration was measured by the DC protein assay (Bio-Rad) and samples of equal protein concentration were boiled for 5 min in sample buffer (50mM Tris-HCl [pH 6.8], 2% SDS, 5% glycerol, 0.005% bromophenol blue, and 1.6% β -mercaptoethanol). Proteins (25 μ g) were separated on denatured 10% polyacrylamide Tris-glycine gels (Appendix A), transferred to Immobilon-FL membrane (Millipore), blocked in 5% non-fat dry milk powder in PBS for 1 hour at RT and incubated overnight at 4°C in shaker with anti-Cadherin 23 polyclonal antibody (LifeSpan BioSciences, Seattle, WA; Catalog# LS-C354296; 1:500) in 5% non-fat milk powder in PBS/0.1% Tween-20 (PBST) or for 1 hr at RT with anti- β actin antibody (Sigma; Catalog#:A5441; 1:3000). Following five washes in PBST, the membrane was then incubated for 1 hr with the appropriate fluorescent tagged secondary antibody diluted 1:15,000 (IRDye 800 or IRDye 680; Rockland, Limerick, PA), washed five times in PBST in the dark chamber and protein bands were visualized/imaged using a Li-COR Odyssey detector (Mandel Scientific, Guelph, ON).

5.2.5 Immunohistochemistry

Organoids were fixed in 4% paraformaldehyde (PFA) (Electron Microscopy Sciences, Hatfield, PA, USA) at RT for 1 hr, followed by three washes with PBS and overnight incubation in 30% sucrose at 4°C. Organoids were embedded in Polyfreeze medium (Polysciences), incubated

overnight at -20°C and sectioned (14mm) on a Cryostat (MICROM HM525). Polyfreeze was removed by hydrating the cryosections in PBS for 20 min followed by blocking for 1 hr at RT in blocking buffer (2% normal goat serum, 0.1% Triton-X100 in PBS) and then overnight incubation at 4°C with primary antibody diluted in blocking buffer. After three washes in PBS/0.1% Tween-20, sections were incubated with species-specific fluorophore conjugated secondary antibodies diluted 1:500 in PBS/0.05% Tween-20 for 1 hr in the dark at RT (Alexa Fluor488 or 594; Thermo Fisher). Slides were gently washed three times with PBS/0.1% Tween-20 and one time with PBS and mounted in Fluoromount-G, containing the DAPI for nuclei (SouthernBiotech, Birmingham AL, USA). Slides were visualized and images acquired using a Zeiss LSM 510 META confocal laser scanning system. Primary antibodies used for immunohistochemistry and their dilution factor were: anti-Recoverin polyclonal antibody (Catalog#:5585; Millipore; 1:1000); anti-blue Opsin polyclonal antibody (Catalog#:ab5407; Millipore; 1:300); anti-Rhodopsin monoclonal antibody (Catalog#:ab5417; Abcam; 1:500); anti-visual Arrestin monoclonal antibody (Catalog#:5580; Millipore, 1:300).

5.2.6 Terminal deoxynucleotidyl transferase dUTP nick end labeling (TUNEL)

To quantify the level of apoptotic cell death, day 60 retinal organoid cryosections were post-fixed in ethanol:acetic acid (2:1) for 5 min at -20°C followed by 2 washes in PBS, 5 min each wash. The ApopTag® Fluorescein *In-Situ* Apoptosis Detection Kit (Millipore) was used according to the manufacturer's instructions, and apoptotic and total cells numbers were calculated by a masked individual that was not aware of the identity of the sections (N=6).

5.2.7 Statistical analysis

The percentage of cell death was determined by calculating the fraction of apoptotic cells out of the total cell number. Results were plotted as mean \pm SEM. Percentages were statistically compared using a paired Student's *t*-test. For qRT-PCR experiments, data were analyzed using an unpaired two-tailed Student's *t*-test. P-values are indicated as *P<0.05, **P<0.01 and ***P<0.005.

5.3 Results

5.3.1 Generation and characterization of iPSCs from patients with CDH23 mutations

With support from the Centre for Commercialization of Regenerative Medicine (CCRM, Toronto), we generated human iPSC cell lines from peripheral blood mononuclear cells isolated from the affected individuals which express compound heterozygous variants in the cadherin 23 gene (*CDH23: Arg1437X;Thr2545Thr*) and from an unaffected control individual with no history of ocular disease.

These newly developed human iPSCs cell lines derived from patient and control were tested with various pluripotency markers and quality assessment at CCRM. Tests included: expression of pluripotency-associated proteins by FACS or qRT-PCR; germ layer differentiation by qPCR; karyotype, post-thaw viability and residual Sendai viral contents. An example of the quality control data for one control patient and one *CDH23* affected cell line is presented in Table 4.1 and 4.2, respectively.

Test Description	Method	Expected Result	Result												
Expression of pluripotency-associated proteins	Flow cytometry	≥ 80% of population is positive for expression of surface markers (SSEA4, Tra-1-60), and intracellular marker (OCT4).	<table border="1"> <thead> <tr> <th>Antigen</th> <th>% Expressing-cells</th> </tr> </thead> <tbody> <tr> <td>SSEA4</td> <td>90.6%</td> </tr> <tr> <td>Tra-1-60</td> <td>98.7%</td> </tr> <tr> <td>OCT4</td> <td>96.2%</td> </tr> <tr> <td>SOX2</td> <td>97.3%</td> </tr> </tbody> </table> (Histograms shown in Figure 1)	Antigen	% Expressing-cells	SSEA4	90.6%	Tra-1-60	98.7%	OCT4	96.2%	SOX2	97.3%		
Antigen	% Expressing-cells														
SSEA4	90.6%														
Tra-1-60	98.7%														
OCT4	96.2%														
SOX2	97.3%														
Gene expression of pluripotency markers	qRT-PCR	≥ 80% expression measured in hESC reference standard (HES2 hESCs on Matrigel).	<table border="1"> <thead> <tr> <th>Gene</th> <th>Relative Expression</th> </tr> </thead> <tbody> <tr> <td>OCT4</td> <td>97%</td> </tr> <tr> <td>NANOG</td> <td>87%</td> </tr> <tr> <td>DNMT3B</td> <td>106%</td> </tr> </tbody> </table>	Gene	Relative Expression	OCT4	97%	NANOG	87%	DNMT3B	106%				
Gene	Relative Expression														
OCT4	97%														
NANOG	87%														
DNMT3B	106%														
Germ layer differentiation	Directed Differentiation Followed by qPCR	Increased expression of germ lineage-specific marker relative to starting pluripotent cell population	<table border="1"> <thead> <tr> <th>Germ Layer</th> <th>Gene</th> <th>Fold Induction</th> </tr> </thead> <tbody> <tr> <td>Endoderm</td> <td>SOX17</td> <td>1,930</td> </tr> <tr> <td>Mesoderm</td> <td>HAND1</td> <td>13,600</td> </tr> <tr> <td>Ectoderm</td> <td>SOX1</td> <td>144</td> </tr> </tbody> </table>	Germ Layer	Gene	Fold Induction	Endoderm	SOX17	1,930	Mesoderm	HAND1	13,600	Ectoderm	SOX1	144
Germ Layer	Gene	Fold Induction													
Endoderm	SOX17	1,930													
Mesoderm	HAND1	13,600													
Ectoderm	SOX1	144													
Mycoplasma	Lonza MycoAlert Plus kit	None detected	None detected												
Identity	STR: PCR profiling of 9 STR regions plus Amelogenin for gender determination.	Consistent with expected ¹	Consistent with parental - Amel: XY CSF1PO:10,10 D21S11:32,32.2 TH01:9,9 D13S317:8,11 D5S818:10,12 TPOX: 8,11 D16S539:11,12 D7S820:10,10 vWA:14,17												
Karyotype	G-banding analysis detecting structural abnormality of size >3-10Mb	Normal karyotype, 46 XX or 46 XY 19/20 cells normal ²	Normal karyotype, 46 XY at passage 3												
Post-Thaw Viability	Cell count and viability using Nucleocounter	Viable cell count and viability within 7 days post thaw	<table border="1"> <tbody> <tr> <td>Viable cell count</td> <td>9.36E+05</td> </tr> <tr> <td>Viability</td> <td>79.8%</td> </tr> </tbody> </table>	Viable cell count	9.36E+05	Viability	79.8%								
Viable cell count	9.36E+05														
Viability	79.8%														
Residual Sendai	RT-PCR against Sendai viral elements	None detected in PCR amplification	None detected												

Table 5.1: Test results for characterization of control iPSC line

Test Description	Method	Expected Result	Result												
Expression of pluripotency-associated proteins	Flow cytometry	≥ 80% of population is positive for expression of surface markers (SSEA4, Tra-1-60), and intracellular marker (OCT4).	<table border="1"> <thead> <tr> <th>Antigen</th> <th>% Expressing-cells</th> </tr> </thead> <tbody> <tr> <td>SSEA4</td> <td>94.6%</td> </tr> <tr> <td>Tra-1-60</td> <td>98.2%</td> </tr> <tr> <td>OCT4</td> <td>99.2%</td> </tr> <tr> <td>SOX2</td> <td>97.5%</td> </tr> </tbody> </table> (Histograms shown in Figure 1)	Antigen	% Expressing-cells	SSEA4	94.6%	Tra-1-60	98.2%	OCT4	99.2%	SOX2	97.5%		
Antigen	% Expressing-cells														
SSEA4	94.6%														
Tra-1-60	98.2%														
OCT4	99.2%														
SOX2	97.5%														
Gene expression of pluripotency markers	qRT-PCR	≥ 80% expression measured in hESC reference standard (HES2 hESCs on Matrigel).	<table border="1"> <thead> <tr> <th>Gene</th> <th>Relative Expression</th> </tr> </thead> <tbody> <tr> <td>OCT4</td> <td>102%</td> </tr> <tr> <td>NANOG</td> <td>99%</td> </tr> <tr> <td>DNMT3B</td> <td>108%</td> </tr> </tbody> </table>	Gene	Relative Expression	OCT4	102%	NANOG	99%	DNMT3B	108%				
Gene	Relative Expression														
OCT4	102%														
NANOG	99%														
DNMT3B	108%														
Germ layer differentiation	Directed Differentiation Followed by qPCR	Increased expression of germ lineage-specific marker relative to starting pluripotent cell population	<table border="1"> <thead> <tr> <th>Germ Layer</th> <th>Gene</th> <th>Fold Induction</th> </tr> </thead> <tbody> <tr> <td>Endoderm</td> <td>SOX17</td> <td>6670</td> </tr> <tr> <td>Mesoderm</td> <td>HAND1</td> <td>8880</td> </tr> <tr> <td>Ectoderm</td> <td>SOX1</td> <td>137</td> </tr> </tbody> </table>	Germ Layer	Gene	Fold Induction	Endoderm	SOX17	6670	Mesoderm	HAND1	8880	Ectoderm	SOX1	137
Germ Layer	Gene	Fold Induction													
Endoderm	SOX17	6670													
Mesoderm	HAND1	8880													
Ectoderm	SOX1	137													
Mycoplasma	Lonza MycoAlert Plus kit	None detected	None detected												
Identity	STR: PCR profiling of 9 STR regions plus Amelogenin for gender determination.	Consistent with expected ¹	Consistent with parental - Amel: XY CSF1PO:11,12 D21S11:29,31.2 TH01:7,9 D13S317:11,12 D5S818:11,11 TPOX: 8,11 D16S539:10,12 D7S820:9,10 vWA:16,18												
Karyotype	G-banding analysis detecting structural abnormality of size >3-10Mb	Normal karyotype, 46 XX or 46 XY 19/20 cells normal ²	Normal karyotype, 46 XY at passage 3												
Post-Thaw Viability	Cell count and viability using Nucleocounter	Viable cell count and viability within 7 days post thaw	<table border="1"> <tbody> <tr> <td>Viable cell count</td> <td>1.41 E+05</td> </tr> <tr> <td>Viability</td> <td>81.4%</td> </tr> </tbody> </table>	Viable cell count	1.41 E+05	Viability	81.4%								
Viable cell count	1.41 E+05														
Viability	81.4%														
Residual Sendai	RT-PCR against Sendai viral elements	None detected in PCR amplification	None detected												

Table 5.2: Test results for characterization of CDH23 iPSC line

In addition, to demonstrate the pluripotency, iPSCs generated from the *CDH23* patient at passage 5 were subjected to immunocytochemistry with antibodies to OCT4, NANOG, and SOX2 (Fig 4.1A-C). All three antibodies resulted in positive labelling compared to no antibody controls. Gene expression analysis by qPCR with Taqman probes to *NANOG* and *SOX2* was also carried out (Fig. 4.1E). In comparison to the undifferentiated human iPSCs, the differentiated human iPSCs at passage 5 displayed a 3-fold decrease in *NANOG* ($P < 0.001$, $N = 3$). There was a smaller but significant down-regulation of *SOX2* in differentiated iPSCs (0.33 fold decrease, $P < 0.05$, $N = 3$). These results demonstrated the successful generation of patient-specific iPSCs.

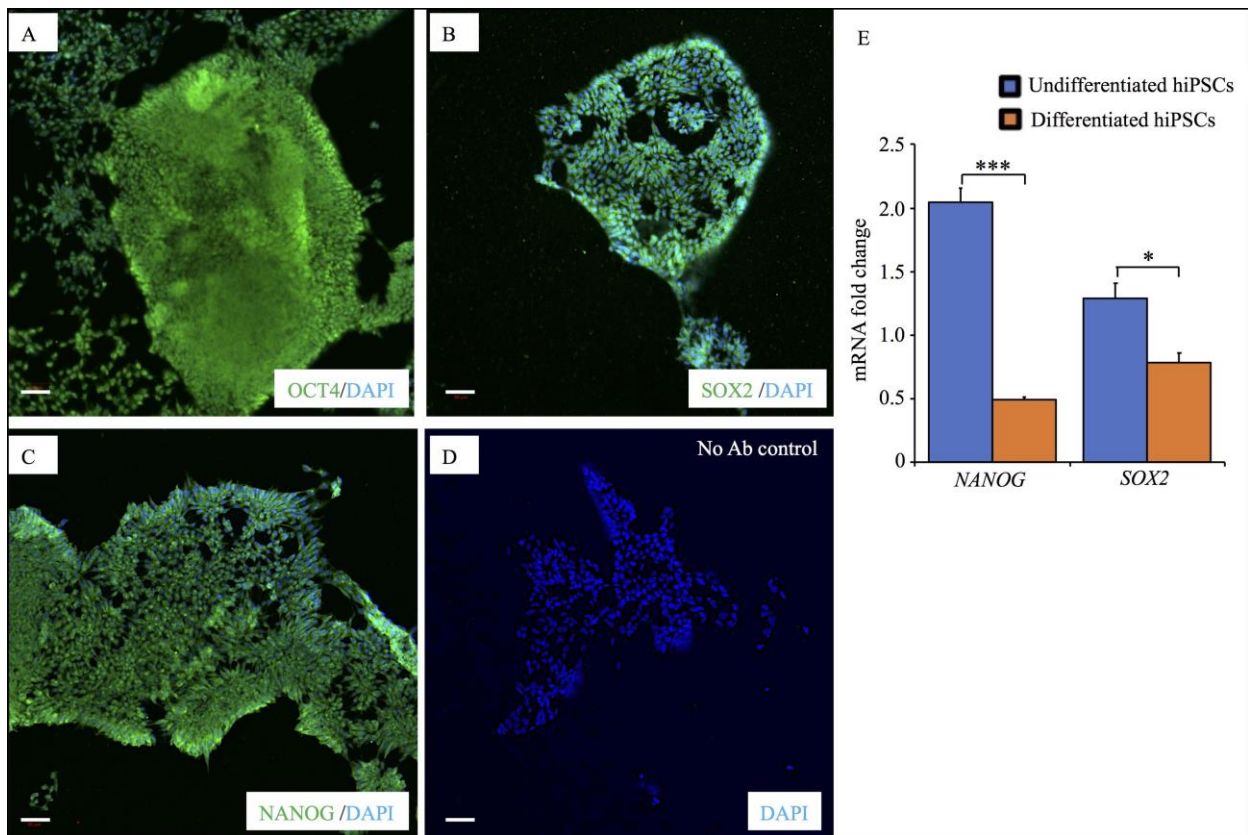


Figure 5.1: Pluripotent human iPSCs express pluripotency markers.

Expression of the pluripotency markers in iPSC. (A) OCT4; (B) SOX2; (C) NANOG. (D) Cells counterstained with DAPI. Size bar =50µm (E) qRT-PCR results showing down-regulation of

NANOG and SOX2 pluripotent mRNA expression in differentiated iPSCs; *P<0.05; ***P<0.001, N=3.

5.3.2 Generation of 3D retinal organoids for disease modeling

In an attempt to study the effect of *CDH23* mutations on intracellular trafficking and photoreceptor development, patient and control iPSCs were differentiated to 3D retinal organoids using our 3D differentiation protocol which was adapted from previously published data (Small et al., 2016; Wiley et al., 2016a). We found that the differentiation of organoids from control iPSCs progressed as expected in that PAX6 started to be expressed at day 33 in the developing retinal organoid in the neural differentiation medium (Fig. 4.2).

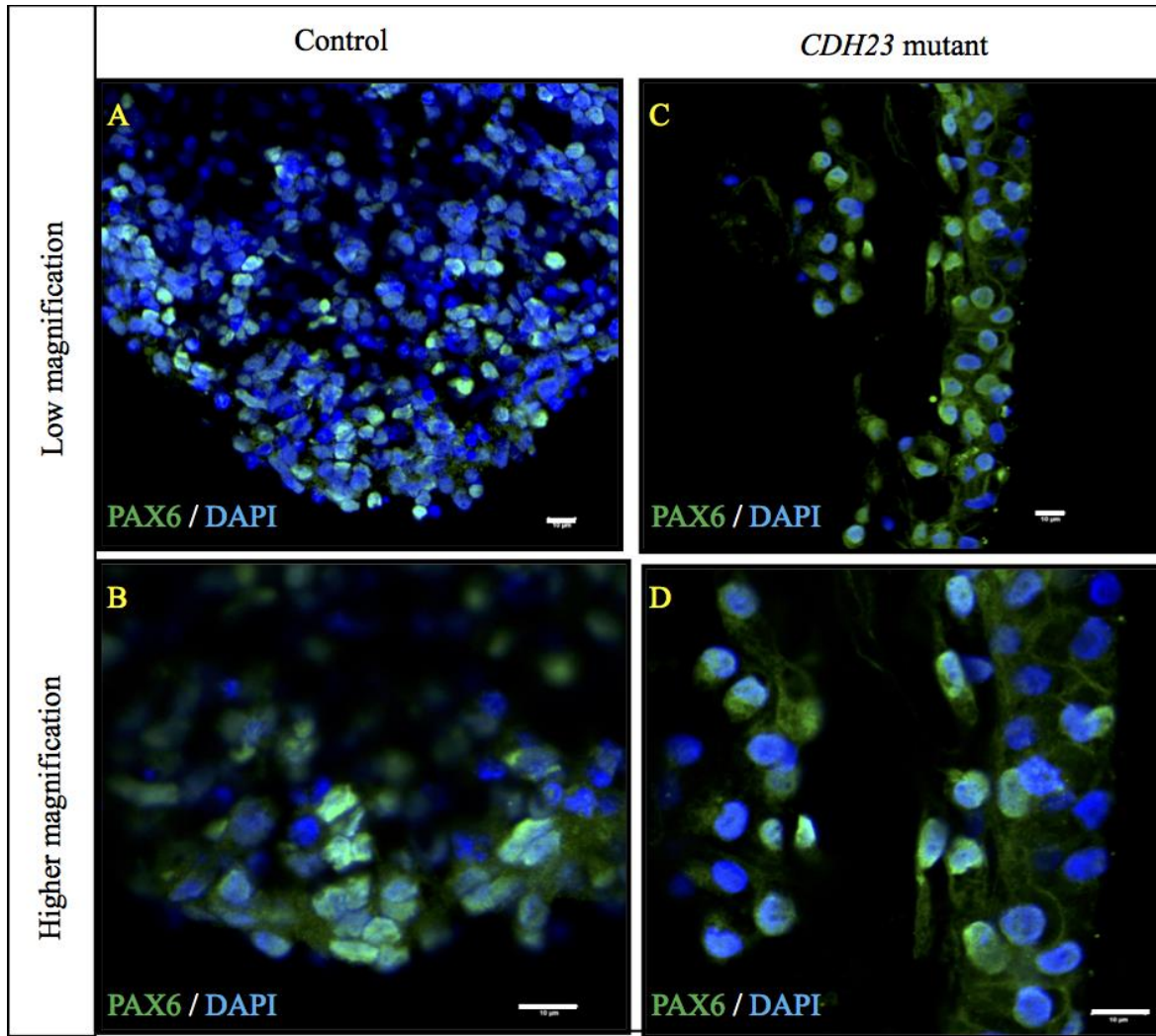


Figure 5.2: Expression of PAX6 in retinal organoids.

Representative images of control cells (A,B) and *CD23* mutant cells (C,D) seeded in Matrigel-coated wells showing neuroepithelial fate by expression of PAX6. Nuclei stained with DAPI. Size bar = 10µm

Following the expression of PAX6, the retinal organoid consisted of a rounded, transparent neuroretina that was continuous with the pigmented RPE at day 40 as shown by phase contrast microscopy (Fig. 4.3A, B). Furthermore, developing photoreceptors in organoids were stained with peanut agglutinin, to visualize the developing cone precursors in the stratified neuroretina (Fig. 4.3C, D).

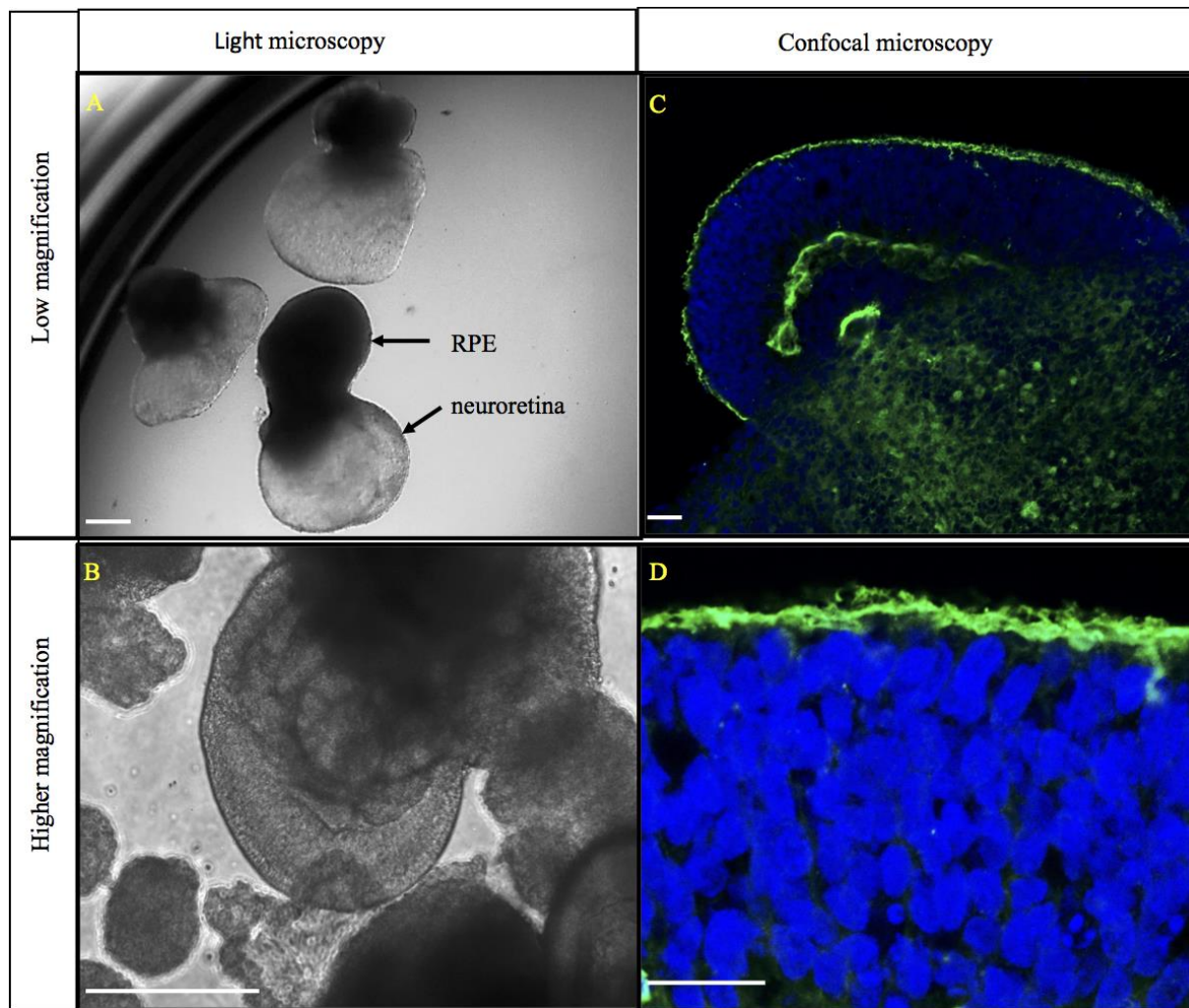


Figure 5.3: Generation of 3D retinal organoids for disease modeling.

(A) Phase contrast image of retinal organoids at P40 and at higher magnification in (B). Size bar = 1mm. (C) Confocal image of neuroretina in day 40 retinal organoids and at higher magnification in (D). Size bar = 50µm Cryosections labelled with peanut agglutinin (green) to identify cones precursors and nuclei labelled with DAPI.

5.3.3 Effect of *CDH23* mutation on photoreceptor protein expression in patient-derived retinal organoids

CDH23 is expressed in the connecting cilium of photoreceptors and the absence of CDH23 protein leads to photoreceptor dysfunction through light-induced protein translocation defects. To examine whether CDH23 is expressed in patient-derived retinal organoids, we performed western

blotting. We found that patient-derived retinal organoids from *CDH23* mutant iPSCs fail to produce CDH23 in contrast to control retinal organoid (Fig.4.4A). We then examined the expression of two retinal proteins that are trafficked through the photoreceptor cilium in a light-dependent manner. Immunohistochemistry in retinal organoids at day 150 demonstrated high levels of expression of rod-specific arrestin and S-opsin in control organoids whereas expression of these proteins was undetectable in *CDH23* mutant organoids (Fig. 4.4B).

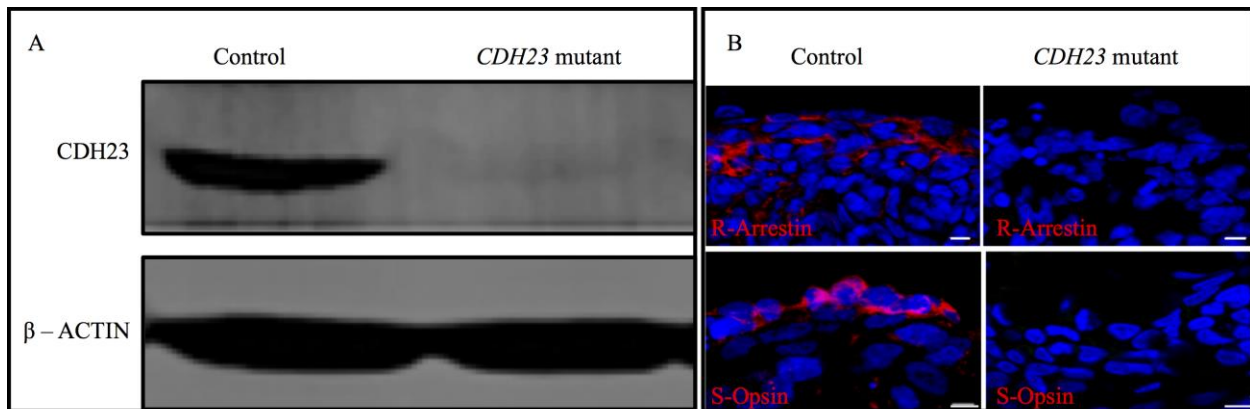


Figure 5.4: CDH23 and photoreceptor protein expression in patient-derived retinal organoids.

(A) Western blot of CDH23 in control and *CDH23* mutant retinal organoid lysates. β -Actin was used as a loading control. (B) Confocal imaging of rod-specific arrestin (R-Arrestin) in upper panels and S-Opsin in lower panels. Nuclei were stained with DAPI. Size bar = 10 μ m.

5.3.4 Nonsense suppression therapy in retinal organoids

In sham-treated *CDH23*-mutant retinal organoids at day 40 of differentiation, only 31% (\pm 3.46) developed neuroepithelium which appeared stunted compared to control organoids (95% \pm 1.45) (Fig. 4.5A,B). However, with continuous treatment up to day 40 using the nonsense suppression drug Ataluren® (1mg/ml), we found that neuroepithelium maturation was present in 53% (\pm 3.48) of *CDH23*-mutant retinal organoids, whereas at a higher concentration of Ataluren® (10 mg/ml) 67% (\pm 4.04) of retinal organoids developed neuroepithelium (Fig. 4.5C,D).

Quantitative assessment of these data revealed that significantly more retinal organoids developed neuroepithelium when treated with Ataluren® compared to untreated organoids (Fig. 4.5E). The neuroepithelium of treated retinal organoids appeared very similar in structure to control organoids.

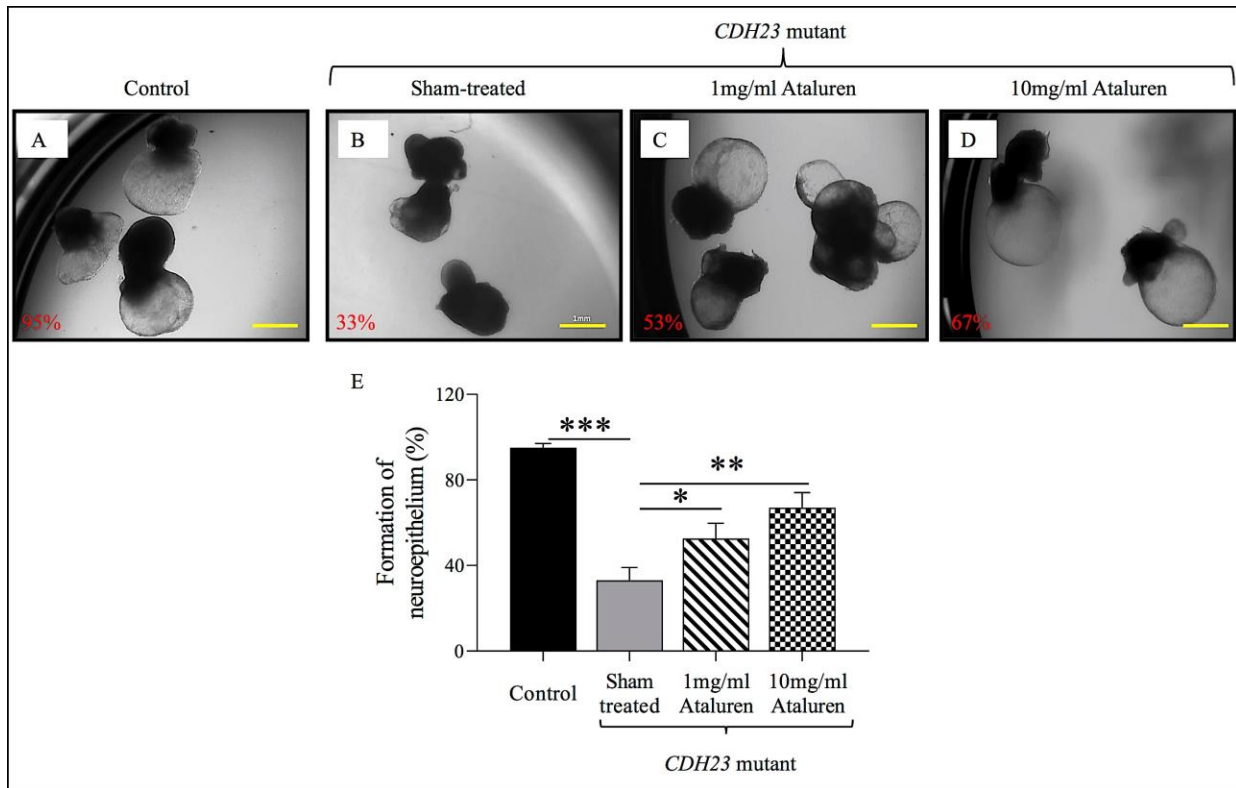


Figure 5.5: Formation of neuroepithelium in control and *CDH23*-mutant organoids.

(A) Most (95%) sham-treated control organoids exhibit the formation of neuroepithelium; (B) Presence of neuroepithelium in 33% of sham-treated *CDH23*-mutant organoids. (C) Neuroepithelium in 53% of *CDH23*-mutant organoids treated with 1 mg/ml Ataluren®. (D) Neuroepithelium in 67% of *CDH23*-mutant organoids treated with 10 mg/ml Ataluren®. Size bar = 1mm. (E) Quantitation of neuroepithelium formation in retinal organoids. *** P<0.001; ** P<0.01; * P<0.05. N=4.

Cell death is a major hallmark of late stage retinal degeneration. We observed loss of neuroepithelium stratification in *CDH23*-mutant retinal organoids at about day 60 of differentiation. TUNEL staining was performed at day 60 to quantify the level of cell death in

CDH23-mutant organoids, and in organoids treated with two concentrations of Ataluren® (1 mg/ml and 10 mg/ml) (Fig. 4.6A-F). Approximately 60% of the cells in the *CDH23*-mutant organoids were labelled by TUNEL staining (Fig. 4.6G). However, cell death was reduced to 13% and 18% in mutant retinal organoids treated with 1 mg/ml and 10 mg/ml Ataluren®, respectively ($P < 0.001$, $N = 3$)

To determine if the mechanism of cell death was caspase-dependent, retinal organoid cell lysates from 2 independent iPSC-derived clones were tested for the presence of cleaved caspase-3 using western blot analysis. No cleaved caspase-3 was detected in the control organoids, whereas both *CDH23* mutant organoids expressed the cell death protein (Fig. 4.6H).

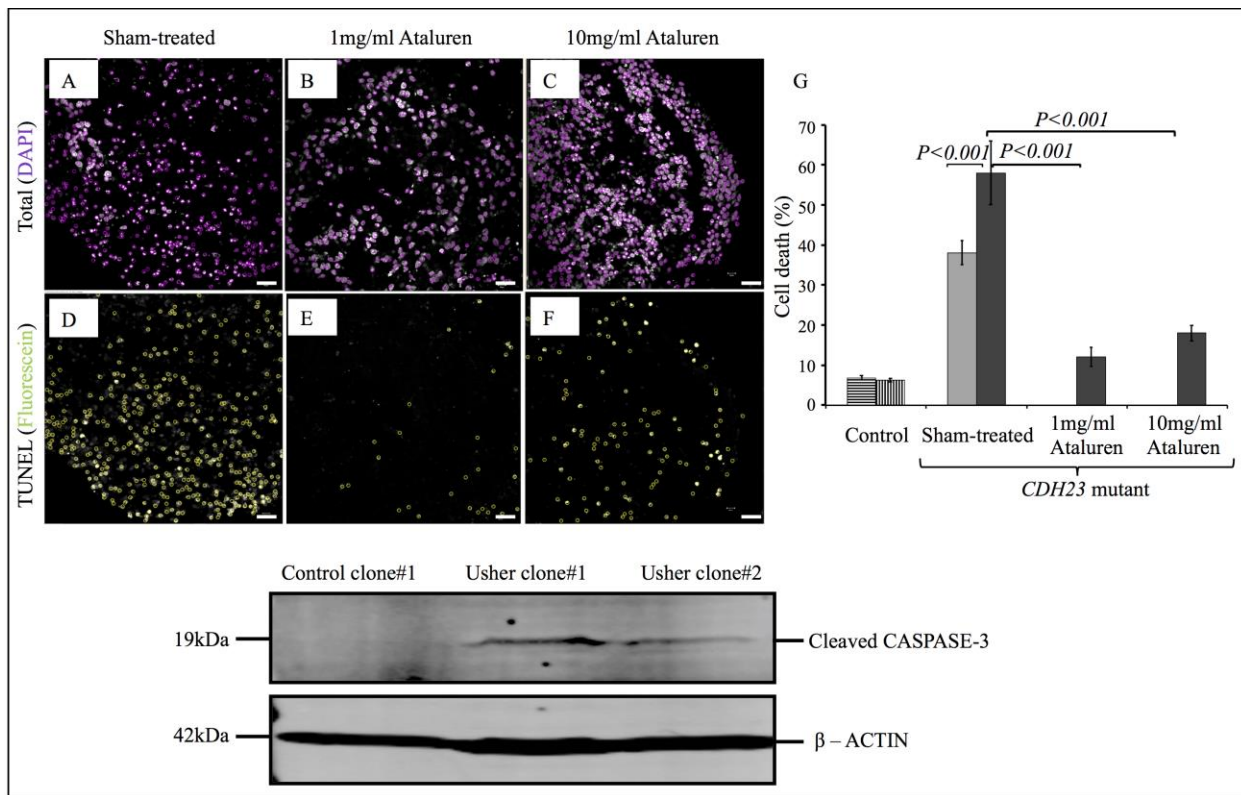


Figure 5.6: Cell death in retinal organoids.

(A-C) *CDH23* retinal organoids stained with DAPI (pseudo-coloured purple) showing all cell nuclei in the presence or absence of Ataluren®. (D-E) TUNEL labelling (fluorescein) of the same *CDH23* retinal organoids in the presence or absence of Ataluren®. (G) Quantification of cell death in retinal organoids comparing treated and untreated organoids. $P < 0.001$, $N = 3$ (H) Representative

western blot image showing cleaved caspase-3 only in *CDH23* retinoid organoids. β -Actin was used as a loading control.

To determine if Ataluren® treatment changed the expression of photoreceptor cell markers at a later stage of differentiation (day 150), retinal organoids were processed for western blotting and immunohistochemistry. Western blot analysis demonstrated CDH23 protein expression was only increased above background in the retinal organoids treated with 10 mg/ml Ataluren® (Fig. 4.7 A). Therefore, this concentration of Ataluren® (10 mg/ml) was used to test for expression of other photoreceptor markers. Untreated retinal organoids did not express either rod-arrestin (labelling rod photoreceptors) or S-opsin (labelling blue cone photoreceptors), whereas treatment with 10mg/ml Ataluren® resulted in both proteins being expressed in the retinal organoids (Fig. 4.7 B-G). The expression of recoverin was also assessed because it is trafficked through the connecting cilium in a light-dependent manner. In the presence of 10 mg/ml Ataluren® the expression of recoverin was similar to the control organoids, whereas very little was detected in the untreated retinal organoids (Fig. 4.7 H-J).

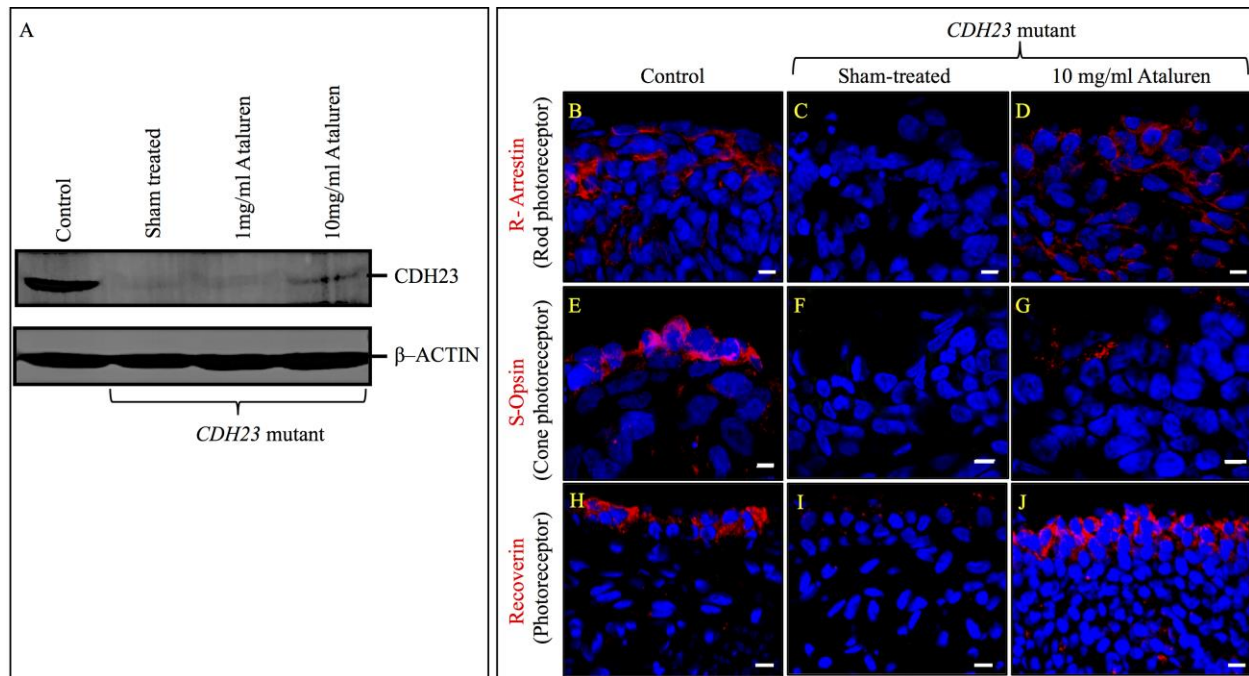


Figure 5.7: The effect of nonsense suppression on photoreceptor protein expression at day 150.

A) Western blot analysis of CDH23 in control and Ataluren® treated groups. β - Actin was used as loading control. (B-D) Immunostaining of control and *CDH23* mutant retinal organoids for rod-arrestin in the presence or absence of 10 mg/ml Ataluren®. (E-G) Expression of S-opsin in the presence or absence of 10 mg/ml Ataluren®. (H-I) Expression of recoverin in the presence or absence of 10 mg/ml Ataluren®. Size bar in all images = 10 μ m.

To determine whether cells in the *CDH23* mutant retinal organoids (that expressed photoreceptor markers) had begun to develop outer segments with Ataluren® treatment, transmission electronmicroscopy imaging was carried out in day 150 organoids. In the iPSC-derived photoreceptors the formation of a few photoreceptor disks was observed (Fig. 4.8) but we were not able to image the photoreceptor cilium.

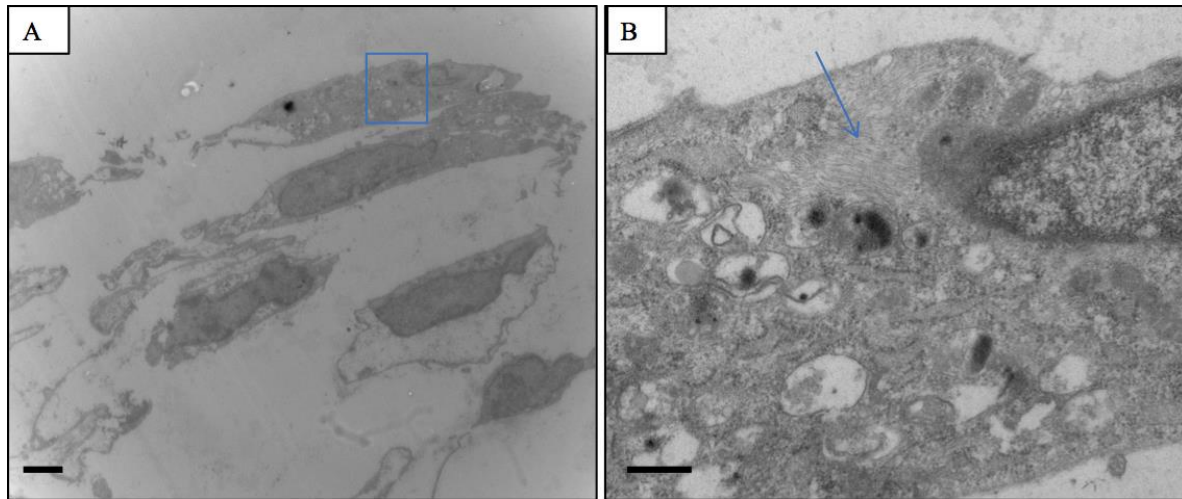


Figure 5.8: Transmission electron microscopy of *CDH23* mutant retinal organoids treated with 10 mg/ml Atauren®.

(A) Low magnification of iPSCs-derived photoreceptors. Size bar = 2 μ m. (B) A higher magnification image as indicated by the blue box in (A). Blue arrow indicates photoreceptor disks. Size bar = 400nm

5.4 Discussion

Under appropriate conditions, retinal organoids can be used to recapitulate human retinal development and disease that are not easily and accurately modeled in animals (Li & Izpisua Belmonte, 2019). Our study is the first to investigate the effect of *CDH23* gene mutation using 3D retinal organoid technology. In this study, patient-derived iPSCs were differentiated into retinal organoids to test the ability of nonsense suppression to rescue the *CDH23* mutant phenotype, because relevant animal models only display a very modest retinal phenotype. In addition, the knowledge generated could be used to support the use of nonsense therapy in a human clinical trial. We characterized the phenotype in *CDH23* mutant retinal organoids obtained from a patient that harboured compound heterozygous mutations (*CDH23: Arg1437X;Thr2454Thr*). Retinal organoids started losing structural integrity at about day 60 of differentiation co-incident with high levels of cell death. We characterized the expression of several photoreceptor markers (*CDH23*,

rod-arrestin, S-opsin, recoverin) and found their expression was undetectable. Since one of the *CDH23* mutations was a premature nonsense mutation (Arg1437X) we assessed the effect of the nonsense suppression drug Ataluren® on the retinal organoid phenotype. In Ataluren®-treated retinal organoids, the photoreceptor marker expression was restored and we observed the initiation of photoreceptor disk formation. These proof-of-concept data suggest that nonsense suppression could be a viable therapy for patients with Usher syndrome type 1D caused by nonsense mutations.

The efficacy of response to nonsense therapy needs to be improved as most nonsense suppression drugs have a read-through capacity of only 5-30% (Wang, X. & Gregory-Evans, 2015). The read-through efficacy varies depending on various factors including the specific nonsense codon that is mutated and relative to surrounding sequences (Namy, Hatin, & Rousset, 2001); absorption of the drug to the ocular tissue; the amino acid replacing the nonsense codon or presence of baseline modified transcript. (Linde et al., 2007). Despite the low level of read-through nonsense suppression drugs are being evaluated in clinical trials. Ataluren (Drug Name Translarna®, PTC Therapeutics) is currently being tested in aniridia (ClinicalTrials.gov: NCT02647359), Dravet syndrome (NCT02758626), and Duchenne muscular dystrophy in the USA (NCT03648827) (Wang et al., 2020). Furthermore, new generation nonsense suppression drugs that have increased neuronal penetration and better pharmacokinetics are being tested (Du, L. et al., 2013; M et al., 2016). Despite these advances in nonsense suppression approaches it should be noted that there are potential off-target effects that may occur. For instance, patients with other in-frame nonsense mutations that are susceptible to nonsense suppression therapy, leading to deleterious proteins being made. With the opportunity for whole exome sequencing, patients who are suitable for nonsense suppression therapy could be pre-screened for nonsense mutations.

Patient-derived iPSCs that are differentiated into specific tissues can assist scientists in modelling various diseases and can be used as drug screening systems if they exhibit the relevant disease phenotype. Patient-derived retinal organoids are paving the way for examining the pathophysiological changes especially in inherited retinal diseases (IRDs). For example, retinal organoids have been generated from patients with Leber congenital amaurosis, Usher syndrome, retinitis pigmentosa and Best's disease (Chuang, Fields, & Del Priore, 2017).

LCA is an inherited eye disorder that primary affects the retina which leads to severe vision loss in childhood. Mutations in genes highly expressed in retinal cells have been identified in patients with LCA (*ALMS1, AIPL1, CABP4, CNGA3, CRX, CRB1, CEP290, GDF6, GUCY2D, IQCB1, IMPDH1, LCA5, LRAT, , MYO7A, NMNAT1, RPGRIP1, RPE65, RD3, RDH12, TULP1*). Animal models are very helpful for understanding the retinal function and pathogenic mechanisms underlying retinal degeneration. However, solid evidence supporting the function of genes involved phototransduction is still difficult to obtain for the human retina. Mouse and cat models of LCA have been previously established, but the causative mutations are different than human (Chang, 2016; Lyons et al., 2016). One group (Parfitt et al., 2016) has recently developed human 3D optic cup organoids from a patient with an intronic mutation in the ciliary gene *CEP290* for studying LCA disease mechanisms in a cellular and genomic context. This model system will also be very useful in designing therapeutic regimens that use antisense oligonucleotide to restored functional CEP290 protein levels.

Retinitis pigmentosa (RP) is a hereditary retinal disorder characterized by progressive loss of rod and cone photoreceptors leading to partial or complete vision loss. It can be inherited in autosomal dominant, recessive, X-linked or through mitochondrial inheritance. In a recent study (Zhong et al., 2014) human iPSCs-derived 3D retinal cups contained functionally matured rod and

cone photoreceptors with outer segment discs, which could be useful model system for studying human retinogenesis, retinal disease modelling and subsequently open windows for future therapeutic development. Most recently, another group (Lane et al., 2020) developed iPSC-derived retinal organoids from an RP2 patient and also used CRISPR/Cas9 to make RP2 gene knockout iPSCs. Interestingly, both types of organoids showed rod photoreceptor cell death occurring between day-150 and day-180 of culture, with reduced the thickness of the ONL in RP2 null organoids by day-180 when compared to control organoids. They also showed RP2 null effect can be rescued by adeno-associated virus-mediated gene augmentation. These data revealed that 3D retinal organoids can be used to model inherited retinal degeneration and could be a useful tool to test potential therapies to rescue photoreceptor cell loss.

Usher syndrome is a rare genetic disorder primarily affecting hearing and vision. Mutation of the USHERIN protein coding gene *USH2A* is the most common cause. Early studies used 3D retinal organoids derived from *USH2A* patient iPSCs to determine the pathophysiology of disease mechanisms *in vitro* (Tucker et al 2013). Similarly, recent studies have shown early developmental abnormalities in patient-derived retinal organoids caused by significant changes in cytoarchitectural structure (Guo et al 2010).

In our study, we have studied the role of CDH23 protein in patient-derived compound heterozygous variants in the cadherin 23 gene (*CDH23: Arg1437X;Thr2545Thr*). Our work has demonstrated that patient-derived retinal organoids in the context of congenital Usher syndrome type 1D are an important tool for the preclinical testing of small molecules drugs. However, there are still significant barriers to overcome before drug development using 3D retinal organoids is mainstream. For example, the time to generate a laminated retina is in the order of months to a year mirroring fetal development, which is a challenge for industrial scale use. One route that is

being used to overcome this is rotating bioreactors that might allow continuous production of organoids for on-demand experimentation (DiStefano et al., 2018). Also relating to the time constraint is that many inherited retinal diseases occur in later life and may also be influenced by a lifetime of epigenetic modifications and environmental insults. This would be very difficult to model in organoids as they are more suited to developmental abnormalities.

Another limitation of retinal organoids is that they lack some structures that are associated with ocular disease. For example, the fovea in the retina is absent therefore investigating foveal development and diseases with foveal hypoplasia such as aniridia is not currently possible. Retinal organoids also lack a vasculature and do not express inflammatory cell types, so the inflammatory aspects of diseases such as diabetic retinopathy and age-related macular degeneration could not be studied. Normally the retina is situated next to the retinal pigment epithelium *in vivo* and very important interactions occur between these two tissues such as phagocytosis of outer segments. Some forms of retinitis pigmentosa are caused by mutations in genes in the RPE (e.g. *MERTK*), thus retinal diseases involving the RPE could not be studied. However, recently co-culturing retinal organoids with RPE has been tested to overcome this barrier (Akhtar et al., 2019).

Although many barriers need to be overcome including cost and scalability, further improvements to the retinal organoid culture could improve pathological modelling and eventually provide the opportunity for personalized medicine.

Chapter 6: Conclusion

Genetic defects have become a leading factor causing partial to complete vision loss in humans. With mainstream availability of genetic testing it has become apparent that there is widespread genetic heterogeneity in inherited eye diseases, meaning that more than one gene can cause a specific phenotype, that different mutations in the same gene cause different phenotypes and there are variable clinical phenotypes even in a family with the same genetic mutation. This means that there is no ‘magic bullet’ to cure all diseases and that precision medicine is going to be an important factor for each inherited eye disease, which will in part direct the type of therapeutic that can be offered.

Several advanced technologies are undergoing testing for vision loss such as cell-based therapies for replacing and rescuing cell loss (Wang, Y., Tang, & Gu, 2020); gene augmentation to replace missing full length functional proteins (Bashar et al., 2016; Beltran et al., 2014); pharmacological therapies that inhibit or enhance protein activity (Liu et al., 2020; Samanta et al., 2019; Schwarz et al., 2015; Wang et al., 2017); induced pluripotent stem cells (iPSCs) for differentiating into a variety of eye cell types for autologous transplantation (Mandai et al., 2017; Tucker et al., 2013) and generation of *in vitro* 3D model systems for screening drugs and studying disease mechanisms (Du, Y. et al., 2020; Fang & Eglén, 2017); gene editing tools (CRISPR/Cas9) for mutation correction or knockdown studies (Mirjalili Mohanna et al., 2020). Application of these advanced approaches for genetic eye diseases is very attractive since they have the potential to provide a cure the eye defects, or at least prevent the progressive nature of some diseases. In addition, such approaches may reduce the number of invasive medical interventions, particularly for conditions like aniridia, where multiple different treatments are required to address the different problems that these patients experience.

For many genetic eye diseases the natural outcome is often progressive loss of vision that sometimes begins in early childhood. For example, since the *PAX6* gene is involved in early eye development, then mutations affecting this gene causes disruption to early morphogenesis of the anterior and posterior segment of the eye. Consequently, morphological defects such as partial or complete absence of the iris and foveal hypoplasia are present at birth. However, since *PAX6* has a maintenance function, progressive defects such as corneal opacity, cataract and glaucoma develop over time. To overcome the severity of disease and improve vision, several *in-vitro* and *in-vivo* model systems and novel translational therapies have been attempted for this disease. Analysis of nonsense suppression was previously tested by the Gregory-Evans lab, where the tissue malformation defects in the retina, lens and cornea were reversed when treatment was given in the early postnatal period by topical Ataluren® delivery (Gregory-Evans et al., 2014; Wang et al., 2017). In addition, the functional testing of electrical and behavioral responses of the retina were normalized. These data led to an on-going clinical trial for Ataluren® that is being delivered by an oral route (NCT02647359 at ClinicalTrials.gov). Although the oral route is not ideal, because the cornea does not receive a blood supply, this approach could address the systemic features of the disease including pancreatic and brain defects.

Although nonsense suppression has shown some promise, treatments are still needed for other types of *PAX6* defects. A number of other approaches have been tested including inhibiting microRNAs which results in an increase in Pax6 protein from the wildtype Pax6 mRNA (Yongblah, Alford, Ryan, Chow, & Howard, 2018); gene augmentation, however, this negatively affected ocular development (Schedl et al., 1996) and germline CRISPR gene editing to correct the *Pax6*^{sey/+} mutation (Mirjalili Mohanna et al., 2020), although whether this is possible in somatic cells remains to be determined. My work adds to these approaches. I have shown that

nonsense suppression rescues the development of Schlemm's canal and the trabecular meshwork, which normally develop in the early postnatal period. Once these two structures are formed correctly, the drug treatment would no longer be necessary. Future work would involve measuring intraocular pressure over time to see if it remains stable after drug treatment. Thus, it is possible with a short drug treatment that increased intraocular pressure would not occur, removing the need for complicated glaucoma surgeries in aniridia. In a second approach, I tested the notion that treatments aimed at downstream targets of Pax6 could bypass the tightly controlled levels of Pax6 that are required in the postnatal eye. Using a single injection of MSCs to deliver Tgf β 2 protein there was significant remodelling of the anterior chamber in the *Pax6*^{Sev/+} eye. MSCs have been extensively studied for treating genetic eye diseases by sub-retinal (Bashar et al., 2016; Guan et al., 2013), intravitreal (Çerman et al., 2016) and intraocular routes (Ding, Kumar, & Mok, 2017). Interestingly, only the sub-retinal route has shown deleterious effects such as inflammation (Davis, Gregori, MacLaren, & Lam, 2019; Gramlich et al., 2016). We only injected the anterior chamber of one eye to determine if MSCs would cross the blood-retinal barrier and get into the contralateral eye. MSCs were only found in the injected eye, so both eyes would need to be injected to improve the anterior chamber abnormalities. Although injection of MSCs into the *Pax6*^{Sev/+} eye is challenging due to the microphthalmia that is present, microphthalmia does not occur in the human eye, thus cell injections would most likely be easier.

Since nonsense suppression was very effective in the *Pax6*^{Sev/+} mouse we also tested this approach in the new USH1D mouse model (*Cdh23*^{m1btr/-}) of deafness and blindness. These mice exhibited circling behaviour and did not survive past 60 days of age. Furthermore, we did not see the expected Mendelian inheritance rate of 25% of offspring being affected (typically we only saw 1 pup per litter of 8). Homozygotes had abnormal ERG responses, however, on histology there

did not appear to be any structural defects in the retina as with most other Usher syndrome mouse models. Interestingly though, we observed atypical trafficking of photoreceptor proteins that would account for the abnormal ERGs. Treatment with Ataluren® improved survivability, rescued the trafficking defect, and produced Cdh23 protein in the connecting cilium. Due to the lack of affected mice we were unable to determine if nonsense suppression also improved the cochlea defect, although the circling behavior was reduced, suggesting there was an improvement in the vestibular system. Despite the low number of affected offspring in this line, it represents a new Usher model that actually has a retinal phenotype and could therefore be valuable for other researchers.

Taking advantage of iPSC technology we also tested nonsense suppression in retinal organoids produced from anUSH1D patient carrying a compound heterozygous nonsense mutation. Similarly, with Ataluren® treatment we saw improvements in retinal organoid phenotype (i.e. reduced cell death, restored CDH23 protein expression, and expression of photoreceptor proteins). Thus, retinal organoids from patients may be very useful for testing new therapeutic approaches and disease mechanisms. Currently, iPSCs from patients with genetic eye conditions including Leber congenital amaurosis, retinitis pigmentosa, and USH2A syndrome are being used to study disease mechanisms, testing gene editing protocols and drug treatments (Tucker et al, 2013; Burnight ER et al, 2017; Sanjurjo-Soriano C et al., 2019; Lane et al 2020). However, the major obstacle in developing new treatments and understanding disease mechanisms in iPSC-derived retinal organoids is that it takes 250-300 days for the retina to fully mature, mirroring normal human gestation. Thus, data acquisition is slow and very expensive.

Although the nonsense suppression data for *Cdh23/CDH23* mutations in the mouse and iPSC studies showed that there was a positive benefit, this may have limited translation at the

clinical setting, particularly for the hearing deficit of certain types of Usher patient. Patients with type I Usher syndrome (which includesUSH1D) are typically born profoundly deaf, thus nonsense suppression would need to be given during the window of hair cell development. The immature hair cells in the cochlea are formed between 12-14 weeks gestation and are mature by week 22 (Rabbitt et al., 2016). Thus, nonsense suppression treatment would need to be in the second trimester. Although most teratogenic effects related to drug therapy occur during the first trimester, there would be significant regulatory hurdles to overcome for such a treatment to be considered. Usher syndrome types 2 and 3 exhibit hearing loss later in life so postnatal use of nonsense suppression would be possible. All types of Usher syndrome patients have normal vision at birth; thus it would be possible to use nonsense suppression to prevent the progressive vision loss that occurs.

In conclusion, from my experiments and findings treatment strategies such as cell-based gene therapy and nonsense suppression therapy may have a role in improving vision loss in childhood genetic disease such as aniridia and Usher Syndrome 1D. Although these strategies would not necessarily cure each disease, it may reduce the number of complicated medical and surgical interventions that are required in the management of the disease throughout life.

Chapter 7: Future directions

The aim of this thesis was to develop several novel therapies for the treatment of childhood blindness, specifically aniridic glaucoma and Usher syndrome. In my research I performed nonsense suppression therapy and cell-based gene therapeutic strategies to rescue the structural abnormalities in the anterior segment of the eye and improve visual function in preclinical models of aniridic glaucoma and Usher syndrome. Several observations were made that can help to direct future research in improving the visual outcomes by these approaches in animal models.

In Chapter 2, further assessment of the functional benefit of the treatments in the $Pax6^{Sey+/-}$ mouse is warranted. For example, measurement of intraocular pressure using a tonometer in the treated $Pax6^{Sey+/-}$ mouse model may help differentiate the effectiveness of nonsense suppression versus stem cell therapy. Furthermore, utilizing a combination of cell-based approach given at P4 and then nonsense suppression therapy from P5 until P45 in a same cohort. This may provide a synergistic effect compared to single treatment therapies.

Additional studies using different genotypic animal models of aniridic glaucoma are also needed to further test the potential of these therapeutic strategies. For example, $Pax6^{leca3}$ would be an ideal candidate for the nonsense suppression therapy since it has point mutation leading to stop codon in the PST region of the $Pax6$ gene (Thaung et al., 2002). The $Pax6^{sey-neu}$ has a missense mutation in the PST domain causing severe abnormalities in the eye (Chhabra et al., 2020; Douvaras et al., 2013) and this model could be utilized as potential model to study the effects of the cell-based treatment strategy.

In Chapter 4, preliminary *in vivo* data showed that nonsense suppression significantly improved retinal function, restored Cdh23 protein expression and corrected the abnormal localization of photoreceptor proteins in the retina of the homozygous $Cdh23$ mouse model of

Usher syndrome. This study however was undertaken in a relatively small number of animals and further studies are needed to better measure the effectiveness of the treatment. In addition, changes in expression of *Cdh23* mRNA could be measured using quantitative RT-PCR in the treated mice. Further, we could study the functional benefits of hearing deficiency using the Auditory Brainstem Response (ABR) test and evaluate the effectiveness of treatment on improving the developmental malformations in the hair cells of the cochlea of the inner ear.

Human retinal organoids differentiated from patient specific iPSCs allow us to investigate diseases mechanisms and evaluate novel therapies for untreatable retinal disorders. Advancement of molecular technologies, cellular phenotyping by FACS, single cell RNA sequencing, advanced non-invasive imaging techniques (optical coherence tomography), next generation electrophysiology (image guided electroretinogram), and high-throughput drug screening approaches are considerably expanded the application of functional retinal cells and organoids for developing individualized medicines for autologous therapies.

In Chapter 5, cultured 3D retinal organoids, derived from patient iPSCs expressing a nonsense mutation in *CDH23* gene, exhibited increased cell death. Treatment with Ataluren® reduced cell death and restored the expression of various photoreceptors protein. Due to time limits we stopped the study at day 200, however, it would be useful to continue culturing to P300 when the retinal organoids are expected to have fully functioning photoreceptors cells. Further studies would include electrophysiological testing, imaging of transportation of proteins through the cilium, assessment of cell death pathway signaling and structural analysis by electron microscopy.

The work presented in this thesis provides a foundation for the above-mentioned future studies. These proposed studies will provide further support to the effectiveness of nonsense

suppression and cell-based delivery of proteins in animal models, paving the way to accelerate the development of more effective treatment for some forms of childhood blindness.

Bibliography

- Adachi, M., Dickens, C. J., Hetherington, J., Hoskins, H. D., Iwach, A. G., Wong, P. C., et al. (1997). Clinical experience of trabeculotomy for the surgical treatment of aniridic glaucoma. *Ophthalmology*, *104*(12), 2121-2125.
- Agarwal, P., Daher, A. M., & Agarwal, R. (2015). Aqueous humor TGF- β 2 levels in patients with open-angle glaucoma: A meta-analysis. *Molecular Vision*, *21*, 612.
- Akhtar, T., Xie, H., Khan, M. I., Zhao, H., Bao, J., Zhang, M., et al. (2019). Accelerated photoreceptor differentiation of hiPSC-derived retinal organoids by contact co-culture with retinal pigment epithelium. *Stem Cell Research*, *39*, 101491. doi:10.1016/j.scr.2019.101491
- Akhurst, R. J., FitzPatrick, D. R., Gatherer, D., Lehnert, S. A., & Millan, F. A. (1990). Transforming growth factor betas in mammalian embryogenesis. *Progress in Growth Factor Research*, *2*(3), 153-168. doi:[https://doi-org.ezproxy.library.ubc.ca/10.1016/0955-2235\(90\)90002-2](https://doi-org.ezproxy.library.ubc.ca/10.1016/0955-2235(90)90002-2)
- Al-Jaibaji, O., Swioklo, S., & Connon, C. J. (2019). Mesenchymal stromal cells for ocular surface repair. *Expert Opinion on Biological Therapy*, *19*(7), 643-653.
- Almoussa, R., Almoussa, R., Lake, D. B., & Lake, D. B. (2014). Intraocular pressure control with ahmed glaucoma drainage device in patients with cicatricial ocular surface disease-associated or aniridia-related glaucoma. *International Ophthalmology*, *34*(4), 753-760.

- Altmann, C. R., Chow, R. L., Lang, R. A., & Hemmati-Brivanlou, A. (1997). Lens induction by pax-6 in *Xenopus laevis*. *Developmental Biology*, *185*(1), 119-123. doi:<https://doi-org.ezproxy.library.ubc.ca/10.1006/dbio.1997.8573>
- Alward, W. L. M., Semina, E. V., Small, K. W., Datson, N. A., Siegel-Bartelt, J., Murray, J. C., et al. (1996). Cloning and characterization of a novel bicoid -related homeobox transcription factor gene, RIEG, involved in rieger syndrome. *Nature Genetics*, *14*(4), 392-399.
- Ambati, B. K., Nozaki, M., Singh, N., Takeda, A., Jani, P. D., Suthar, T., Ambati, J. (2006a). Corneal avascularity is due to soluble VEGF receptor-1. *Nature*, *443*(7114), 993-997. doi:[10.1038/nature05249](https://doi.org/10.1038/nature05249)
- Arroyave, C. P., Scott, I. U., Gedde, S. J., Parrish, R. K., & Feuer, W. J. (2003). Use of glaucoma drainage devices in the management of glaucoma associated with aniridia. *American Journal of Ophthalmology*, *135*(2), 155-159.
- Ashery-Padan, R., Marquardt, T., Zhou, X., & Gruss, P. (2000). Pax6 activity in the lens primordium is required for lens formation and for correct placement of a single retina in the eye. *Genes & Development*, *14*(21), 2701-2711. doi:[10.1101/gad.184000](https://doi.org/10.1101/gad.184000) [doi]
- Azaiez, H., Booth, K. T., Ephraim, S. S., Crone, B., Black-Ziegelbein, E. A., Marini, R. J., et al. (2018). Genomic landscape and mutational signatures of deafness-associated genes. *American Journal of Human Genetics*, *103*(4), 484-497. doi:[10.1016/j.ajhg.2018.08.006](https://doi.org/10.1016/j.ajhg.2018.08.006)

Bashar, A. E., Metcalfe, A. L., Viringipurampeer, I. A., Yanai, A., Gregory-Evans, C. Y., & Gregory-Evans, K. (2016a). An ex vivo gene therapy approach in X-linked retinoschisis. *Molecular Vision*, 22, 718-733.

Bashar, A. E., Metcalfe, A. L., Viringipurampeer, I. A., Yanai, A., Gregory-Evans, C. Y., & Gregory-Evans, K. (2016b). An ex vivo gene therapy approach in X-linked retinoschisis. *Molecular Vision*, 22, 718-733.

Bashar, A. E., Metcalfe, A., Yanai, A., Laver, C., Hafeli, U. O., Gregory-Evans, C. Y., et al. (2013). Influence of iron oxide nanoparticles on innate and genetically modified secretion profiles of mesenchymal stem cells. *IEEE Transactions on Magnetics*, 49(1), 389-393.
doi:10.1109/TMAG.2012.2225829

Baulmann, D. C., Ohlmann, A., Flügel-Koch, C., Goswami, S., Cvekl, A., & Tamm, E. R. (2002). *Pax6 heterozygous eyes show defects in chamber angle differentiation that are associated with a wide spectrum of other anterior eye segment abnormalities* doi:[https://doi-org.ezproxy.library.ubc.ca/10.1016/S0925-4773\(02\)00260-5](https://doi-org.ezproxy.library.ubc.ca/10.1016/S0925-4773(02)00260-5)

Beebe, D. C., & Coats, J. M. (2000). The lens organizes the anterior segment: Specification of neural crest cell differentiation in the avian eye. *Developmental Biology*, 220(2), 424-431.

Beltran, W. A., Cideciyan, A. V., Lewin, A. S., Hauswirth, W. W., Jacobson, S. G., & Aguirre, G. D. (2014). Gene augmentation for X-linked retinitis pigmentosa caused by mutations in RPGR. *Cold Spring Harbor Perspectives in Medicine*, 5(2), a017392.
doi:10.1101/cshperspect.a017392

- Berry, F. B., Lines, M. A., Footz, T., Underhill, D. A., Gage, P. J., & Walter, M. A. (2006). Functional interactions between FOXC1 and PITX2 underlie the sensitivity to FOXC1 gene dose in axenfeld-rieger syndrome and anterior segment dysgenesis. *Human Molecular Genetics*, *15*(6), 905-919
- Bhuvanagiri, M., Lewis, J., Putzker, K., Becker, J. P., Leicht, S., Krijgsveld, J., . . . Kulozik, A. E. (2014). 5-azacytidine inhibits nonsense-mediated decay in a MYC-dependent fashion. *EMBO Molecular Medicine*, *6*(12), 1593-1609. doi:10.15252/emmm.201404461
- Biasco, L., Rothe, M., Büning, H., & Schambach, A. (2018). Analyzing the genotoxicity of retroviral vectors in hematopoietic cell gene therapy. *Molecular Therapy. Methods & Clinical Development*, *8*(C), 21-30. doi:10.1016/j.omtm.2017.10.002
- Bolz, H., von Brederlow, B., Ramírez, A., Bryda, E. C., Kutsche, K., Nothwang, H. G., et al. (2001). Mutation of CDH23, encoding a new member of the cadherin gene family, causes usher syndrome type 1D. *Nature Genetics*, *27*(1), 108-112. doi:10.1038/83667
- Boughman, J. A., Vernon, M., & Shaver, K. A. (1983). Usher syndrome: Definition and estimate of prevalence from two high-risk populations. *Journal of Chronic Diseases*, *36*(8), 595-603. doi:10.1016/0021-9681(83)90147-9
- Brauner, S. C., Walton, D. S., & Chen, T. C. (2008). Aniridia. *International Ophthalmology Clinics*, *48*(2), 79-85. doi:10.1097/IIO.0b013e318169314b

- Braunger, B. M., Fuchshofer, R., & Tamm, E. R. (2015). The aqueous humor outflow pathways in glaucoma: A unifying concept of disease mechanisms and causative treatment. *European Journal of Pharmaceutics and Biopharmaceutics*, 95(Pt B), 173-181.
- Brigid L. M. Hogan, Elizabeth M. A. Hirst, Horsburgh, G., & Hetherington, C. M. (1988). Small eye (sey): A mouse model for the genetic analysis of craniofacial abnormalities. *Development*, 103(Supplement), 115.
- Brill, E., Malanson, K. M., Radu, R. A., Boukharov, N. V., Wang, Z., Chung, H., et al. (2007). A novel form of transducin-dependent retinal degeneration: Accelerated retinal degeneration in the absence of rod transducin. *Investigative Ophthalmology & Visual Science*, 48(12), 5445-5453. doi:10.1167/iovs.06-1402
- Çerman, E., Akkoç, T., Eraslan, M., Şahin, Ö, Özkara, S., Vardar Aker, F., et al. (2016). Retinal electrophysiological effects of intravitreal bone marrow derived mesenchymal stem cells in streptozotocin induced diabetic rats. *PLoS ONE*, 11(6) doi:10.1371/journal.pone.0156495
- Chang, B. (2016). Mouse models as tools to identify genetic pathways for retinal degeneration, as exemplified by leber's congenital amaurosis. *Methods in Molecular Biology (Clifton, N.J.)*, 1438, 417-430. doi:10.1007/978-1-4939-3661-8_21
- Chang, B., Smith, R. S., Peters, M., Savinova, O. V., Hawes, N. L., Zabaleta, A., et al. (2001). Haploinsufficient Bmp4 ocular phenotypes include anterior segment dysgenesis with elevated intraocular pressure. *BMC Genetics*, 2(1), 18. doi:10.1186/1471-2156-2-18

- Chen, H., Lun, Y., Ovchinnikov, D., Kokubo, H., Oberg, K. C., Pepicelli, C. V., et al. (1998). Limb and kidney defects in *Lmx1b* mutant mice suggest an involvement of LMX1B in human nail patella syndrome. *Nature Genetics*, *19*(1), 51-55. doi:10.1038/ng0598-51
- Chen, L. S., & Gage, P. J. (2016). Heterozygous *Pitx2* null mice accurately recapitulate the ocular features of axenfeld-rieger syndrome and congenital glaucoma. *Investigative Ophthalmology & Visual Science*, *57*(11), 5023-5030.
- Chhabra, N. F., Amarie, O. V., Wu, M., Amend, A., Rubey, M., Gradinger, D., Hrabě de Angelis, M. (2020). PAX6 mutation alters circadian rhythm and β cell function in mice without affecting glucose tolerance. *Communications Biology*, *3*(1), 628. doi:10.1038/s42003-020-01337-x
- Chuang, K., Fields, M. A., & Del Priore, L. V. (2017). Potential of gene editing and induced pluripotent stem cells (iPSCs) in treatment of retinal diseases. *The Yale Journal of Biology and Medicine*, *90*(4), 635-642. Retrieved from <https://www.ncbi.nlm.nih.gov/pmc/articles/PMC5733854/>
- Collinson, J. M., Hill, R. E., & West, J. D. (2000). Different roles for Pax6 in the optic vesicle and facial epithelium mediate early morphogenesis of the murine eye. *Development*, *127*(5), 945.
- Collinson, J. M., Quinn, J. C., Hill, R. E., & West, J. D. (2003). The roles of Pax6 in the cornea, retina, and olfactory epithelium of the developing mouse embryo. *Developmental Biology*, *255*(2), 303-312. doi:S0012160602000957 [pii]

- Concepcion, F., Mendez, A., & Chen, J. (2002). The carboxyl-terminal domain is essential for rhodopsin transport in rod photoreceptors. *Vision Research*, 42(4), 417-426.
doi:10.1016/s0042-6989(01)00195-x
- Conley, S. M., Cai, X., & Naash, M. I. (2008). Non-viral ocular gene therapy: Assessment and future directions. *Current Opinion in Molecular Therapeutics*, 10(5), 456-463. Retrieved from <https://www.ncbi.nlm.nih.gov/pmc/articles/PMC2938038/>
- Cosgrove, D., & Zallocchi, M. (2014). Usher protein functions in hair cells and photoreceptors. *International Journal of Biochemistry and Cell Biology*, 46, 80-89.
doi:10.1016/j.biocel.2013.11.001
- Cousins, S. W., McCabe, M. M., Danielpour, D., & Streilein, J. W. (1991). Identification of transforming growth-factor-beta as an immunosuppressive factor in aqueous-humor. *Investigative Ophthalmology & Visual Science*, 32(8), 2201-2211.
- Cvekl, A., & Callaerts, P. (2017). Experimental eye research. *Experimental Eye Research*, 156, 10-21. Retrieved from <http://www.sciencedirect.com/science/article/pii/S0014483516300902>
- Cvekl, A., & Tamm, E. R. (2004). Anterior eye development and ocular mesenchyme: New insights from mouse models and human diseases. *BioEssays*, 26(4), 374-386.
- Dang, Y., Low, W., Xu, J., Gehring, N. H., Dietz, H. C., Romo, D., & Liu, J. O. (2009). Inhibition of nonsense-mediated mRNA decay by the natural product pateamine A through

eukaryotic initiation factor 4AIII. *The Journal of Biological Chemistry*, 284(35), 23613-23621. doi:10.1074/jbc.M109.009985

Dastiridou, A. I., Katsanos, A., Denis, P., Francis, B. A., Mikropoulos, D. G., Teus, M. A., et al. (2018). Cyclodestructive procedures in glaucoma: A review of current and emerging options. *Advances in Therapy*, 35(12), 2103-2127.

Davis, J. L., Gregori, N. Z., MacLaren, R. E., & Lam, B. L. (2019). Surgical technique for subretinal gene therapy in humans with inherited retinal degeneration. *Retina*, 39, S2. doi:10.1097/IAE.0000000000002609

Ding, S. L. S., Kumar, S., & Mok, P. L. (2017). Cellular reparative mechanisms of mesenchymal stem cells for retinal diseases. *International Journal of Molecular Sciences*, 18(8) doi:10.3390/ijms18081406

DiStefano, T., Chen, H. Y., Panebianco, C., Kaya, K. D., Brooks, M. J., Gieser, L., et al. (2018). Accelerated and improved differentiation of retinal organoids from pluripotent stem cells in rotating-wall vessel bioreactors. *Stem Cell Reports*, 10(1), 300-313. doi:10.1016/j.stemcr.2017.11.001

Douvaras, P., Mort, R. L., Edwards, D., Ramaesh, K., Dhillon, B., Morley, S. D., . . . West, J. D. (2013). Increased corneal epithelial turnover contributes to abnormal homeostasis in the Pax6(+/-) mouse model of aniridia. *PloS One*, 8(8), e71117. doi:10.1371/journal.pone.0071117

- Du, L., Jung, M. E., Damoiseaux, R., Completo, G., Fike, F., Ku, J., et al. (2013). A new series of small molecular weight compounds induce read through of all three types of nonsense mutations in the ATM gene. *Molecular Therapy: The Journal of the American Society of Gene Therapy*, 21(9), 1653-1660. doi:10.1038/mt.2013.150
- Du, M., Liu, X., Welch, E. M., Hirawat, S., Peltz, S. W., & Bedwell, D. M. (2008). PTC124 is an orally bioavailable compound that promotes suppression of the human CFTR-G542X nonsense allele in a CF mouse model. *Proceedings of the National Academy of Sciences of the United States of America*, 105(6), 2064-2069.
- Du, Y., Li, X., Niu, Q., Mo, X., Qui, M., Ma, T., et al. (2020). Development of a miniaturized 3D organoid culture platform for ultra-high-throughput screening. *Journal of Molecular Cell Biology*, 12(8), 630-643. doi:10.1093/jmcb/mjaa036
- Durand, S., Cougot, N., Mahuteau-Betzer, F., Nguyen, C., Grierson, D. S., Bertrand, E., . . . Lejeune, F. (2007). Inhibition of nonsense-mediated mRNA decay (NMD) by a new chemical molecule reveals the dynamic of NMD factors in P-bodies. *The Journal of Cell Biology*, 178(7), 1145-1160. doi:10.1083/jcb.200611086
- Evans, A. L., & Gage, P. J. (2005). Expression of the homeobox gene Pitx2 in neural crest is required for optic stalk and ocular anterior segment development. *Human Molecular Genetics*, 14(22), 3347-3359.
- Fang, Y., & Eglen, R. M. (2017). Three-dimensional cell cultures in drug discovery and development. *Slas Discovery*, 22(5), 456-472. doi:10.1177/1087057117696795

- Fantes, J., Redeker, B., Breen, M., Boyle, S., Brown, J., Fletcher, J., et al. (1995). Aniridia-associated cytogenetic rearrangements suggest that a position effect may cause the mutant phenotype. *Human Molecular Genetics*, 4(3), 415-422. doi:10.1093/hmg/4.3.415
- Foltz, L. P., & Clegg, D. O. (2019). Patient-derived induced pluripotent stem cells for modelling genetic retinal dystrophies. *Progress in Retinal and Eye Research*, 68, 54-66. doi:10.1016/j.preteyeres.2018.09.002
- Frick, K. D., Roebuck, M. C., Feldstein, J. I., McCarty, C. A., & Grover, L. L. (2012). Health services utilization and cost of retinitis pigmentosa. *Archives of Ophthalmology*, 130(5), 629-634. doi:10.1001/archophthalmol.2011.2820
- French, L. S., Mellough, C. B., Chen, F. K., & Carvalho, L. S. (2020). A review of gene, drug and cell-based therapies for usher syndrome. *Frontiers in Cellular Neuroscience*, 14 doi:10.3389/fncel.2020.00183
- Fuchshofer, R., & Tamm, E. R. (2009). Modulation of extracellular matrix turnover in the trabecular meshwork. *Experimental Eye Research*, 88(4), 683-688.
- Fusaki, N., Ban, H., Nishiyama, A., Saeki, K., & Hasegawa, M. (2009). Efficient induction of transgene-free human pluripotent stem cells using a vector based on sendai virus, an RNA virus that does not integrate into the host genome. *Proceedings of the Japan Academy. Series B, Physical and Biological Sciences*, 85(8), 348-362. doi:10.2183/pjab.85.348

- Gage, P. J., Rhoades, W., Prucka, S. K., & Hjalt, T. (2005). Fate maps of neural crest and mesoderm in the mammalian eye. *Investigative Ophthalmology & Visual Science*, *46*(11), 4200-4208.
- Gage, P. J., Kuang, C., & Zacharias, A. L. (2014). The homeodomain transcription factor PITX2 is required for specifying correct cell fates and establishing angiogenic privilege in the developing cornea. *Developmental Dynamics*, *243*(11), 1391-1400.
- Gage, P. J., & Zacharias, A. L. (2009). Signaling “cross-talk” is integrated by transcription factors in the development of the anterior segment in the eye. *Developmental Dynamics*, *238*(9), 2149-2162.
- Gaudin, C., Forster, V., Sahel, J., Dreyfus, H., & Hicks, D. (1996). Survival and regeneration of adult human and other mammalian photoreceptors in culture. *Investigative Ophthalmology & Visual Science*, *37*(11), 2258-2268.
- Gehring, W. J., & Ikeo, K. (1999). Pax 6: Mastering eye morphogenesis and eye evolution. *Trends in Genetics: TIG*, *15*(9), 371-377. doi:10.1016/s0168-9525(99)01776-x
- Gehring, W. J. (2002). The genetic control of eye development and its implications for the evolution of the various eye-types. *The International Journal of Developmental Biology*, *46*(1), 65-73.
- Glaser, T., Jepeal, L., Edwards, J. G., Young, S. R., Favor, J., & Maas, R. L. (1994). PAX6 gene dosage effect in a family with congenital cataracts, aniridia, anophthalmia and central nervous system defects. *Nature Genetics*, *7*(4), 463-471. doi:10.1038/ng0894-463

- Goldmann, T., Overlack, N., Wolfrum, U., & Nagel-Wolfrum, K. (2011). PTC124-mediated translational readthrough of a nonsense mutation causing usher syndrome type 1C. *Human Gene Therapy*, 22(5), 537-547. doi:10.1089/hum.2010.067
- Goldmann, T., Overlack, N., Möller, F., Belakhov, V., Wyk, M. v., Baasov, T., et al. (2012). A comparative evaluation of NB30, NB54 and PTC124 in translational read-through efficacy for treatment of anUSH1C nonsense mutation. *EMBO Molecular Medicine*, 4(11), 1186-1199. doi:10.1002/emmm.201201438
- Gonzalez-Hilarion, S., Beghyn, T., Jia, J., Debreuck, N., Berte, G., Mamchaoui, K., . . . Lejeune, F. (2012). Rescue of nonsense mutations by amlexanox in human cells. *Orphanet Journal of Rare Diseases*, 7, 58. doi:10.1186/1750-1172-7-58
- Gould, D. B., Smith, R. S., & John, S. W. M. (2004). Anterior segment development relevant to glaucoma. *The International Journal of Developmental Biology*, 48(8-9), 1015-1029. doi:10.1387/ijdb.041865dg
- Gramlich, O. W., Burand, A. J., Brown, A. J., Deutsch, R. J., Kuehn, M. H., & Ankrum, J. A. (2016). Cryopreserved mesenchymal stromal cells maintain potency in a retinal ischemia/reperfusion injury model: Toward an off-the-shelf therapy. *Scientific Reports*, 6, 26463. doi:10.1038/srep26463
- Grant, M. K., Bobiley, A. M., Pierce, J. E., DeWitte, J., & Lauderdale, J. D. (2017). Structural brain abnormalities in 12 persons with aniridia [version 2; peer review: 2 approved]. *F1000Research*, 6(255) doi:10.12688/f1000research.11063.2

- Grant, W. M., & Walton, D. S. (1974). Progressive changes in the angle in congenital aniridia, with development of glaucoma. *American Journal of Ophthalmology*, 78(5), 842.
- Green, E. S., Menz, M. D., LaVail, M. M., & Flannery, J. G. (2000). Characterization of rhodopsin mis-sorting and constitutive activation in a transgenic rat model of retinitis pigmentosa. *Investigative Ophthalmology & Visual Science*, 41(6), 1546-1553.
- Gregory-Evans, C. Y., Wang, X., & Gregory-Evans, K. (2019). Prospects and modalities for the treatment of genetic ocular anomalies. *Human Genetics*, 138(8), 1019-1026.
- Gregory-Evans, C. Y., Wang, X., Wasan, K. M., Zhao, J., Metcalfe, A. L., & Gregory-Evans, K. (2014). Postnatal manipulation of Pax6 dosage reverses congenital tissue malformation defects. *The Journal of Clinical Investigation*, 124(1), 111-116. doi:10.1172/JCI70462
- Guan, Y., Cui, L., Qu, Z., Lu, L., Wang, F., Wu, Y., et al. (2013). Subretinal transplantation of rat MSCs and erythropoietin gene modified rat MSCs for protecting and rescuing degenerative retina in rats. *Current Molecular Medicine*, 13(9), 1419-1431. doi:10.2174/15665240113139990071
- Guerin, K., Gregory-Evans, C. Y., Hodges, M. D., Moosajee, M., Mackay, D. S., Gregory-Evans, K., et al. (2008). Systemic aminoglycoside treatment in rodent models of retinitis pigmentosa. *Experimental Eye Research*, 87(3), 197-207.
- Hanson, I. M., Fletcher, J. M., Jordan, T., Brown, A., Taylor, D., Adams, R. J., et al. (1994). Mutations at the PAX6 locus are found in heterogeneous anterior segment malformations including peters' anomaly. *Nature Genetics*, 6(2), 168-173. doi:10.1038/ng0294-168

- Hanson, I., & Van Heyningen, V. (1995). Pax6: More than meets the eye. *Trends in Genetics*, 11(7), 268-272. doi:[https://doi-org.ezproxy.library.ubc.ca/10.1016/S0168-9525\(00\)89073-3](https://doi-org.ezproxy.library.ubc.ca/10.1016/S0168-9525(00)89073-3)
- Harz, C., Ludwig, N., Lang, S., Werner, T. V., Galata, V., Backes, C., et al. (2014). Secretion and immunogenicity of the meningioma-associated antigen TXNDC16. *Journal of Immunology (Baltimore, Md.: 1950)*, 193(6), 3146-3154. doi:10.4049/jimmunol.1303098
- Hashimoto, T., Gibbs, D., Lillo, C., Azarian, S. M., Legacki, E., Zhang, X., et al. (2007). Lentiviral gene replacement therapy of retinas in a mouse model for usher syndrome type 1B. *Gene Therapy*, 14(7), 584-594. doi:10.1038/sj.gt.3302897
- Hill, R. E. (1991). Mouse small eye results from mutations in a paired-like homeobox-containing gene. *Nature (London)*, 354(6354), 522.
- Hingorani, M., Hanson, I., & van Heyningen, V. (2012). Aniridia. *European Journal of Human Genetics: EJHG*, 20(10), 1011-1017. doi:10.1038/ejhg.2012.100
- Hodgkinson, C. P., Gomez, J. A., Mirotsov, M., & Dzau, V. J. (2010). Genetic engineering of mesenchymal stem cells and its application in human disease therapy. *Human Gene Therapy*, 21(11), 1513-1526. doi:10.1089/hum.2010.165 [doi]
- Hodgson, S. V., & Saunders, K. E. (1980). A probable case of the homozygous condition of the aniridia gene. *Journal of Medical Genetics*, 17(6), 478-480. Retrieved from <https://www.ncbi.nlm.nih.gov/pmc/articles/PMC1885928/>

- Holme, R. H., & Steel, K. P. (2002). Stereocilia defects in waltzer (Cdh23), shaker1 (Myo7a) and double waltzer/shaker1 mutant mice. *Hearing Research*, 169(1-2), 13-23.
doi:10.1016/s0378-5955(02)00334-9
- Hu, K., Yu, J., Suknuntha, K., Tian, S., Montgomery, K., Choi, K., et al. (2011). Efficient generation of transgene-free induced pluripotent stem cells from normal and neoplastic bone marrow and cord blood mononuclear cells. *Blood*, 117(14), e109-e119. doi:10.1182/blood-2010-07-298331
- Huang, D., Fletcher, S., Wilton, S. D., Palmer, N., McLenachan, S., Mackey, D. A., et al. (2017). Inherited retinal disease therapies targeting precursor messenger ribonucleic acid. *Vision (Basel, Switzerland)*, 1(3) doi:10.3390/vision1030022
- Hug, N., Longman, D., & Cáceres, J. F. (2016). Mechanism and regulation of the nonsense-mediated decay pathway. *Nucleic Acids Research*, 44(4), 1483-1495.
doi:10.1093/nar/gkw010
- Ittner, L. M., Wurdak, H., Schwerdtfeger, K., Kunz, T., Ille, F., Leveen, P., et al. (2005). Compound developmental eye disorders following inactivation of TGF β signaling in neural-crest stem cells. *Journal of Biology*, 4(3), 11. doi:10.1186/jbiol29
- Iwao, K., Inatani, M., Matsumoto, Y., Ogata-Iwao, M., Takihara, Y., Irie, F., et al. (2009). Heparan sulfate deficiency leads to peters anomaly in mice by disturbing neural crest TGF-[beta]² signaling. *Journal of Clinical Investigation*, 119(7), 1997.

- Jeon, S., Ahn, J., Halder, D., Cho, H., Lim, J., Jun, S. Y., et al. (2019). TIPRL potentiates survival of lung cancer by inducing autophagy through the eIF2 α -ATF4 pathway. *Cell Death & Disease*, 10(12), 959. doi:10.1038/s41419-019-2190-0
- Jia, F., Wilson, K. D., Sun, N., Gupta, D. M., Huang, M., Li, Z., et al. (2010). A nonviral minicircle vector for deriving human iPS cells. *Nature Methods*, 7(3), 197-199. doi:10.1038/nmeth.1426
- Jm, M., E, A., T, J., F, B., A, G. & C, A. (2011). *An update on the genetics of usher syndrome*. Retrieved Dec 18, 2020, from <https://pubmed-ncbi-nlm-nih.gov.ezproxy.library.ubc.ca/21234346/?dopt=Abstract>
- Joensuu, T., Hämäläinen, R., Yuan, B., Johnson, C., Tegelberg, S., Gasparini, P., et al. (2001). Mutations in a novel gene with transmembrane domains underlie usher syndrome type 3. *American Journal of Human Genetics*, 69(4), 673-684. doi:10.1086/323610
- Johnson, C. E., & Tee, A. R. (2017). Exploiting cancer vulnerabilities: mTOR, autophagy, and homeostatic imbalance. *Essays in Biochemistry*, 61(6), 699-710. doi:10.1042/EBC20170056
- Johnson, T. V., Bull, N. D., Hunt, D. P., Marina, N., Tomarev, S. I., & Martin, K. R. (2010). Neuroprotective effects of intravitreal mesenchymal stem cell transplantation in experimental glaucoma. *Investigative Ophthalmology & Visual Science*, 51(4), 2051-2059.
- Junglas, B., Kuespert, S., Seleem, A. A., Struller, T., Ullmann, S., Bösl, M., et al. (2012). Connective tissue growth factor causes glaucoma by modifying the actin cytoskeleton of the trabecular meshwork. *American Journal of Pathology, The*, 180(6), 2386-2403.

- Junglas, B., Yu, A. H. L., Welge-Lüssen, U., Tamm, E. R., & Fuchshofer, R. (2009). Connective tissue growth factor induces extracellular matrix deposition in human trabecular meshwork cells. *Experimental Eye Research*, 88(6), 1065-1075.
- Kalcheim, C. (2015). Epithelial–Mesenchymal transitions during neural crest and somite development. *Journal of Clinical Medicine*, 5(1) doi:10.3390/jcm5010001
- Kaufman, M. H., Chang, H. H., & Shaw, J. P. (1995). Craniofacial abnormalities in homozygous small eye (sey/sey) embryos and newborn mice. *Journal of Anatomy*, 186(Pt 3), 607-617.
Retrieved from <https://www.ncbi.nlm.nih.gov/pmc/articles/PMC1167018/>
- Kay, M. A., Glorioso, J. C., & Naldini, L. (2001). Viral vectors for gene therapy: The art of turning infectious agents into vehicles of therapeutics. *Nature Medicine*, 7(1), 33-40.
doi:10.1038/83324
- Kazmierczak, P., Sakaguchi, H., Tokita, J., Wilson-Kubalek, E. M., Milligan, R. A., Müller, U., et al. (2007). Cadherin 23 and protocadherin 15 interact to form tip-link filaments in sensory hair cells. *Nature*, 449(7158), 87-91. doi:10.1038/nature06091
- Khan, S. H. (2019). Genome-editing technologies: Concept, pros, and cons of various genome-editing techniques and bioethical concerns for clinical application. *Molecular Therapy. Nucleic Acids*, 16, 326-334. doi:10.1016/j.omtn.2019.02.027
- Ken K. Nischal, Jane C. Swoden. (2016). Anterior segment: Developmental anomalies.
Retrieved from <https://entokey.com/anterior-segment-developmental-anomalies/>

- Kidson, S. H., Kume, T., Deng, K., Winfrey, V., & Hogan, B. L. M. (1999). The forkhead/winged-helix gene, Mf1, is necessary for the normal development of the cornea and formation of the anterior chamber in the mouse eye. *Developmental Biology*, *211*(2), 306-322.
- Kim, D., Kim, C., Moon, J., Chung, Y., Chang, M., Han, B., et al. (2009). Generation of human induced pluripotent stem cells by direct delivery of reprogramming proteins. *Cell Stem Cell*, *4*(6), 472-476.
- Kimberling, W. J., Hildebrand, M. S., Shearer, A. E., Jensen, M. L., Halder, J. A., Trzuppek, K., et al. (2010). Frequency of usher syndrome in two pediatric populations: Implications for genetic screening of deaf and hard of hearing children. *Genetics in Medicine: Official Journal of the American College of Medical Genetics*, *12*(8), 512-516.
doi:10.1097/GIM.0b013e3181e5afb8
- Kong, L., Li, F., Soleman, C. E., Li, S., Elias, R. V., Zhou, X., et al. (2006). Bright cyclic light accelerates photoreceptor cell degeneration in tubby mice. *Neurobiology of Disease*, *21*(3), 468-477. doi:10.1016/j.nbd.2005.08.017
- Kremer, H., van Wijk, E., Märker, T., Wolfrum, U., & Roepman, R. (2006). Usher syndrome: Molecular links of pathogenesis, proteins and pathways. *Human Molecular Genetics*, *15*(suppl_2), R262-R270. doi:10.1093/hmg/ddl205
- Kroeber, M., Davis, N., Holzmann, S., Kritzenberger, M., Shelah-Goraly, M., Ofri, R., et al. (2010). Reduced expression of Pax6 in lens and cornea of mutant mice leads to failure of

chamber angle development and juvenile glaucoma. *Human Molecular Genetics*, 19(17), 3332-3342.

Labrador-Velandia, S., Alonso-Alonso, M. L., Alvarez-Sanchez, S., González-Zamora, J., Carretero-Barrio, I., Pastor, J. C., et al. (2016). Mesenchymal stem cell therapy in retinal and optic nerve diseases: An update of clinical trials. *World Journal of Stem Cells*, 8(11), 376-383. doi:10.4252/wjsc.v8.i11.376

Lagziel, A., Overlack, N., Bernstein, S. L., Morell, R. J., Wolfrum, U., & Friedman, T. B. (2009). Expression of cadherin 23 isoforms is not conserved: Implications for a mouse model of usher syndrome type 1D. *Molecular Vision*, 15, 1843-1857. doi:196 [pii]

Lane, A., Jovanovic, K., Shortall, C., Ottaviani, D., Panes, A. B., Schwarz, N., et al. (2020). Modeling and rescue of RP2 retinitis pigmentosa using iPSC-derived retinal organoids. *Stem Cell Reports*, 15(1), 67-79. doi:10.1016/j.stemcr.2020.05.007

Lauderdale, J. D., Wilensky, J. S., Oliver, E. R., Walton, D. S., & Glaser, T. (2000). 3' deletions cause aniridia by preventing PAX6 gene expression. *Proceedings of the National Academy of Sciences of the United States of America*, 97(25), 13755-13759. doi:10.1073/pnas.240398797

Lee, H., Khan, R., & O'Keefe, M. (2008). Aniridia: Current pathology and management. *Acta Ophthalmologica*, 86(7), 708-715. doi:10.1111/j.1755-3768.2008.01427.x

Leung, L. -. B., Flynn, T., Tsai, J. C., P. J. G. Maris, Jr, & Al-Aswad, L. A. (2008). The effect of systemic immunosuppression on the hypertensive phase in uveitic glaucoma patients

undergoing ahmed valve implantation (preliminary study). *Investigative Ophthalmology & Visual Science*, 49(13), 4739-4739. Retrieved from

<http://iovs.arvojournals.org/article.aspx?articleid=2380121>

Li, M., & Izpisua Belmonte, J. C. (2019). Organoids — preclinical models of human disease. *The New England Journal of Medicine*, 380(6), 569-579.

Libby, R. T., & Steel, K. P. (2001). Electroretinographic anomalies in mice with mutations in *Myo7a*, the gene involved in human usher syndrome type 1B. *Investigative Ophthalmology & Visual Science*, 42(3), 770-778.

Libby, R. T., Kitamoto, J., Holme, R. H., Williams, D. S., & Steel, K. P. (2003). *Cdh23* mutations in the mouse are associated with retinal dysfunction but not retinal degeneration. *Experimental Eye Research*, 77(6), 731-739.

Linde, L., Boelz, S., Nissim-Rafinia, M., Oren, Y. S., Wilschanski, M., Yaacov, Y., et al. (2007). Nonsense-mediated mRNA decay affects nonsense transcript levels and governs response of cystic fibrosis patients to gentamicin. *The Journal of Clinical Investigation*, 117(3), 683-692. doi:10.1172/JCI28523

Liu, P., & Johnson, R. L. (2010). *Lmx1b* is required for murine trabecular meshwork formation and for maintenance of corneal transparency. *Developmental Dynamics*, 239(8), 2161-2171. doi:<https://doi.org/10.1002/dvdy.22347>

- Liu, W., Lagutin, O. V., Mende, M., Streit, A., & Oliver, G. (2006). Six3 activation of Pax6 expression is essential for mammalian lens induction and specification. *The EMBO Journal*, 25(22), 5383-5395. doi:10.1038/sj.emboj.7601398
- Liu, X., Zhang, Y., Zhang, B., Gao, H., & Qiu, C. (2020). Nonsense suppression induced readthrough of a novel PAX6 mutation in patient-derived cells of congenital aniridia. *Molecular Genetics & Genomic Medicine*, 8(5), e1198-n/a.
- Lopes, V. S., Gibbs, D., Libby, R. T., Aleman, T. S., Welch, D. L., Lillo, C., et al. (2011). The usher 1B protein, MYO7A, is required for normal localization and function of the visual retinoid cycle enzyme, RPE65. *Human Molecular Genetics*, 20(13), 2560-2570. doi:10.1093/hmg/ddr155
- Lundstrom, K. (2018). Viral vectors in gene therapy. *Diseases*, 6(2) doi:10.3390/diseases6020042
- Lyons, L. A., Creighton, E. K., Alhaddad, H., Beale, H. C., Grahn, R. A., Rah, H., et al. (2016). Whole genome sequencing in cats, identifies new models for blindness in AIPL1 and somite segmentation in HES7. *BMC Genomics*, 17(1), 265. doi:10.1186/s12864-016-2595-4
- Ma, A. S., Grigg, J. R., & Jamieson, R. V. (2019). Phenotype–genotype correlations and emerging pathways in ocular anterior segment dysgenesis. *Human Genetics*, 138(8), 899-915. doi:10.1007/s00439-018-1935-7
- M, M., et al. (2016). *Functional rescue of REP1 following treatment with PTC124 and novel derivative PTC-414 in human choroideremia fibroblasts and the nonsense-mediated*

zebrafish model. Retrieved Jul 6, 2020, from <https://pubmed-ncbi-nlm-nih-gov.ezproxy.library.ubc.ca/27329764/?dopt=Abstract>

MacDonald, I. M., & Mah, D. Y. (2000). Summary of heritable ocular disorders and selected systemic conditions with eye findings. *Ophthalmic Genetics*, *21*(1), 29-49.

Machon, O., Kreslova, J., Ruzickova, J., Vacik, T., Klimova, L., Fujimura, N., et al. (2010). Lens morphogenesis is dependent on Pax6-mediated inhibition of the canonical wnt/beta-catenin signaling in the lens surface ectoderm. *Genesis (New York, N.Y.: 2000)*, *48*(2), 86-95.
doi:10.1002/dvg.20583

Mandai, M., Watanabe, A., Kurimoto, Y., Hiram, Y., Morinaga, C., Daimon, T., et al. (2017). Autologous induced stem-cell-derived retinal cells for macular degeneration. *The New England Journal of Medicine*, *376*(11), 1038-1046. doi:10.1056/NEJMoa1608368

Margo, C. E. (1983). Congenital aniridia: A histopathologic study of the anterior segment in children. *Journal of Pediatric Ophthalmology and Strabismus*, *20*(5), 192.

Massagué, J., Seoane, J., & Wotton, D. (2005). Smad transcription factors. *Genes & Development*, *19*(23), 2783-2810. doi:10.1101/gad.1350705

Mathebula, S. (2012). A review of ocular genetics and inherited eye diseases. *African Vision and Eye Health*, *71* doi:10.4102/aveh.v71i4.81

- Mathur, P., & Yang, J. (2015). *Usher syndrome: Hearing loss, retinal degeneration and associated abnormalities* doi:<https://doi-org.ezproxy.library.ubc.ca/10.1016/j.bbadis.2014.11.020>
- McDonald, C. M., Campbell, C., Torricelli, R. E., Finkel, R. S., Flanigan, K. M., Goemans, N., et al. (2017). *Ataluren in patients with nonsense mutation duchenne muscular dystrophy (ACT DMD): A multicentre, randomised, double-blind, placebo-controlled, phase 3 trial* doi:[https://doi.org/10.1016/S0140-6736\(17\)31611-2](https://doi.org/10.1016/S0140-6736(17)31611-2)
- McGinnis, J. F., Whelan, J. P., & Donoso, L. A. (1992). Transient, cyclic changes in mouse visual cell gene products during the light-dark cycle. *Journal of Neuroscience Research*, 31(3), 584-590. doi:10.1002/jnr.490310325
- Mears, A. J., Jordan, T., Mirzayans, F., Dubois, S., Kume, T., Parlee, M., et al. (1998). Mutations of the forkhead/winged-helix gene, FKHL7, in patients with axenfeld-rieger anomaly. *The American Journal of Human Genetics*, 63(5), 1316-1328.
- Mirjalili Mohanna, S. Z., Hickmott, J. W., Lam, S. L., Chiu, N. Y., Lengyell, T. C., Tam, B. M., et al. (2020). Germline CRISPR/Cas9-mediated gene editing prevents vision loss in a novel mouse model of aniridia. *Molecular Therapy. Methods & Clinical Development*, 17, 478-490. doi:10.1016/j.omtm.2020.03.002
- Mishra, R., Gorlov, I. P., Chao, L. Y., Singh, S., & Saunders, G. F. (2002). PAX6, paired domain influences sequence recognition by the homeodomain. *Journal of Biological Chemistry*, 277(51), 49488-49494. doi:10.1074/jbc.M206478200

- Montini, E., Cesana, D., Schmidt, M., Sanvito, F., Bartholomae, C. C., Ranzani, M., et al. (2009). The genotoxic potential of retroviral vectors is strongly modulated by vector design and integration site selection in a mouse model of HSC gene therapy. *The Journal of Clinical Investigation*, 119(4), 964-975. doi:10.1172/JCI37630
- Moosajee, Maria Toms, Waheeda Pagarkar, Mariya. (2020). Usher syndrome: Clinical features, molecular genetics and advancing therapeutics - maria toms, waheeda pagarkar, mariya moosajee, 2020. *Therapeutic Advances in Ophthalmology*, 12 Retrieved from <https://journals-sagepub-com.ezproxy.library.ubc.ca/doi/10.1177/2515841420952194>
- Moosajee, M., Gregory-Evans, K., Ellis, C. D., Seabra, M. C., & Gregory-Evans, C. Y. (2008). Translational bypass of nonsense mutations in zebrafish rep1, pax2.1 and lamb1 highlights a viable therapeutic option for untreatable genetic eye disease. *Human Molecular Genetics*, 17(24), 3987-4000.
- Namy, O., Hatin, I., & Rousset, J. P. (2001). Impact of the six nucleotides downstream of the stop codon on translation termination. *EMBO Reports*, 2(9), 787-793. doi:10.1093/embo-reports/kve176
- Nascimento e Silva, R., Shen, L. Q., Chiou, C. A., Shanbhag, S. S., Paschalis, E. I., Pasquale, L. R., et al. (2019). *Glaucoma management in patients with aniridia and boston type 1 keratoprosthesis* doi:<https://doi-org.ezproxy.library.ubc.ca/10.1016/j.ajo.2019.06.018>

- Netland, P. A., Scott, M. L., Boyle, J. W., & Lauderdale, J. D. (2011). *Ocular and systemic findings in a survey of aniridia subjects* doi:<https://doi-org.ezproxy.library.ubc.ca/10.1016/j.jaapos.2011.07.009>
- Neuhaus, C., Eisenberger, T., Decker, C., Nagl, S., Blank, C., Pfister, M., et al. (2017). Next-generation sequencing reveals the mutational landscape of clinically diagnosed usher syndrome: Copy number variations, phenocopies, a predominant target for translational read-through, and PEX26 mutated in heimler syndrome. *Molecular Genetics & Genomic Medicine*, 5(5), 531. doi:10.1002/mgg3.312
- Ng, T. K., Fortino, V. R., Pelaez, D., & Cheung, H. S. (2014). Progress of mesenchymal stem cell therapy for neural and retinal diseases. *World Journal of Stem Cells*, 6(2), 111-119. doi:10.4252/wjsc.v6.i2.111
- Nguyen, L. S., Wilkinson, M. F., & Gecz, J. (2014). Nonsense-mediated mRNA decay: Inter-individual variability and human disease. *Neuroscience & Biobehavioral Reviews*, 46, 175-186. doi:10.1016/j.neubiorev.2013.10.016
- Nienhuis, A. W., Dunbar, C. E., & Sorrentino, B. P. (2006). Genotoxicity of retroviral integration in hematopoietic cells. *Molecular Therapy*, 13(6), 1031-1049. doi:10.1016/j.ymthe.2006.03.001
- Ocansey, D. K. W., Pei, B., Yan, Y., Qian, H., Zhang, X., Xu, W., et al. (2020). Improved therapeutics of modified mesenchymal stem cells: An update. *Journal of Translational Medicine*, 18(1), 42. doi:10.1186/s12967-020-02234-x

Okano, S., Makita, Y., Katada, A., Harabuchi, Y., Kohmoto, T., Naruto, T., et al. (2019). Novel compound heterozygous CDH23 variants in a patient with usher syndrome type I. *Human Genome Variation*, 6(1), 8-4. doi:10.1038/s41439-019-0037-y

Okita, K., Matsumura, Y., Sato, Y., Okada, A., Morizane, A., Okamoto, S., et al. (2011). A more efficient method to generate integration-free human iPS cells. *Nature Methods*, 8(5), 409-412. doi:10.1038/nmeth.1591

Oshima, A., Jaijo, T., Aller, E., Millan, J. M., Carney, C., Usami, S., et al. (2008). Mutation profile of the CDH23 gene in 56 probands with usher syndrome type I. *Human Mutation*, 29(6), E37. doi:10.1002/humu.20761

Overlack, N., Goldmann, T., Wolfrum, U., & Nagel-Wolfrum, K. (2012). Gene repair of an usher syndrome causing mutation by zinc-finger nuclease mediated homologous recombination. *Investigative Ophthalmology & Visual Science*, 53(7), 4140-4146. doi:10.1167/iovs.12-9812

Papermaster, D. S. (2002). The birth and death of photoreceptors : The Friedenwald lecture. *Investigative Ophthalmology & Visual Science*, 43(5), 1300-1309. Retrieved from <http://iovs.arvojournals.org/article.aspx?articleid=2122965>

Parfitt, D. A., Lane, A., Ramsden, C. M., Carr, A. F., Munro, P. M., Jovanovic, K., et al. (2016). Identification and correction of mechanisms underlying inherited blindness in human iPSC-derived optic cups. *Cell Stem Cell*, 18(6), 769-781. doi:10.1016/j.stem.2016.03.021

Park, D., Lee, J., Park, I., Choi, D., Lee, S., Song, S., et al. (2014). Lymphatic regulator PROX1 determines schlemm's canal integrity and identity. *The Journal of Clinical Investigation*, *124*(9), 3960-3974. doi:10.1172/JCI75392

Peltz, S. W., Morsy, M., Welch, E. M., & Jacobson, A. (2013). Ataluren as an agent for therapeutic nonsense suppression. *Annual Review of Medicine*, *64*(1), 407-425.

Peng, Y., Zallocchi, M., Wang, W., Delimont, D., & Cosgrove, D. (2011). Moderate light-induced degeneration of rod photoreceptors with delayed transducin translocation in shaker1 mice. *Investigative Ophthalmology & Visual Science*, *52*(9), 6421-6427.
doi:10.1167/iovs.10-6557

Pressman, C. L., Chen, H., & Johnson, R. L. (2000). LMX1B, a LIM homeodomain class transcription factor, is necessary for normal development of multiple tissues in the anterior segment of the murine eye. *Genesis (New York, N.Y.: 2000)*, *26*(1), 15-25.

Proetzel, G., Pawlowski, S. A., Yin, M., Howles, P. N., Ferguson, M. W. J., Wiles, M. V., et al. (1995). Transforming growth factor- β 3 is required for secondary palate fusion. *Nature Genetics*, *11*(4), 409-414. doi:10.1038/ng1295-409

Rathod, R., Surendran, H., Battu, R., Desai, J., & Pal, R. (1988). Journal of chemical neuroanatomy. *Journal of Chemical Neuroanatomy*, *95*, 81-88. Retrieved from <http://www.sciencedirect.com/science/article/pii/S0891061817301205>

Rabbitt, R. D., Brichta, A. M., Tabatabaee, H., Boutros, P. J., Ahn, J., Della Santina, C. C., Lim, R. (2016). Heat pulse excitability of vestibular hair cells and afferent neurons. *Journal of Neurophysiology*, *116*(2), 825-843. doi:10.1152/jn.00110.2016

Reiners, J., Reidel, B., El-Amraoui, A., Boëda, B., Huber, I., Petit, C., et al. (2003). Differential distribution of harmonin isoforms and their possible role in usher-1 protein complexes in mammalian photoreceptor cells. *Investigative Ophthalmology & Visual Science*, *44*(11), 5006-5015. doi:10.1167/iovs.03-0483

Reneker, L. W., Silversides, D. W., Xu, L., & Overbeek, P. A. (2000). Formation of corneal endothelium is essential for anterior segment development - a transgenic mouse model of anterior segment dysgenesis. *Development*, *127*(3), 533-542.

Richardson, R., Smart, M., Tracey-White, D., Webster, A. R., & Moosajee, M. (2017). Mechanism and evidence of nonsense suppression therapy for genetic eye disorders. *Experimental Eye Research*, *155*, 24-37.

Robert, M., & Colby, K. (2017). Corneal diseases in children: Congenital anomalies. In K. Colby (Ed.), *Corneal diseases in children: Challenges and controversies* (pp. 69-85). Cham: Springer International Publishing. doi:10.1007/978-3-319-55298-9_6 Retrieved from https://doi.org/10.1007/978-3-319-55298-9_6

Sahly, I., Dufour, E., Schietroma, C., Michel, V., Bahloul, A., Perfettini, I., et al. (2012). Localization of usher 1 proteins to the photoreceptor calyceal processes, which are absent from mice. *Journal of Cell Biology*, *199*(2), 381-399.

- Saika, S., Saika, S., Liu, C. Y., Azhar, M., Sanford, L. P., Doetschman, T., et al. (2001). TGFbeta2 in corneal morphogenesis during mouse embryonic development. *Developmental Biology*, 240(2), 419-432. doi:S0012-1606(01)90480-4 [pii]
- Saika, S. (2006). TGFβ pathobiology in the eye. *Laboratory Investigation*, 86(2), 106-115. doi:10.1038/labinvest.3700375
- Samanta, A., Stingl, K., Kohl, S., Ries, J., Linnert, J., & Nagel-Wolfrum, K. (2019). Ataluren for the treatment of usher syndrome 2A caused by nonsense mutations. *International Journal of Molecular Sciences*, 20(24), 6274.
- Sambhara, D., & Aref, A. A. (2014). *Glaucoma management: Relative value and place in therapy of available drug treatments*. London, England: SAGE Publications. doi:10.1177/2040622313511286
- Schedl, A., Ross, A., Lee, M., Engelkamp, D., Rashbass, P., van Heyningen, V., et al. (1996). Influence of PAX6 gene dosage on development: Overexpression causes severe eye abnormalities. *Cell*, 86(1), 71-82. doi:10.1016/s0092-8674(00)80078-1
- Schietroma, C., Parain, K., Estivalet, A., Aghaie, A., Monvel, J. B. d., Picaud, S., et al. (2017). Usher syndrome type 1–associated cadherins shape the photoreceptor outer segment. *The Journal of Cell Biology*, 216(6), 1849. doi:10.1083/jcb.201612030
- Schmittgen, T. D., & Livak, K. J. (2008). Analyzing real-time PCR data by the comparative C(T) method. *Nature Protocols*, 3(6), 1101-1108. doi:10.1038/nprot.2008.73

- Schultz, J. M., Bhatti, R., Madeo, A. C., Turriff, A., Muskett, J. A., Zalewski, C. K., et al. (2011). Allelic hierarchy of CDH23 mutations causing non-syndromic deafness DFNB12 or usher syndrome USH1D in compound heterozygotes. *Journal of Medical Genetics*, 48(11), 767-775.
- Schwarz, N., Carr, A., Lane, A., Moeller, F., Chen, L. L., Aguilà, M., et al. (2015). Translational read-through of the RP2 Arg120stop mutation in patient iPSC-derived retinal pigment epithelium cells. *Human Molecular Genetics*, 24(4), 972. doi:10.1093/hmg/ddu509
- Scofield, D. G., Hong, X., & Lynch, M. (2007). Position of the final intron in full-length transcripts: Determined by NMD? *Molecular Biology and Evolution*, 24(4), 896-899. doi:10.1093/molbev/msm010
- Seo, S., Singh, H. P., Lacal, P. M., Sasman, A., Fatima, A., Liu, T., et al. (2012). Forkhead box transcription factor FoxC1 preserves corneal transparency by regulating vascular growth. *Proceedings of the National Academy of Sciences of the United States of America*, 109(6), 2015-2020.
- Siemens, J., Kazmierczak, P., Reynolds, A., Sticker, M., Littlewood-Evans, A., & Müller, U. (2002). The usher syndrome proteins cadherin 23 and harmonin form a complex by means of PDZ-domain interactions. *Proceedings of the National Academy of Sciences of the United States of America*, 99(23), 14946-14951. doi:10.1073/pnas.232579599

- Silla, Z. T. V., Naidoo, J., Kidson, S. H., & Sommer, P. (2014). Signals from the lens and Foxc1 regulate the expression of key genes during the onset of corneal endothelial development. *Experimental Cell Research*, 322(2), 381-388.
- Simpson, T. I., & Price, D. J. (2002). Pax6; A pleiotropic player in development. *BioEssays*, 24(11), 1041-1051. doi:10.1002/bies.10174
- Sisodiya, S. M., Free, S. L., Williamson, K. A., Mitchell, T. N., Willis, C., Stevens, J. M., et al. (2001). PAX6 haploinsufficiency causes cerebral malformation and olfactory dysfunction in humans. *Nature Genetics*, 28(3), 214-216. doi:10.1038/90042
- Slepak, V. Z., & Hurley, J. B. (2008). Mechanism of light-induced translocation of arrestin and transducin in photoreceptors: Interaction-restricted diffusion. *IUBMB Life*, 60(1), 2-9. doi:10.1002/iub.7
- Slijkerman, R. W. N., Song, F., Astuti, G. D. N., Huynen, M. A., van Wijk, E., Stieger, K., et al. (2015). The pros and cons of vertebrate animal models for functional and therapeutic research on inherited retinal dystrophies. *Progress in Retinal and Eye Research*, 48, 137-159.
- Smith, J. R., & Rosenbaum, J. T. (2000). Management of immune-mediated uveitis. *BioDrugs: Clinical Immunotherapeutics, Biopharmaceuticals and Gene Therapy*, 13(1), 9-20. doi:10.2165/00063030-200013010-00002

- Smith, R. S., Zabaleta, A., Kume, T., Savinova, O. V., Kidson, S. H., Martin, J. E., et al. (2000). Haploinsufficiency of the transcription factors FOXC1 and FOXC2 results in aberrant ocular development. *Human Molecular Genetics*, 9(7), 1021-1032.
- Smith, R. S., Zabaleta, A., Savinova, O. V., & John, S. W. (2001). The mouse anterior chamber angle and trabecular meshwork develop without cell death. *BMC Developmental Biology*, 1(1), 3. doi:10.1186/1471-213X-1-3
- Sowden, J. C. (2007). Molecular and developmental mechanisms of anterior segment dysgenesis. *Eye*, 21(10), 1310-1318. doi:10.1038/sj.eye.6702852
- Sridhar, A., Hoshino, A., Finkbeiner, C. R., Chitsazan, A., Dai, L., Haugan, A. K., et al. (2020). Single-cell transcriptomic comparison of human fetal retina, hPSC-derived retinal organoids, and long-term retinal cultures. *Cell Reports*, 30(5), 1644-1659.e4.
- Staerk, J., Dawlaty, M. M., Gao, Q., Maetzel, D., Hanna, J., Sommer, C. A., et al. (2010). Reprogramming of peripheral blood cells to induced pluripotent stem cells. *Cell Stem Cell*, 7(1), 20-24. doi:10.1016/j.stem.2010.06.002
- Strissel, K. J., Lishko, P. V., Trieu, L. H., Kennedy, M. J., Hurley, J. B., & Arshavsky, V. Y. (2005). Recoverin undergoes light-dependent intracellular translocation in rod photoreceptors. *The Journal of Biological Chemistry*, 280(32), 29250-29255. doi:M501789200 [pii]

- Strungaru, M. H., Dinu, I., & Walter, M. A. (2007). Genotype-phenotype correlations in axenfeld-rieger malformation and glaucoma patients with FOXC1 and PITX2 mutations. *Investigative Ophthalmology & Visual Science*, *48*(1), 228-237.
- Summers, K. M., Withers, S. J., Gole, G. A., Piras, S., & Taylor, P. J. (2008). Anterior segment mesenchymal dysgenesis in a large australian family is associated with the recurrent 17 bp duplication in PITX3. *Molecular Vision*, *14*, 2010-2015. Retrieved from <https://www.ncbi.nlm.nih.gov/pmc/articles/PMC2579936/>
- Swanner, J. C., Walton, D. S., & Chen, T. C. (2004). Prevention of aniridic glaucoma with goniosurgery. *International Ophthalmology Clinics*, *44*(1), 67-71.
- Takahashi, K., & Yamanaka, S. (2006). Induction of pluripotent stem cells from mouse embryonic and adult fibroblast cultures by defined factors. *Cell*, *126*(4), 663-676. doi:10.1016/j.cell.2006.07.024
- Tawara, A., Varner, H. H., & Hollyfield, J. G. (1989). Distribution and characterization of sulfated proteoglycans in the human trabecular tissue. *Investigative Ophthalmology & Visual Science*, *30*(10), 2215-2231.
- Thaug, C., West, K., Clark, B. J., McKie, L., Morgan, J. E., Arnold, K., . . . Cross, S. H. (2002). Novel ENU-induced eye mutations in the mouse: Models for human eye disease. *Human Molecular Genetics*, *11*(7), 755-767. doi:10.1093/hmg/11.7.755

- Tian, G., Lee, R., Ropelewski, P., & Imanishi, Y. (2016). Impairment of vision in a mouse model of usher syndrome type III. *Investigative Ophthalmology & Visual Science*, 57(3), 866-875. doi:10.1167/iovs.15-16946
- Tian, M., Wang, W., Delimont, D., Cheung, L., Zallocchi, M., Cosgrove, D., et al. (2014). Photoreceptors in whirler mice show defective transducin translocation and are susceptible to short-term light/dark changes-induced degeneration. *Experimental Eye Research*, 118, 145-153. doi:10.1016/j.exer.2013.10.021
- Tom Dieck, S., Altrock, W. D., Kessels, M. M., Qualmann, B., Regus, H., Brauner, D., et al. (2005). Molecular dissection of the photoreceptor ribbon synapse: Physical interaction of bassoon and RIBEYE is essential for the assembly of the ribbon complex. *The Journal of Cell Biology*, 168(5), 825-836. doi:10.1083/jcb.200408157
- Torriano, S., Erkilic, N., Baux, D., Cereso, N., Luca, V. D., Meunier, I., et al. (2018). The effect of PTC124 on choroideremia fibroblasts and iPSC-derived RPE raises considerations for therapy. *Scientific Reports*, 8(1), 1-15. doi:10.1038/s41598-018-26481-7
- Tripathi, R. C., Li, J. P., Chan, W., & Tripathi, B. J. (1994). Aqueous-humor in glaucomatous eyes contains an increased level of tgf-beta-2. *Experimental Eye Research*, 59(6), 723-727.
- Tsai, J. H., Freeman, J. M., Chan, C., Schwartz, G. S., Derby, E. A., Petersen, M. R., et al. (2005). A progressive anterior fibrosis syndrome in patients with postsurgical congenital aniridia. *American Journal of Ophthalmology*, 140(6), 1075-1079. doi:10.1016/j.ajo.2005.07.035

- Tucker, B. A., Mullins, R. F., Streb, L. M., Anfinson, K., Eyestone, M. E., Kaalberg, E., et al. (2013). Patient-specific iPSC-derived photoreceptor precursor cells as a means to investigate retinitis pigmentosa. *eLife*, 2 doi:10.7554/eLife.00824
- U, M. (2008). Cadherins and mechanotransduction by hair cells. *Current Opinion in Cell Biology*, 20(5), 557-566. doi:10.1016/j.ceb.2008.06.004
- Ullah, I., Subbarao, R. B., & Rho, G. J. (2015). Human mesenchymal stem cells - current trends and future prospective. *Bioscience Reports*, 35(2), e00191. doi: 10.1042/BSR20150025. doi:10.1042/BSR20150025 [doi]
- van Heyningen, V., & Williamson, K. A. (2002). PAX6 in sensory development. *Human Molecular Genetics*, 11(10), 1161-1167. doi:10.1093/hmg/11.10.1161
- Viringipurampeer, I. A., Metcalfe, A. L., Bashar, A. E., Sivak, O., Yanai, A., Mohammadi, Z., et al. (2016). NLRP3 inflammasome activation drives bystander cone photoreceptor cell death in a P23H rhodopsin model of retinal degeneration. *Human Molecular Genetics*, 25(8), 1501-1516. doi:10.1093/hmg/ddw029
- Wagatsuma, M., Kitoh, R., Suzuki, H., Fukuoka, H., Takumi, Y., & Usami, S. (2007). Distribution and frequencies of CDH23 mutations in japanese patients with non-syndromic hearing loss. *Clinical Genetics*, 72(4), 339-344. doi:10.1111/j.1399-0004.2007.00833.x
- Wahlin, K. J., Maruotti, J. A., Sripathi, S. R., Ball, J., Angueyra, J. M., Kim, C., et al. (2017). Photoreceptor outer segment-like structures in long-term 3D retinas from human pluripotent stem cells. *Scientific Reports*, 7(1), 766-15.

- Wang, H., Wang, C., Peng, G., Yu, D., Cui, X., Sun, Y., et al. (2020). Capping protein regulator and myosin 1 linker 3 is required for tumor metastasis. *Molecular Cancer Research: MCR*, 18(2), 240-252. doi:10.1158/1541-7786.MCR-19-0722
- Wang, X., & Gregory-Evans, C. Y. (2015). Nonsense suppression therapies in ocular genetic diseases. *Cellular and Molecular Life Sciences: CMLS*, 72(10), 1931-1938. doi:10.1007/s00018-015-1843-0
- Wang, X., Gregory-Evans, K., Wasan, K. M., Sivak, O., Shan, X., & Gregory-Evans, C. Y. (2017). Efficacy of postnatal In Vivo nonsense suppression therapy in a Pax6 mouse model of aniridia. *Molecular Therapy - Nucleic Acids*, 7(C), 417-428.
- Wang, X., Shan, X., Gregory-Evans, K., & Gregory-Evans, C. Y. (2020). RNA-based therapies in animal models of leber congenital amaurosis causing blindness. *Precision Clinical Medicine*, 3(2), 113-126. doi:10.1093/pcmedi/pbaa009
- Wang, Y., Tang, Z., & Gu, P. (2020). Stem/progenitor cell-based transplantation for retinal degeneration: A review of clinical trials. *Cell Death & Disease*, 11(9) doi:10.1038/s41419-020-02955-3
- Warren, L., Manos, P. D., Ahfeldt, T., Loh, Y., Li, H., Lau, F., et al. (2010). Highly efficient reprogramming to pluripotency and directed differentiation of human cells with synthetic modified mRNA. *Cell Stem Cell*, 7(5), 618-630.
- Welch, E. M., Barton, E. R., Zhuo, J., Tomizawa, Y., Friesen, W. J., Trifillis, P., et al. (2007). PTC124 targets genetic disorders caused by nonsense mutations. *Nature*, 447(7140), 87-U6.

- Whatley, M., Francis, A., Ng, Z. Y., Khoh, X. E., Atlas, M. D., Dilley, R. J., et al. (2020). Usher syndrome: Genetics and molecular links of hearing loss and directions for therapy. *Frontiers in Genetics, 11*, 1257. Retrieved from <https://www.frontiersin.org/article/10.3389/fgene.2020.565216>
- Whelan, J. P., & McGinnis, J. F. (1988). Light-dependent subcellular movement of photoreceptor proteins. *Journal of Neuroscience Research, 20*(2), 263-270.
doi:10.1002/jnr.490200216 [doi]
- Wiley, L. A., Burnight, E. R., Songstad, A. E., Drack, A. V., Mullins, R. F., Stone, E. M., et al. (2015). Patient-specific induced pluripotent stem cells (iPSCs) for the study and treatment of retinal degenerative diseases. *Progress in Retinal and Eye Research, 44*, 15-35.
doi:10.1016/j.preteyeres.2014.10.002
- Williams, D. S., Aleman, T. S., Lillo, C., Lopes, V. S., Hughes, L. C., Stone, E. M., et al. (2009). Harmonin in the murine retina and the retinal phenotypes of Ush1c-mutant mice and human USH1C. *Investigative Ophthalmology & Visual Science, 50*(8), 3881-3889.
doi:10.1167/iovs.08-3358
- Wolf, L. V., Yang, Y., Wang, J. H., Xie, Q., Braunger, B., Tamm, E. R., et al. (2009a). Identification of Pax6-dependent gene regulatory networks in the mouse lens. *Plos One, 4*(1), e4159.

- Wolf, L. V., Yang, Y., Wang, J., Xie, Q., Braunger, B., Tamm, E. R., et al. (2009b). Identification of pax6-dependent gene regulatory networks in the mouse lens. *PloS One*, 4(1), e4159. doi:10.1371/journal.pone.0004159 [doi]
- Woltjen, K., Michael, I. P., Mohseni, P., Desai, R., Mileikovsky, M., Hämäläinen, R., et al. (2009). piggyBac transposition reprograms fibroblasts to induced pluripotent stem cells. *Nature*, 458(7239), 766-770. doi:10.1038/nature07863
- Wyse, R. D., Dunbar, G. L., & Rossignol, J. (2014). Use of genetically modified mesenchymal stem cells to treat neurodegenerative diseases. *International Journal of Molecular Sciences*, 15(2), 1719-1745. doi:10.3390/ijms15021719
- Xu, J., Dodd, R. L., Makino, C. L., Simon, M. I., Baylor, D. A., & Chen, J. (1997). Prolonged photoresponses in transgenic mouse rods lacking arrestin. *Nature*, 389(6650), 505-509. doi:10.1038/39068
- Xu, W., & Xu, G. (2011). Mesenchymal stem cells for retinal diseases. *International Journal of Ophthalmology*, 4(4), 413-421. doi:10.3980/j.issn.2222-3959.2011.04.19
- Yan, D., & Liu, X. Z. (2010). Genetics and pathological mechanisms of usher syndrome. *Journal of Human Genetics*, 55(6), 327-335. doi:10.1038/jhg.2010.29
- Yanai, A., Laver, C. R. J., Joe, A. W., Viringipurampeer, I. A., Wang, X., Gregory-Evans, C. Y., et al. (2013). Differentiation of human embryonic stem cells using size-controlled embryoid bodies and negative cell selection in the production of photoreceptor precursor cells. *Tissue Engineering. Part C, Methods*, 19(10), 755-764. doi:10.1089/ten.TEC.2012.0524

- Yongblah, K., Alford, S. C., Ryan, B. C., Chow, R. L., & Howard, P. L. (2018). Protecting Pax6 3' UTR from MicroRNA-7 partially restores PAX6 in islets from an aniridia mouse model. *Molecular Therapy.Nucleic Acids*, *13*, 144-153. doi:10.1016/j.omtn.2018.08.018
- Young, T. L. (2003). Ophthalmic genetics/inherited eye disease. *Current Opinion in Ophthalmology*, *14*(5), 296-303.
- Yu, S., Tanabe, T., Dezawa, M., Ishikawa, H., & Yoshimura, N. (2006). Effects of bone marrow stromal cell injection in an experimental glaucoma model. *Biochemical and Biophysical Research Communications*, *344*(4), 1071-1079.
- Zallocchi, M., Meehan, D. T., Delimont, D., Askew, C., Garige, S., Gratton, M. A., et al. (2009). Localization and expression of clarin-1, the Cln1 gene product, in auditory hair cells and photoreceptors. *Hearing Research*, *255*(1-2), 109-120. doi:10.1016/j.heares.2009.06.006
- Zhang, H., Huang, W., Zhang, H., Zhu, X., Craft, C. M., Baehr, W., et al. (2003). Light-dependent redistribution of visual arrestins and transducin subunits in mice with defective phototransduction. *Molecular Vision*, *9*, 231-237. doi:v9/a34 [pii]
- Zhang, Y., Overbeek, P. A., & Govindarajan, V. (2007). Perinatal ablation of the mouse lens causes multiple anterior chamber defects. *Molecular Vision*, *13*(259-60), 2289-2300.
- Zhou, T., Benda, C., Duzinger, S., Huang, Y., Li, X., Li, Y., et al. (2011). Generation of induced pluripotent stem cells from urine. *Journal of the American Society of Nephrology*, *22*(7), 1221-1228.

Zhu, J., Reynolds, J., Garcia, T., Cifuentes, H., Chew, S., Zeng, X., et al. (2018). Generation of transplantable retinal photoreceptors from a current good manufacturing practice-manufactured human induced pluripotent stem cell line. *STEM CELLS Translational Medicine*, 7(2), 210-219. doi:10.1002/sctm.17-0205

Appendix A Supplemental data for chapter 1

A.1 3% TBE Agarose gel preparation

To prepare a 10X stock solution in 1 L of H₂O following reagents are used.

108 g of Tris base

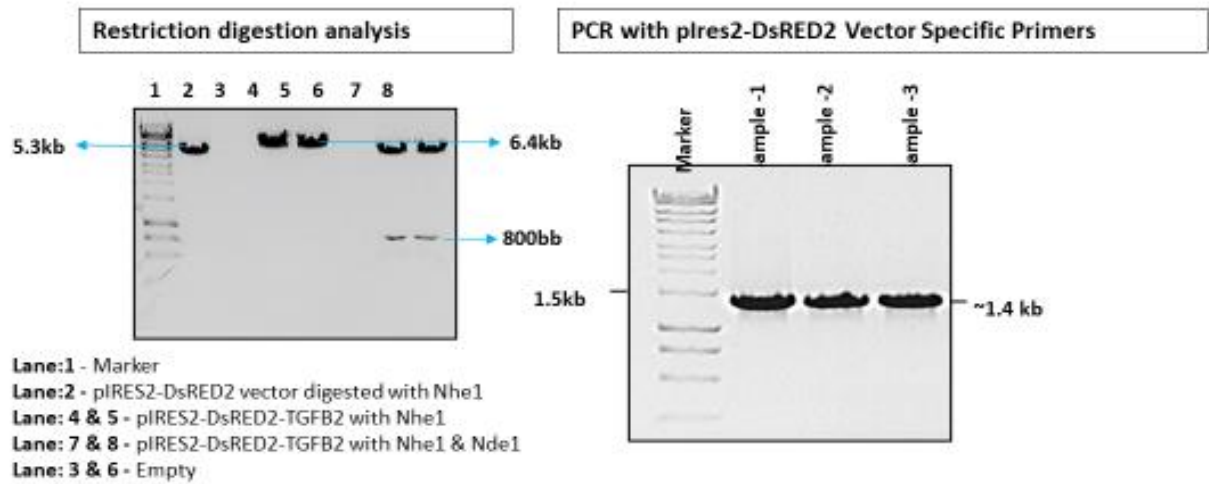
55 g of boric acid

20 mL of 1 M EDTA (pH 8.0)

The 0.5X working solution is 45 mM Tris-borate/1 mM EDTA. TBE is usually made as 10X stock solution, and the pH of the concentrated stock buffer is ~8.3. The concentrated stock buffer was diluted just before to prepare the gel solution and the electrophoresis buffer was prepared from the same concentrated stock solution.

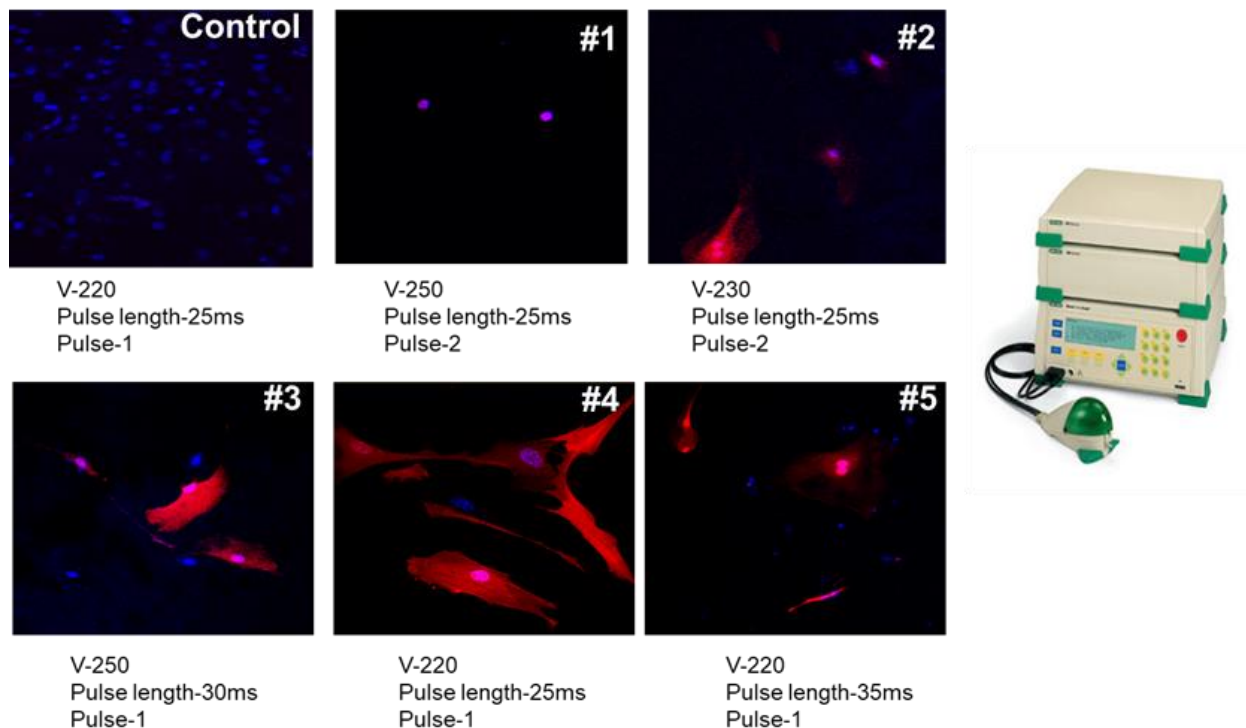
A.2 Confirmation of *Tgfb2* gene in the plasmid pIRES Ds Red 2 vector by restriction digestion analysis.

Cloning confirmation by restriction digestion and PCR



A.3 Optimization of Electroporation of MSCs at different voltage

Plasmid containing *Tgfβ2* electroporated into MSCs



A.4 START formulation for topical treatment.

The 'START' formulation (0.9% Sodium chloride, 1% Tween 80, 1% powdered Ataluren, 1% carboxy methyl cellulose) without preservatives. To improve particle dispersion Ataluren was ground into a very fine powder using mortar and pestle. The ground powder was added to the Tween 80 and NaCl solution and sonicated for 300 sec. Residual particulate material was removed on passing the suspension through a #325 mesh screen, prior to adding carboxy methylcellulose which increased the viscosity of the formulation. The time for re-dispersion was determined by the time it took for the sediment to be fully shaken up manually after standing the container in an upright position for 5 days at 25°C.